LBL-13057

Lawrence Berkeley Laboratory
UNIVERSITY OF CALIFORNIA

Materials & Molecular
Research Division

THE INFLUENCE OF LEAD IONS ON THE MACROMORPHOLOGY OF ELECTRODEPOSITED ZINC

Tetsuaki Tsuda with Charles W. Tobias
(M.S. thesis)

September 1981

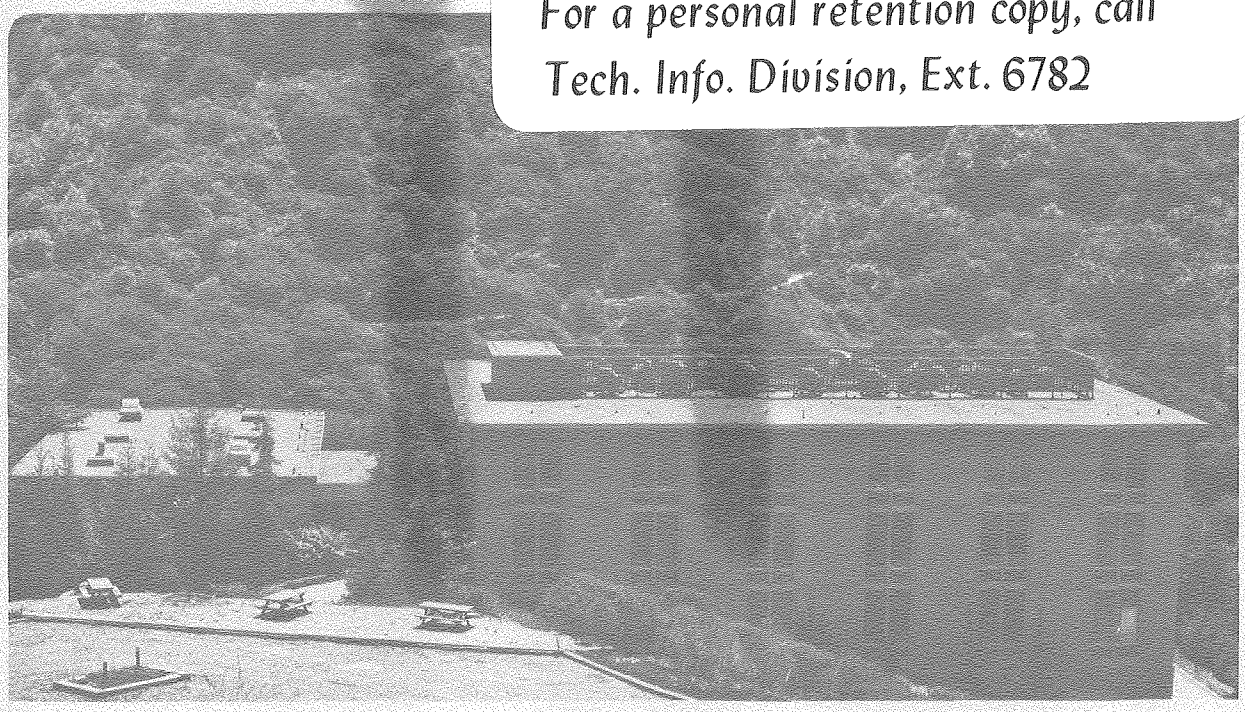

Prepared for the U.S. Department of Energy under Contract W-7405-ENG-48

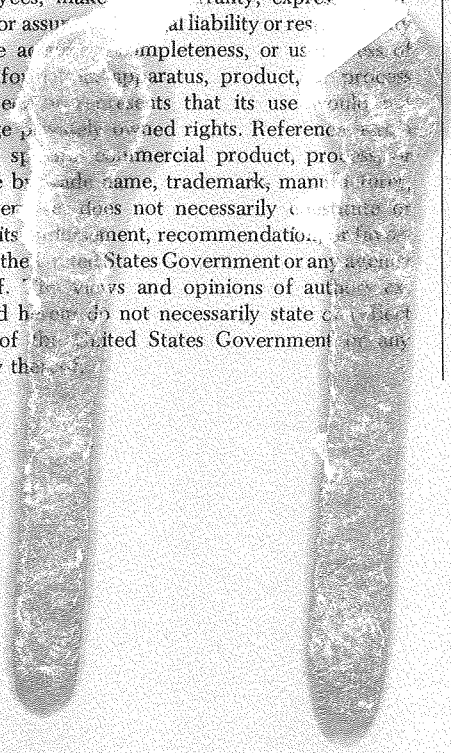

LBL-13057

THE INFLUENCE OF LEAD IONS ON THE MACROMORPHOLOGY OF ELECTRODEPOSITED ZINC

Tetsuaki Tsuda with Charles W. Tobias

Materials and Molecular Research Division
Lawrence Berkeley Laboratory
and
Department of Chemical Engineering
University of California
Berkeley, California 94720

This work was supported by the Director, the Assistant Secretary of Conservation and Renewable Energy, Office of Advanced Conservation Technology, Electrochemical Systems Research Division of the U.S. Department of Energy under Contract No. W-7405-ENG-48.

CONTENTS

THE INFLUENCE OF LEAD IONS ON THE MACROMORPHOLOGY OF ELECTRODEPOSITED ZINC

Tetsuaki Tsuda* with Charles W. Tobias

Materials and Molecular Research Division, Lawrence Berkeley Laboratory

and Department of Chemical Engineering, University of California
Berkeley, California 94720

ABSTRACT

The morphology of zinc as it is electrodeposited from acid solutions demonstrates a remarkable imprint of electrolyte flow conditions. The development of macromorphology of zinc deposits has been investigated under galvanostatic conditions on a rotating platinum disk electrode by use of photomacrography, scanning electron microscopy, electron probe microanalysis and Auger microprobe analysis. Logarithmic spiral markings, which reflect the hydrodynamic flow on a rotating disk, appear in a certain region of current density well below the limiting current density. Morphological observations revealed the major influence of trace lead ions on the amplification of surface roughness through coalescence and preferred growth of initial protrusions. Results obtained from ultra-pure electrolyte suggest preferred crystal growth towards well-mixed orientation in the concentration field caused by slight differences in crystallization overpotential. A qualitative model involving a coupling mechanism between the evolving surface roughness and instability phenomena in the boundary layer is advanced to explain the formation of spiral patterns.

---

*Filed as M.S. thesis.

1. INTRODUCTION

Extensive work has been done to establish the criteria for obtaining smooth and dense deposits electrochemically in the fields of electroplating, electro-winning and -refining, and in rechargeable batteries as well. The evolution of surface morphology during electrolysis often dominates the performance and efficiency of these electrochemical systems.

Several investigators have observed deposit patterns which contain imprints of hydrodynamic events. It is of especially great interest that under certain conditions hydrodynamic effects on the macromorphology of electrodeposits are observed at rates far lower than the mass-transfer controlled regime. Several inadequate explanations have been given which require further study on this subject. A better understanding of the mechanism responsible for this phenomenon will lead to the successful optimization of these systems.

The zinc-chlorine battery is under development for energy-storage use in utility load-levelling and electric vehicle applications. The macromorphological development of zinc deposit during charging and discharging plays a major role in determining the cycle-life, reliability and efficiency of this flow-battery system. Investigations of the hydrodynamic effect on the surface morphology in the electrodeposition of zinc from acidic solutions have been conducted as a portion of this zinc-chlorine battery project. This extensive experimental work serves as an extension of earlier works carried out in this laboratory by M. Jaksić and continued successively by V. Komnenić. Currently investigations are conducted in this laboratory by J. Faltemier on

hydrodynamic effects on the electrocrystallization of zinc in a channel type cell, using large (30 cm long) electrodes. This experimental study is aimed at advancing our understanding of why under certain conditions the surface morphology of zinc deposit carries an imprint of hydrodynamic flow.

It is well known that metallic impurities present in the electrolyte have a major effect on zinc electrodeposition. Preliminary results obtained from purified solutions by means of zinc-particle cementation indicated a large effect of impurities on the formation of spiral patterns on a rotating disk electrode. Since lead is a most common impurity associated with zinc electrolysis and is known to influence the kinetics and micromorphology of the electrocrystallization of zinc, the effect of lead impurity on the formation of spiral patterns are fully examined using rotating disk electrodes.

2. LITERATURE REVIEW

Although spiral markings in metal layers deposited on a rotating disk electrode have been reported by various investigators, the cause of these spirals has not as yet been satisfactorily explained (1, 24).

Johnson and Turner (2) observed spiral patterns obtained from galvanostatic copper deposition in 1M $CuSO_4$ with 1M H_2SO_4 containing 1×10^{-4} M thiourea. A remarkable feature is that the pattern did not change with rotation speed. They considered this shape to be an Archimedes spiral, however it is more likely that this spiral is a logarithmic spiral whose characteristic constant (1/ln a) was measured by the present author to be about 1.37. Polarization curves with thiourea showed a cathode potential plateau where the current density increased markedly with a slight increase in potential.

Rogers and Taylor (3) found spiral markings in deposits obtained in the laminar flow region from Watts-type nickel plating solution with coumarine addition. The appearance of the spirals did not resemble those electrodeposited from zine chloride solution. There were definite protrusions or defects in the surface associated with each spiral. These authors have demonstrated that in this case the spirals are traces of the wakes of hydrogen bubbles growing at these points. It was assumed that the effect of coumarine was to enhance hydrogen coevolution. Protrusions which had different heights generated different shape (angle) of spirals. The height of protrusions was much smaller than the thickness of fluid boundary layer, and hence local Reynolds number was too small to cause local turbulence. Autoradiographic

results indicated that the incorporation of carbon from coumarine in deposits was lower within the spirals than on the uniform surface. They interpreted this result as an indication of lower mass-transport rate of coumarine along spiral wakes.

Hill and Rogers (4) have studied the effect of Polyethylene glycol on copper electrodeposition. Below a critical overpotential very strong inhibition of deposition was observed. Spiral patterns appeared at the critical overpotential plateau where current density rose rapidly with a slight overpotential rise. It should be noted that the Wagner number becomes very small in this region due to low polarization resistance (i.e., $dE/di \simeq 0$). Interestingly, the number of spirals decreased with increasing the current density. The number and shape of spirals did not vary with rotation speed from 910 rpm to 2,600 rpm. The protrusion height was calculated to be about 3 - 5 μm from the characteristic constant, $1/\ln a = 1.27$, of this logarithmic spiral. Although the amplification of surface irregularities with deposition was explained in terms of low polarization resistance at the critical overpotential, the mechanism by which connection of these protrusions and/or depressions occurs was not clarified.

Subsequently Hill et al. (5), found that the formation of spirals in the critical overpotential region can be attributed to submicroscopic defects on the surface. However, Hill et al. do not give satisfactory explanations concerning either the origin of protrusions or the inter-relationship between the number of protrusions and the number of spirals. The mechanism whereby concentration changes in a wake affect the deposition rate below limiting current is also not clarified.

Gregory et al. (6) have studied the vortex generation upstream of transition point within the hydrodynamic boundary layer on a theoretical basis, and observed experimentally spiral streaks on a rotating china-clay disk between the radius at the starting point of instability and radius where transition occurs from laminar to turbulent flow. The characteristic constant (1/ln a) observed was 4.01 for this spiral, a value very different from that obtained for zinc electrodeposition: 1.2 - 1.4. Onset of instability started at Re = 1.78 - 2.12 x 10^5 and transition occurred at Re = 2.70 - 2.99 x 10^5.

Cornet et al. (7) have investigated the effect of surface roughness elements on the rate of mass transfer of dissolved oxygen to the surface of rotating Monel disks. The coarser the surface of a disk, the lower was the observed transition Reynolds number: Re_T = 2.6 x 10^5 for the smooth disk and Re_T = 2.8 x 10^4 for the disk with sand roughness of #16. Results for spiral grooved disks in laminar flow showed that the effective area available for mass transfer to a spiral grooved disk was less than that for a smooth disk. This seems to suggest that mass transfer is less effective into a groove on the surface of a rotating disk.

Previous studies on zinc deposition carried out in A. R. grade electrolytes using 99.99% zinc anode by M. Jaksić, V. Komnenić, J. Faltemier and C. Tobias (8 - 12) may be summarized as follows:

(a) Zinc deposits from $ZnCl_2$, $ZnBr_2$ and $ZnSO_4$ solutions (pH 1-5) show groove striations parallel to the flow direction in a channel cell, starting at the leading edge. Similarly,

logarithmic spiral markings are observed on a rotating disk electrode.

(b) The number density of striations and/or spirals increases with current density. Macroscopically smooth deposits are obtained above a certain current density, approximately 100 mA/cm^2 in zinc chloride solution and 10 mA/cm^2 in zinc sulfate solution.

(c) Since spirals appear in both strongly-complexing $ZnCl_2$ and weakly-complexing $ZnSO_4$ solutions, it is most likely that complexing is not the crucial factor governing the formation of spirals.

(d) The bulk concentration of zinc ions seems to have only minor influence.

(e) pH in the range of 1 - 5 has no significant effect. Markings form over the entire acid range were investigated.

(f) At higher flowrates, ridges and valleys are more sharply drawn and in addition spirals and/or striations develop more rapidly.

(g) Shape angle of spirals is nearly independent of rotational speeds.

(h) Addition of a strongly adsorbing surfactant such as the fluorosurfactant "Zonyl FSB" (Du Pont) refines the surface structure and more rapid growth of these markings occurs.

(i) The close relationship among surface defects, nucleation density and spiral formation is corroborated by use of variable-current step and A.C. pulse techniques.

Preliminary experiments on a rotating ring electrode show that spiral formation is much more pronounced near the outer edge than the inner edge (i.e., a leading edge for this electrode). Similar trend is observed for a rotating disk where the center of rotation serves as a stagnation point (see Appendix B).

Mansfeld and Gilman (13) have investigated the effect of lead ions on the characteristics of a zinc single crystal deposition from 6N KOH and 20 g/l ZnO. In the presence of trace lead ions (10^{-4} M lead acetate) crystalline nodules with layer growth changed to rounded protrusions consisting of numerous small crystallites while zinc deposition tended to initiate only at preferred sites.

MacKinnon et al. (14) have studied the influence of lead on zinc deposit micromorphology and crystallographic orientation galvanostatically from acidic sulphate solutions. Lead concentration in zinc deposits increased with increasing lead content in solution and with decreasing current density because the deposition rate of lead was mass transfer limited. The orientation changed from intermediate (112), (101) to perpendicular (100), finally to basal (002) as lead content in the deposits increased. Activation overpotential, as measured by cyclic voltammetry, increased with a rise of lead content in the zinc deposits up to 0.07%. For lead concentrations of the deposits greater than 0.07%, obtained at low current densities (i.e., 21.5 mA/cm^2), the morphology of zinc crystals became poorly defined; basal orientation was preferred, associated with low activation overpotential.

Bressan and Wiart (15, 16, 17) have studied the influence of additives on the kinetics of zinc electrocrystallization by use of impedance

measurements in the Leclanché cell electrolyte (0.48 - 0.72M $ZnCl_2$, 2.67M NH_4Cl, pH 5.2) and acid sulphate electrolyte (1.5M $ZnSO_4$, 1M Na_2SO_4). Experiments were performed under galvanostatic conditions, because the current varied abruptly with the cathodic overpotential during the electrocrystallization of zinc (i.e., $dE/di \ll 1$). The steady state polarization curves shifted towards more cathodic overpotentials as the lead concentration was increased up to 3×10^{-4} M Pb at 1,000 rpm, and also with increasing rotation speed from 200 rpm to 1,000 rpm. S-shaped polarization curves appeared as a consequence of diffusion-controlled inhibition of zinc electrodeposition by lead acetate. With rotation speeds higher than 1,000 rpm, the polarization curve became single valued. Similarly, a pH decrease eliminated the S-shape in the polarization curve and gave rise to a shift toward more negative overpotentials. The addition of lead acetate modified the impedance diagrams at low frequencies. The results were interpreted in terms of a coupling between the diffusion of the inhibitor and the slow renewal of active growth sites.

3. EXPERIMENTAL

3-1. Materials and Apparatus

Chemicals

Most of the solutions were prepared from "analytical grade" chemicals as a starting material. In some cases "ultra-pure" grade chemical was used.

(1) Zinc chloride

(A) Mallinckrodt, Analytical Reagent $ZnCl_2$

maximum limits given for impurities: Fe 10 ppm

Pb 50 ppm

(B) Alfa Division, Ventron Corp.

anhydrous ultra-pure lump $ZnCl_2$, manufacturer specification:

Fe < 2 ppm, Al < 1 ppm, Si < ppm.

Pb, Cu, below the detection level.

(2) Zinc powder

(A) Matheson Coleman & Bell Manufacturing Chemists.

30 mesh Zn. A.C.S.

maximum limits given for impurities: Fe 100 ppm

Pb 100 pm

As 0.1 ppm

(B) Alfa Division, Ventron Corp.

6 nine 200 mesh Zn powder

Pb, Al, Cd, In, Si 0.1 ppm each.

Fe, Cu, Mg, Ag < 0.1 ppm each.

(3) Hydrochloric acid

J. T. Baker Chemical, Analytical Concentrate

Dilut-It (1N HCl).

(4) Lead acetate

J. T. Baker Chemical, Analyzed Reagent

granular $Pb(CH_3COO)_2.3H_2O$, actual analysis by the manufacturer:

Fe 1 ppm, Cu ppm.

Electrodes

(1) Cathode

Cathodes and some attachments are shown in Figure 3.1.

(A) Large area electrodes (1.65 cm^2)

A platinum disk 1.45cm in diameter was attached to a brass core using silver-epoxy adhesive. The brass core was tapped on one end to screw onto the spindle shaft of the rotating disk assembly. Around this brass core with a platinum disk, epoxy-resin was cast and then oven-cured. Finally it was machined down to produce the cylindrical shape, with an outer diameter of 3.5 cm.

(B) Small area electrodes (1.27 cm^2)

Special electrodes were made for scanning Auger microprobe analysis. A 1/4-20 stainless steel set screw was welded perpendicularly onto a 1/2" diameter stainless steel disk. A platinum disk, 1.27 cm diameter small enough to fit into the specimen holder of the Auger chamber, was silver-soldered onto the other side of this stainless steel disk. It was coated with Kynar (Vinylidene fluoride resin, Pennwalt Corp.) not only to provide corrosion protection and electric insulation during

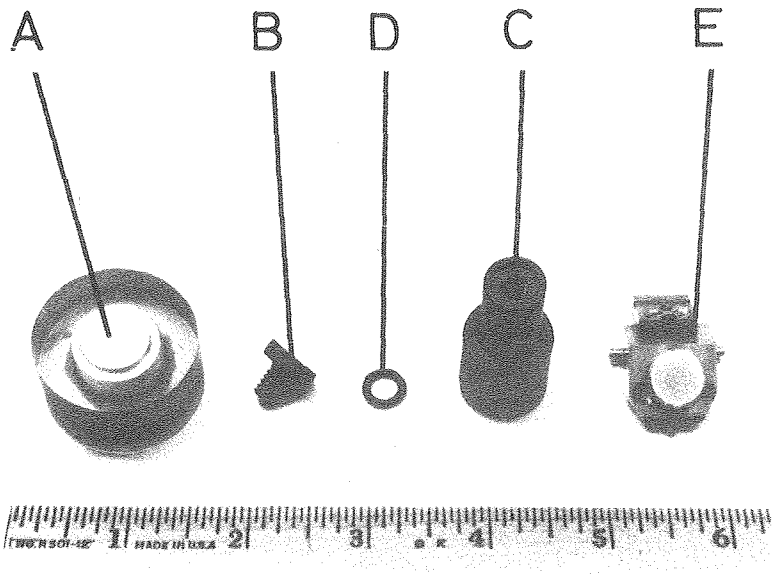

XBB 816-5235 B

Figure 3.1 Cathodes and Attachments

The scale is in inches.

A. The larger RDE
B. The smaller RDE
C. An adaptor for the smaller RDE
D. An O-ring for the adaptor
E. The smaller RDE mounted on a specimen holder for Scanning Auger Microprobe analysis.

electrolysis but also to ensure high vacuum suitable for examination in the scanning Auger microprobe study.

(2) Anode

A large 99.99% zinc disk, 7.5 cm in diameter, had been used in the earlier investigations by Jaksić and Komnenić. The content of lead impurity in these may be roughly estimated to have been in the range of 5 - 30 ppm for electrolytic-refined 4 nine zinc; an actual analysis, however, was not obtained. In this investigation, either,

(A) A pure platinum sheet was used to eliminate contamination of the zinc deposits, or instead,

(B) A 99.9999% zinc wire, 1 mm diameter, (Alpha Division, Ventron Corp.) was used in conjunction with ultra-pure solutions so as to avoid the potential influence of dissolved chlorine or oxygen.

(3) Electrolysis cell

The electrochemical cells were made from borosilicate glass beakers as shown in Figure 3.2. Approximately 0.85 litre of solution was contained in each cell. Previous investigators, Jaksić and Komnenić, had used the one-compartment cell with a 4 nine zinc circular anode located at the bottom of the cell. A two-compartment cell was employed in this investigation to minimize contamination from the anode. The catholyte was separated from the anolyte by a borosilicate fritted glass disk. An acrylate lid covered the top of the cell to prevent spillage and dust-contamination from open air. The rotating disk electrode entered the cell through a hole in the center of the top-lid.

Plastic and glass ware was washed with detergent, rinsed first with copious amounts of hot tap water, and then with distilled water.

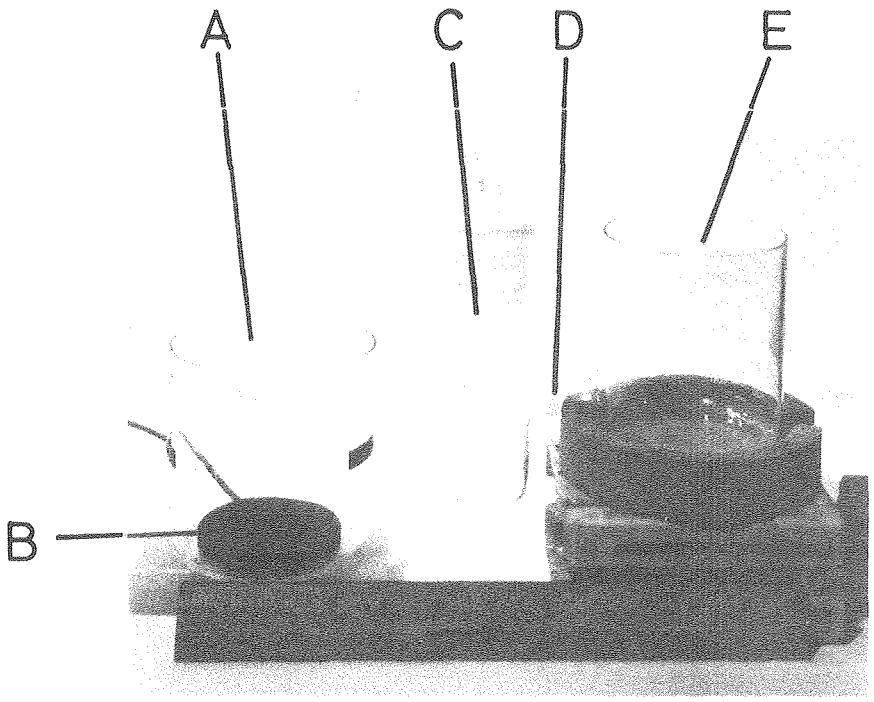

XBB 816-5238 B

Figure 3.2 Electrolysis Cells

The scale shown is in inches.

A. One compartment cell
B. 99.99% zinc anode
C. Anode compartment
D. Anolyte-catholyte separator
E. Cathode compartment

Afterwards, it was soaked in a cleaning solution, consisting of concentrated HCl, H_2SO_4 and H_2O_2, for 24 hours to leach out trace impurities adsorbed on the surface. Finally it was thoroughly rinsed with distilled water.

Apparatus setup

The complete apparatus is shown in Figure 3.3 - 3.4.

(1) Electrical setup

All experiments were conducted in galvanostatic operation using PAR Model 371 Potentiostat-Galvanostat with a Model 178 Electrometer probe. Electronic Measurements Model C618 Constant Current Power Supply was also employed when the current exceeded 165 mA because of insufficient voltage capacity of the PAR Model 371. A PAR Model 175 Universal Programmer controlled the galvanostat in case of pulsed current experiments. Cell current was measured by a Keithley 173A or 179TRMS Digital Multimeter. Deposition time was measured by a Casio F-300 digital watch.

(2) Rotating disk assembly

The disk was attached to a spindle via a screw fitting and a flat annular interface. The spindle and disk were driven by a variable speed motor (Servo-Tek Products, Model STE-231T-1C) with a controller (Servo-Tek Products, Type ST-556 Control Head). At high rotation speed, vibration tended to occur with this assembly, for this reason subsequently a Pine Instrument, Analytical Rotator Model ASRP2 was also used. The latter provided a stable rotation from 100 rpm to 10,000 rpm with very little vibration.

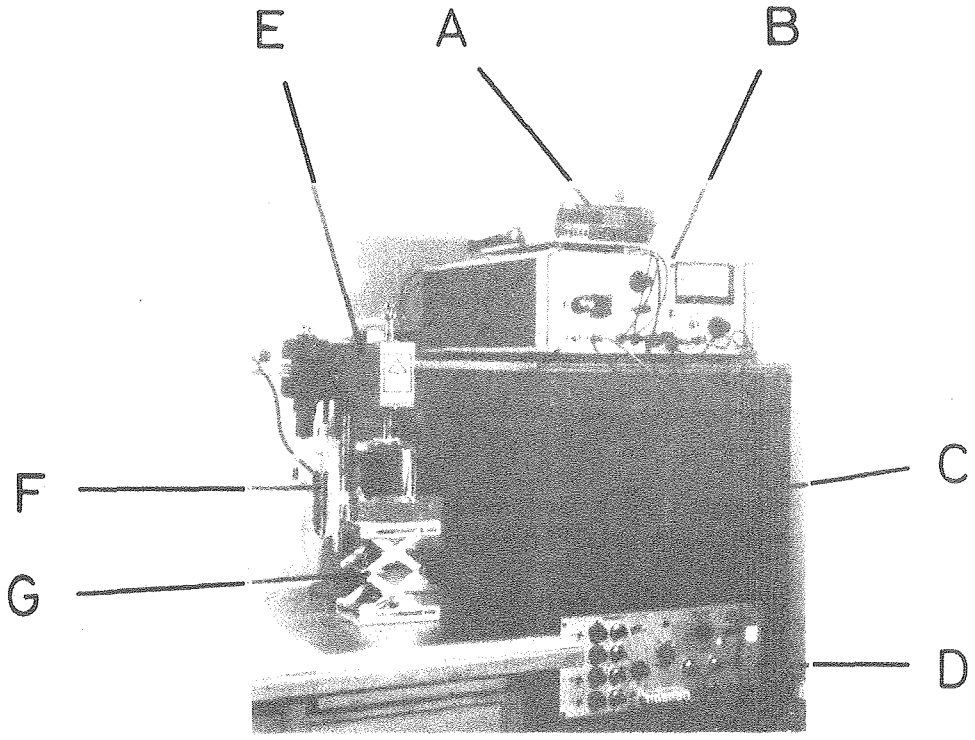

XBB 816-5237B

Figure 3.3 Overall View of the Experimental Apparatus

A. Digital Multimeter , Keithley 173A
B. Potentiostat-Galvanostat , PAR Model 371
C. Electrometer Probe , PAR Model 178
D. Universal Programmer , PAR Model 175
E. Analytical Rotator , Pine Instrument ASRI2
F. Two compartment Cell
G. Scissors-type Jack Positioner

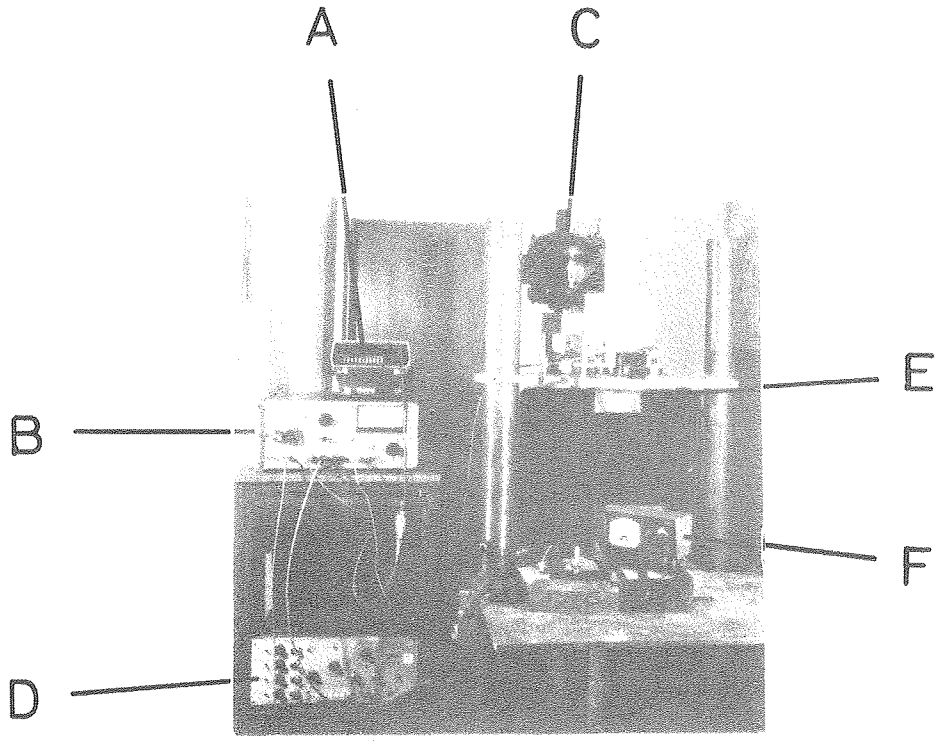

XBB 813-2169C

Figure 3.4 Rotating Disc Assembly and associated Equipment

A. Digital Multimeter , Keithley 179TRMS
B. Potentiostat-Galvanostst , PAR Model 371
C. Variable speed motor , Servo-Tek STE-231T
D. Universal Programmer , PAR Model 175
E. Bearing case with Spindle inside
F. Speed controller , Servo-Tek ST-556

3-2. Procedure

Electrolyte Preparation

(1) Purification by zinc cementation

A stock solution of zinc chloride was prepared using analytical grade chemical and distilled water. An electrolyte concentration of 1M was used in each experiment. 1M zinc chloride solution was purified adding 10 g/l zinc particles (30 mesh Reagent Zn) with vigorous stirring after heating to about 90°C. The mixture, stirred for 24 hours under ambient atmosphere, was kept above 60°C for at least an hour. It was then filtered through a glass microfibre paper (Whatman GF/A, retention 1.6 μm) to remove excess zinc particles and zinc hydroxide precipitate. The filtrate was cooled and set still for 24 hours to settle down any residual fine precipitate, which was then removed by further filtration. A.R. grade 1N HCl was then added to the electrolyte to give pH of about 2.

The solutions were analyzed before and after the zinc cementation treatment by a Perkin Elmer Model 360 flame atomic absorption spectrophotometer. Results are given in Table 3.1. The sensitivity of this analyser, however, was not sufficient to determine the actual content of trace lead impurity below 1 mg/l. Previous study on zinc cementation had shown that the lead content could be reduced below 0.1 mg/l, in fact probably to about 0.05 mg/l as indicated in Appendix A.

The procedure for the preparation of "ultra-pure" solution was essentially identical with that of the A.R. (Analytical Reagent) grade solution, except that the starting chemical was an ultra-pure $ZnCl_2$ and 6 nine (99.99%) 200 mesh Zn powder was used.

TABLE 3.1 Analysis of Electrolyte before and after Zinc Cementation (mg/l)

	1M $ZnCl_2$ A.R. grade	After zinc cementation
Fe	< 0.1	< 0.1
Pb	< 1	< 1
Cd	0.27	< 0.1
Cu	0.55	< 0.01
Co	0.17	0.18
Ni	0.17	0.18
Mn	0.1	0.1

Although Cu was successfully reduced, Co & Ni were difficult to remove, presumably due to the formation of localized solid solution layer at active sites on a zinc particle which retarded further cementation reaction. Pb was below the detection level.

(2) Addition of metallic impurities

Zinc electrolytes were also prepared by addition of either carefully weight metallic compounds or dissolved metals to zinc-powder treated 1M zinc chloride solution. In particular, lead was added to the electrolyte as lead acetate.

Surface Preparation of Cathode

Electrodes were mechanically polished to mirror bright finish on a canvas covered polishing wheel coated with 1 micron diamond paste, after the deposited zinc on the platinum was removed by concentrated HCl. Kerosene was used as a lubricant. The greasy surface was gently rubbed by a cotton-tipped applicator with soap, and then washed thoroughly with running hot water. The surface was again cleaned by the applicator with excess aceton, followed by rinsing with ethyl alcohol, and then dried in an air stream. Just prior to deposition, electrolytic cleaning was applied anodically, oxygen being evolved on the platinum surface, in a solution consisting of 1M KOH and 0.5M K_2HPO_4 for 30 minutes at 300 mA/cm^2. The electrode was then washed with distilled water and immediately submerged in the cell.

Electrolysis

Zinc was electrodeposited galvanostatically onto a rotating disk of platinum at room temperature (20 - 25°C) in a cell open to air. Experiments were carried out at current densities of 10,30,60,90 and 120 mA/cm^2 and rotation speeds of 400,800 and 1,200 rpm.

Five different electrolytes, namely ultra-pure solution, purified AR grade solution, AR grade solution, and purified AR grade solutions containing 1 mg/l i.e., (4.8×10^{-6}M) Pb or 10 mg/l i.e., (4.8×10^{-5}M)

Pb, were used to study the effect of lead codeposition on the formation of spiral patterns.

Pulse parameters used in the case of pulsed current electrodeposition are tabulated below.

pulse parameters			high frequency	low frequency
Peak current density	i_p	(mA/cm^2)	100	100
Average current density	i	(mA/cm^2)	10	10
On - time	T		1ms	1s
Off - time	T'		9ms	9s

The deposition process was interrupted periodically for observations by optical microscopy and photomacrography. During observations, the electrode surfaces were kept wet by the film of distilled water so that the surface did not change significantly in the interval between removal from the cell and observation in the microscope. The macromorphological development of zinc deposit with time was followed by this "interrupted deposition" method.

However, this technique was not applicable to specimens prepared for instrumental surface analysis, such as scanning electron microscopy, electron probe microanalysis and scanning Auger microprobe analysis. For these the deposit was dried before being introduced in the vacuum chamber, hence zinc oxide layer was formed on the deposit. For studying

the effect of deposition time on the character of the deposit for each length of time, a separate electrode was plated with zinc.

Examination of Deposits

The deposits were examined by a selection of the following techniques.

(1) Photomacrography

The evolution of surface topography during interrupted electrodeposition was photographed at x 3-5 using the Polaroid MP-3 Industrial View Land Camera with Polaroid Type 55 P/N 4x5 Land Film. Care was taken not to dry the deposit by adjusting the intensity of light and minimizing the time during which it was exposed to light.

(2) Optical microscopy

A stereo zoom microscope (Bausch & Lomb RBV-1070P, magnification 1-7 X) was occasionally used for a quick examination of spiral patterns prior to photomacrography.

(3) Scanning electron microscopy (SEM)

Certain of the deposits were examined by an AMR Model 1000 scanning electron microscope to determine their surface morphology in detail at higher magnification (20 - 8,000 X). Backscattered electron images were taken for selected specimens to attain higher topographic contrasts.

(4) Electron probe microanalysis (EPMA)

Elemental X-ray images of the deposit surface were obtained by AMR Model 1000 SEM with an attached Kevex X-ray Analyzer Model 7077.

(5) Scanning Auger microprobe analysis (SAM)

Selected specimens were examined by Auger spectrum analysis and

Auger elemental image mapping utilizing Physical Electronics 590A scanning Auger microprobe analyser.

4. RESULTS

4-1. Effect of Electrolyte Purification

An induction time was observed before visible spiral patterns appear on the deposit. We introduce the definition: "Spiral Formation Time" to denote the induction time necessary for spiral patterns to become discernable under suitable magnification (3 - 5X for photomacrography, and 20 - 100X for SEM, Cf. Table 4.2). Spiral Formation Time was affected by zinc cementation treatment and the anode employed. The results obtained from galvanostatic deposition at 30 mA/cm^2 and 800 rpm, are summarized in Table 4.1. Onset of spiral formation was examined by photomacrographs of the deposits during interrupted electrodeposition. Due to chemical corrosion of the anode, the pH rose sharply during electrolysis for pH 2 solutions using 4 nine zinc anode.

When "preliminary purification" by zinc cementation was carried out at room temperature for 2 hours, the spiral formation time was significantly increased. Addition of trace amounts of lead to this purified electrolyte reduced the spiral formation time close to that of A.R. grade zinc chloride solution. The four nine zinc anode is suspected as a possible additional source of contaminants. The number density and the shape (angle) of spirals did not vary significantly with the purity of the solutions. However, it was rather difficult to make a quantitative judgment; as shown in Figure 4.1, unlike in deposits obtained from solutions with added lead ions, the profiles of ridges and valleys on the deposit were not sharply delineated in the deposit obtained from this purified solution.

Afterwards, reaction temperature was raised and agitation duration was prolonged in order to ensure complete cementation: the solution was stirred with addition of 10 g/l zinc particles (30 mesh reagent grade Zn) for 24 hours, and was kept above $60^{o}C$ for the first hour. In further experiments the temperature during cementation was raised, and time during which the suspension was agitated was extended. Formation time of spirals obtained from this standard "purified A.R. grade solution" was 10 - 20 minutes at 30 mA/cm^2 and 800 rpm. As is seen in Figure 4.2 the deposit obtained from standard "purified A.R. grade solution" rather resembles the deposit from "ultra-pure" solution, but it strongly differs in appearance from a deposit obtained from a "preliminary purified solution". The bare platinum surface was partially exposed in the case of former two deposits. This indicates the possibility of insufficient removal of lead when agitation period is brief and the temperature is low.

TABLE 4.1 Effect of Electrolyte Purification on Spiral Formation Times

All experiments were carried out at 30 mA/cm^2 and 800 rpm in 1M zinc chloride solution.

	Electrolytes	Anode	Run	Time (min.)
1.	A.R. grade	4 nine Zn[(a)]	1st	10 - 20
	A.R. grade	4 nine Zn	2nd	5 - 10
2.	After	4 nine Zn	1st	30 - 45
	"Preliminary"	4 nine Zn	2nd	0 - 10
	Purification	Platinum	1st	30 - 45
		Platinum	2nd	30 - 45
3.	Addition of			
	5.8×10^{-6} M Pb	4 nine Zn	1st	0 - 10
	4.8×10^{-5} M Pb	4 nine Zn	1st	0 - 10
4.	After "Standard" Purification	Platinum	1st	10 - 20
5.	Ultra-pure	Platinum	1st	10 - 20

(a) 4 nine Zn = 99.99% Zn

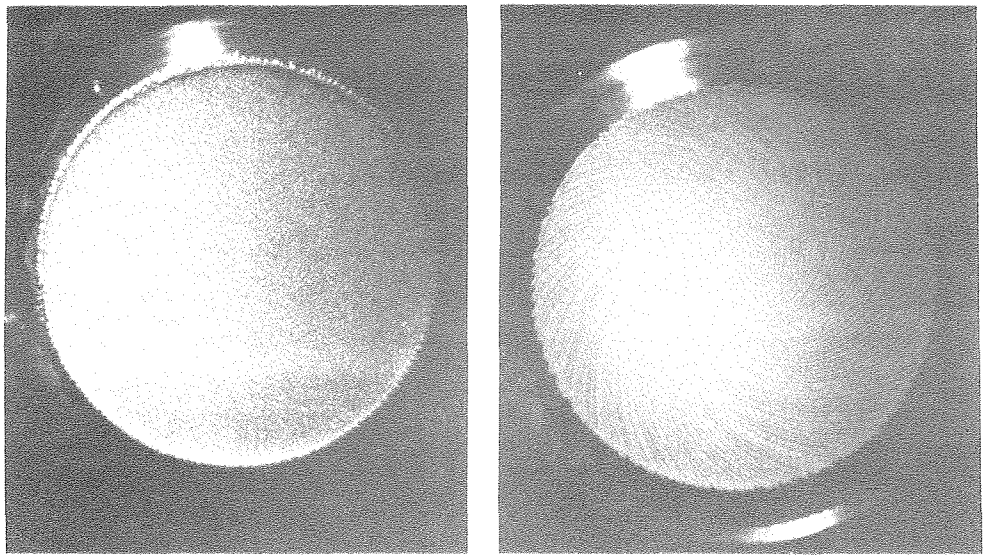

(a) (b)

XBB 817-5960A

Figure 4.1 Spiral Patterns obtained from,

(a) Purified solution.
30 mA/cm^2 x 105 min., 800 rpm, Pt anode

(b) Lead containing solution (4.8 x 10^{-5} M)
30 mA/cm^2 x 30 min., 800 rpm, Pt anode

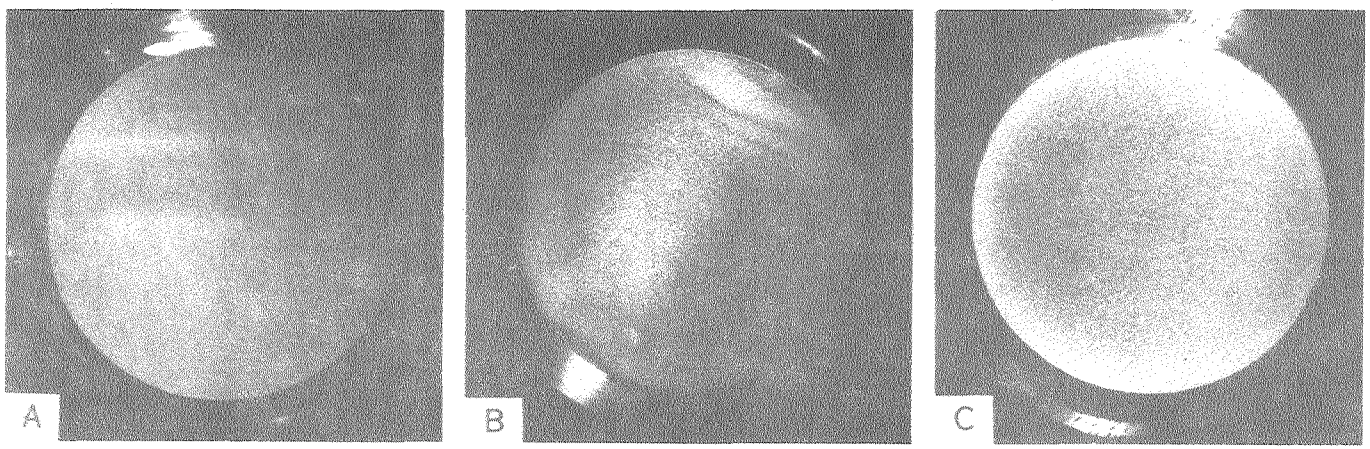

XBB 817-6760 A

Figure 4.2 Influence of the purity of electrolytes on spiral formation.

(A) After preliminary purification.
(B) After standard purification ("purified A. R. grade").
(C) Ultrapure solution.

30 mA/cm^2 X 10 min., 800 rpm.

4-2. Electrolytes Containing Lead Ions

Morphological Observations of Spirals

(1) Influence of current density

Spirals electrodeposited from A.R. grade $ZnCl_2$ solution appear within a specific region of the current density, which was previously reported by Jaksić and Tobias to be 1 - 100 mA/cm^2 (9). This spiral forming region is in fair agreement with that found in the present investigation for solutions containing 4.8×10^{-6} - 4.8×10^{-5} M Pb. The number density of spirals increased with an increase in current density, and above certain critical current density macroscopically smooth deposit was produced, as shown in Figure 4.3.

Komnenić et al. reported (11) that the spiral formation time decreases with increasing current density. This would imply that spirals would become visible when the same number of coulombs passed. The present results confirm that the spiral formation time is almost independent of current density in this region. These observations, however, are subjet to some doubts; since the determination of the formation of spirals is subject to relatively large errors. When zinc was deposited for 30 seconds on the platinum substrate at 120 mA/cm^2 until the surface was completely covered by a smooth deposit, and then deposition was continued at 10 mA/cm^2, the spiral formation time increased. Table 4.2 presents a summary of the spiral formation time, as it depends on current density, rotation speed and lead content of the solution.

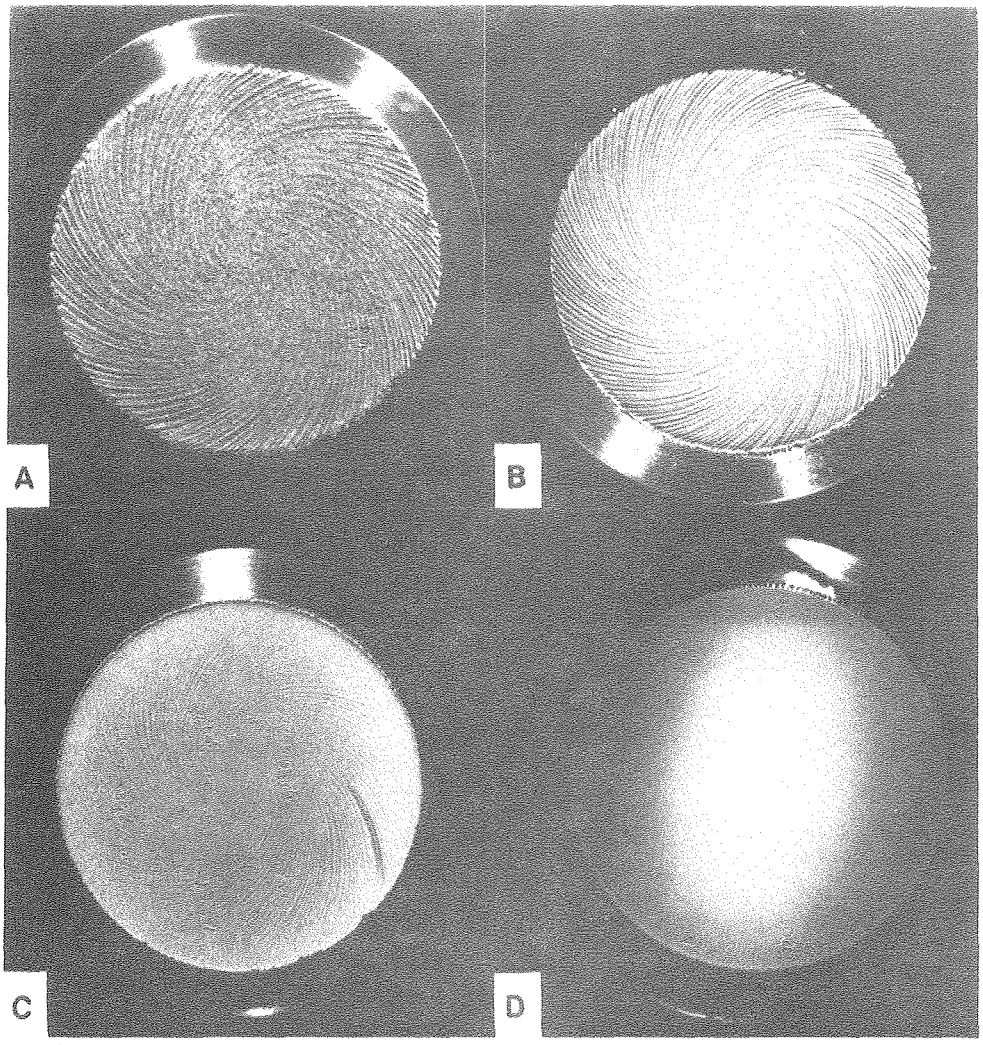

XBB 817-6476 A

Figure 4.3 Effect of current density on the number density of spirals.
(A) 10 mA/cm^2 X 45 min. (B) 30 mA/cm^2 X 20 min.
(C) 60 mA/cm^2 X 10 min. (D) 90 mA/cm^2 X 10 min.

1M zinc chloride with 4.8 X 10^{-5} M Pb, 800 rpm.

The shape of striations was close to a logarithmic spiral, described by $r = a^{\theta}$ or $\theta - \theta o = \ln(r/r_o)/\ln a$, but deviated from an Archimedes spiral described by $r = a\theta$. The shape (angle) of spirals was independent of current density (see Figure 4.43).

(2) Influence of rotational speed

The number density of spirals hardly varied at all with rotation speed. The number of spiral lines was much larger near the periphery than in the center region of a disk. Typical examples are shown in Figure 4.4. However, in the case of spirals obtained from A.R. grade 1M $ZnSO_4$ solution on a rotating ring electrode, the number density of spirals increased with an increase in rotation speed, as may be seen from Figure B. in Appendix B.

Spiral formation time declined with an increase in rotation speed, as shown in Table 4.2. This result agreed with the previous observations of spirals, by Komnenić et al. (11) obtained from A.R. grade 1M zinc chloride solutions.

Ridges and valleys became sharply delineated as the rotation speed was increased. The higher the rotation speed, the more well-defined spirals were obtained, as shown in Figure 4.5 and 4.6. At the lower rotation speeds, spiral lines consisted of protrusions vaguely connecting each other along spiral patterns.

The shape (angle) of spirals seems to be nearly independent of rotation speed as shown in Table 4.3, however an accurate measurement of characteristic constants (1/ln a) was difficult.

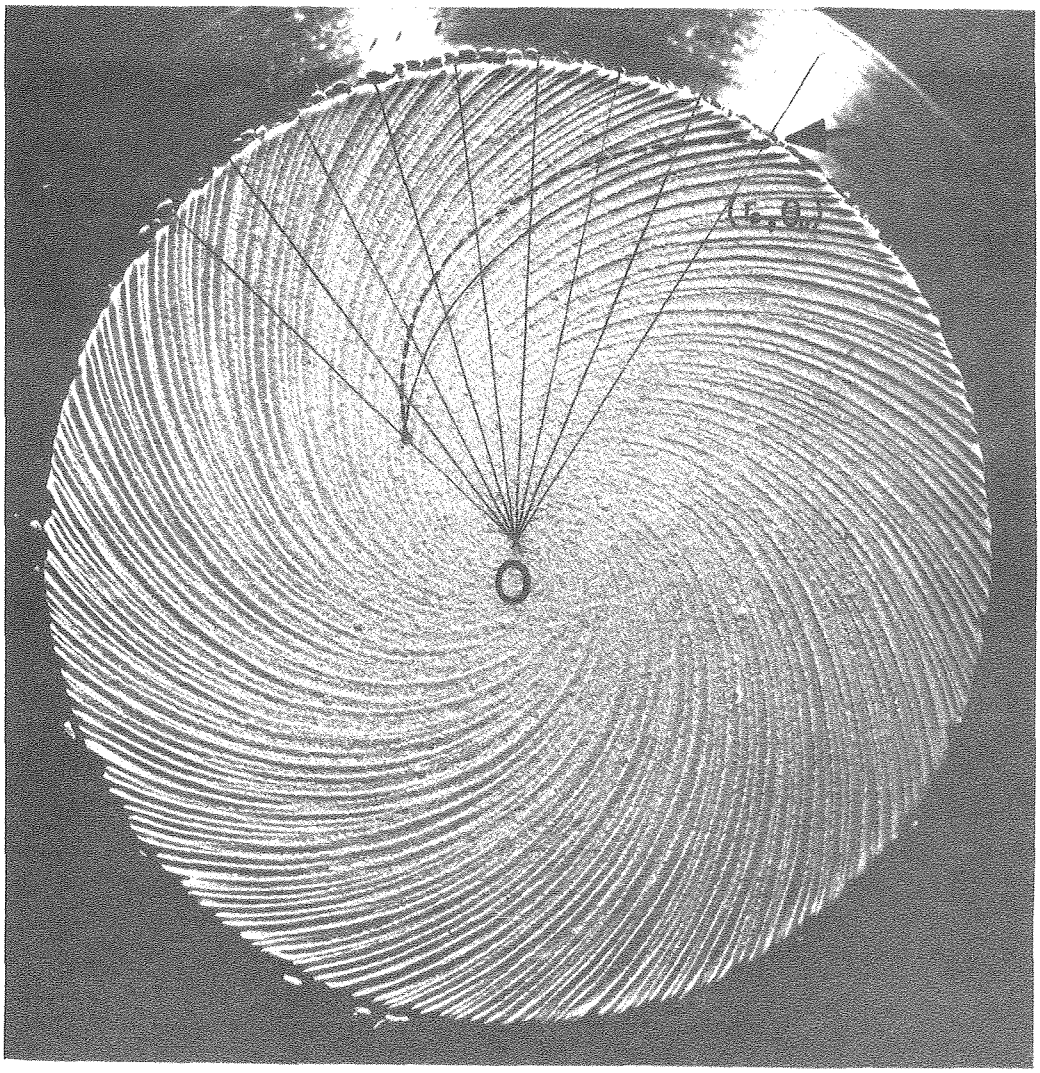

XBB 817-6215A

Figure 4.43 The dotted line is an Archimedes spiral described by, $\theta - \theta_o = .0304 (r - r_o)$. The fine solid curve is a logarithmic spiral described by, $\theta - \theta_o = 1.25 \ln r / r_o$ Note that the Archimedes spiral deviates greatly from the striation.

TABLE 4.2 Spiral Formation Time

lead content ($\times 10^{-6}$ M)	current density (mA/cm^2)	rotation speed (rpm)	Spiral Formation Time (a) min.	(b) min.
4.8	10	800	3 - 6	---
4.8	30	800	6 - 9	5 - 10
48	10	800	0 - 1.5	0 - 5
48	30	400	---	10 - 20
48	30	800	1.5 - 3	5 - 7.5
48	30	1,200	---	0 - 5
48	60	800	1.5 - 3	5 - 10
48	90	800	no spirals	no spirals
48	120	800	no spirals	no spirals
48	120 x 30 sec. --- 10	800	1.5 - 3	---

(a) determined by means of SEM photographs (X 20 - 100)

(b) determined by means of photomacrographs (X 3 - 5)

TABLE 4.3 Effect of rotation speed on shape angle of spiral lines

lead content ($\times 10^{-6}$ M)	current density (mA/cm^2)	rotation speed (rpm)	(a) 1/ln a
48	10	400	1.26
48	10	800	1.21
48	10	1,200	1.29
48	30	800	1.22
4.8	10	800	1.24
ultrapure	30	800	1.21

(a) Each value is the average of three measurements. The amount of scatter in measured values is approximately $\pm$ 0.1.

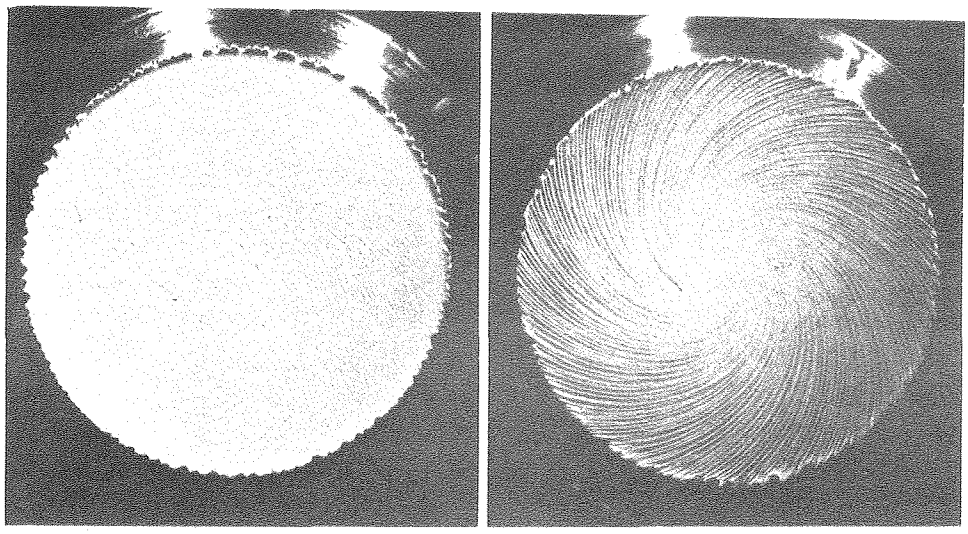

XBB 817-6769A

Figure 4.4 Photomacrographs showing the effect of rotation speed on the formation of spirals.

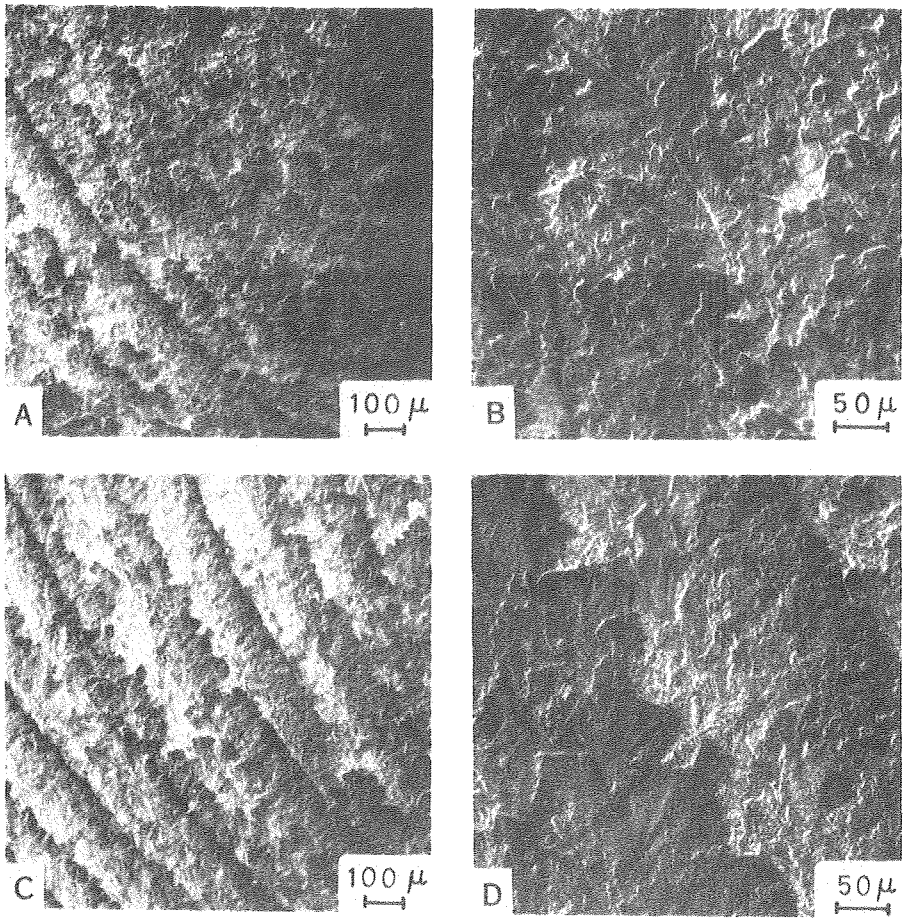

XBB 817-6788 A

Figure 4.5 SEM photographs showing the influence of rotation speed on the morphology of spirals electrodeposited at 10 mA/cm^2.

(A), (B) 400 rpm
(C), (D) 1,200 rpm

1M zinc chloride containing 4.8 X 10^{-5} M Pb.

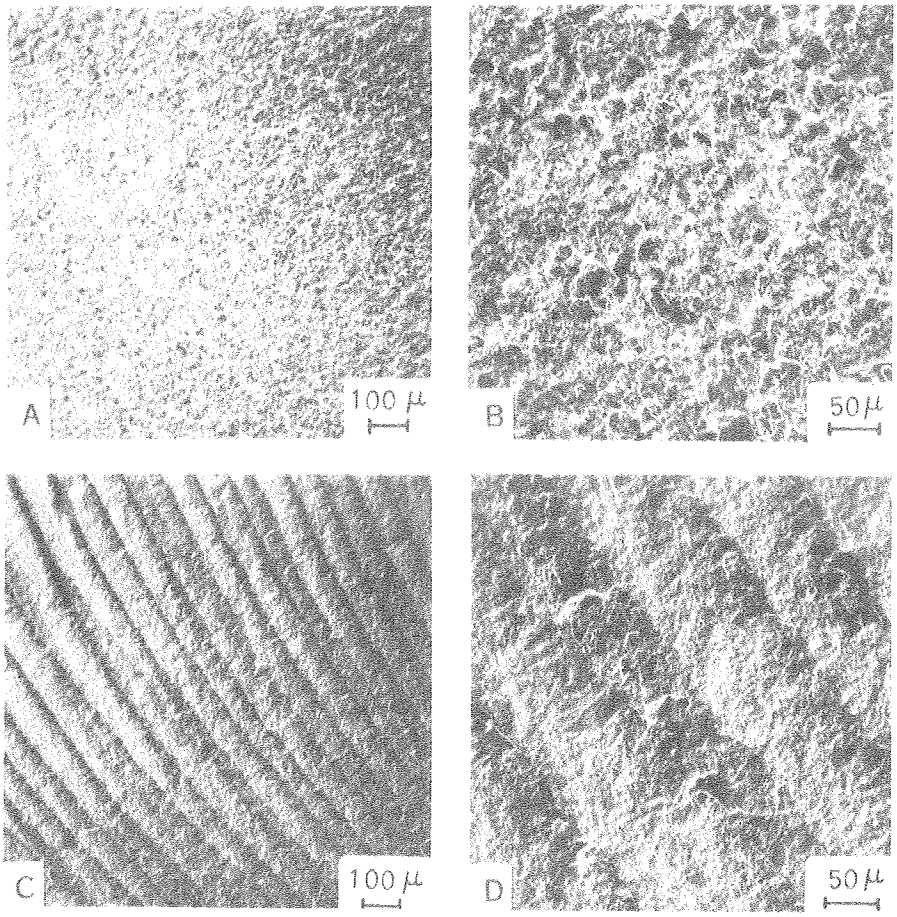

XBB 817-6787 A

Figure 4.6 SEM photographs showing the influence of rotation speed on the morphology of spirals electrodeposited at 30 mA/cm^2.

(A), (B) 200 rpm
(C), (D) 1,200 rpm

1M zinc chloride containing 4.8 X 10^{-5} M Pb

(3) Influence of artificial surface imperfections

Macroscopic depressions were artificially introduced on the surface by pressing a point against the platinum disk. Dimensions of the depressions were 120 - 130 μm by 70 - 80 μm, and the depth was estimated to be about 20 - 30 μm. These depressions are probably large enough to cause separation and reattachment of flow resulting in enhanced eddy mixing along the spiral stream lines.

At 10 mA/cm^2, a well established spiral was generated behind this depression, superimposed on other regular spiral patterns, as is shown in Figure 4.7. The shape (angle) of this spiral was nearly the same as that of other regular spirals. Even at 120 mA/cm^2 above the spiral forming region, a single spiral was formed behind the depression. However, it was very short in length and the ridge of this spiral descended by a gradual slope to the flat smooth surface as shown in Figure 4.7.

(4) Influence of lead content

The number density and the shape (angle) of spirals did not vary with the lead content of the electrolytes. Spiral formation time decreased as lead content increased. The profile of spirals were more delineated with a decrease in lead content. Results are depicted in Figure 4.8, Table 4.2 and Figure 4.9.

(5) Influence of pulsed current

The aim of introducing pulse techniques was to increase the nucleation rate associated with high peak current density.

As a result the spiral formation time and the number density of spiral lines increased for spirals obtained from A.R. grade solution and solution containing 4.8×10^{-6} M Pb, as shown in Table 4.4,

Figure 4.10 and Figure 4.11. Obscured results, however, were obtained from a solution containing 4.8×10^{-5} M lead, as shown in Table 4.4 and Figure 4.12. In addition, the appearance of the deposit was blackish gray, probably indicating higher lead content in the zinc deposit.

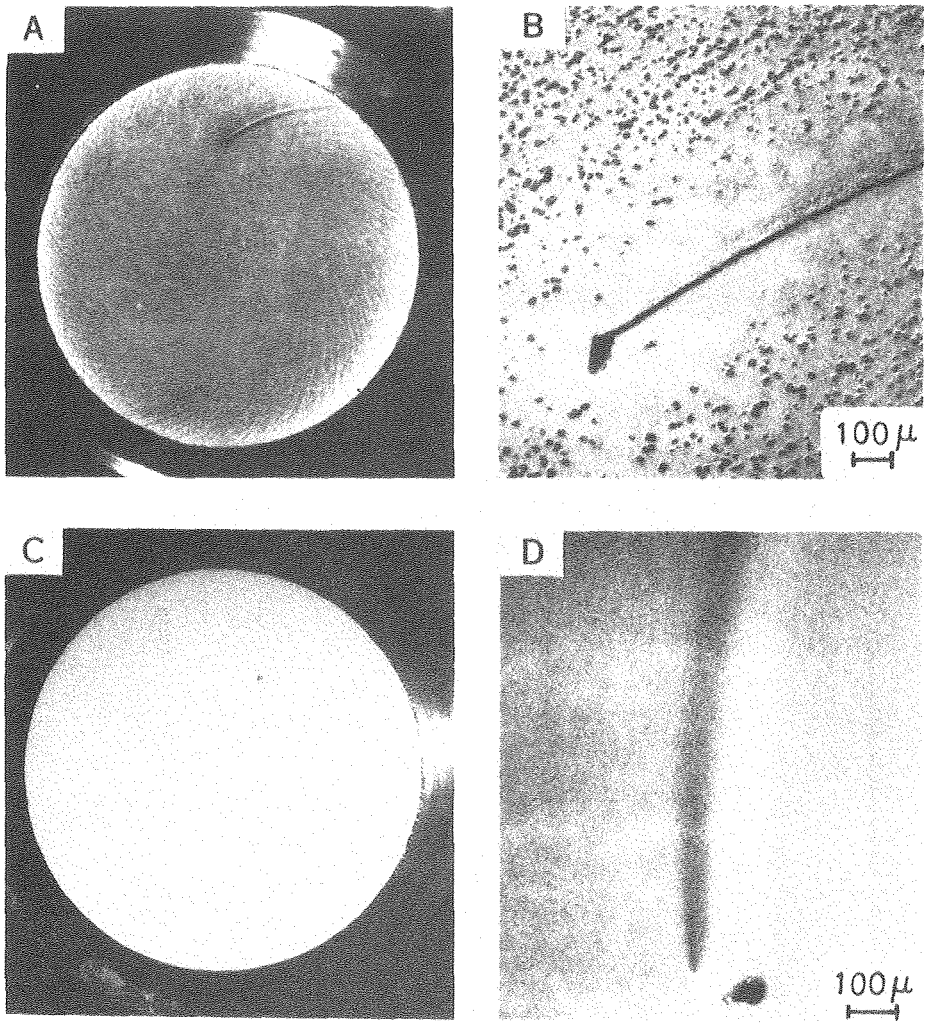

XBB 817 6789A

Figure 4.7 Effect of artificial depressions.

(A),(B) 10 mA/cm^2 X 3 min.
(C),(D) 120 mA/cm^2 X 15 sec.

1M zinc chloride with 4.8 X 10^{-5} M Pb
800 rpm.

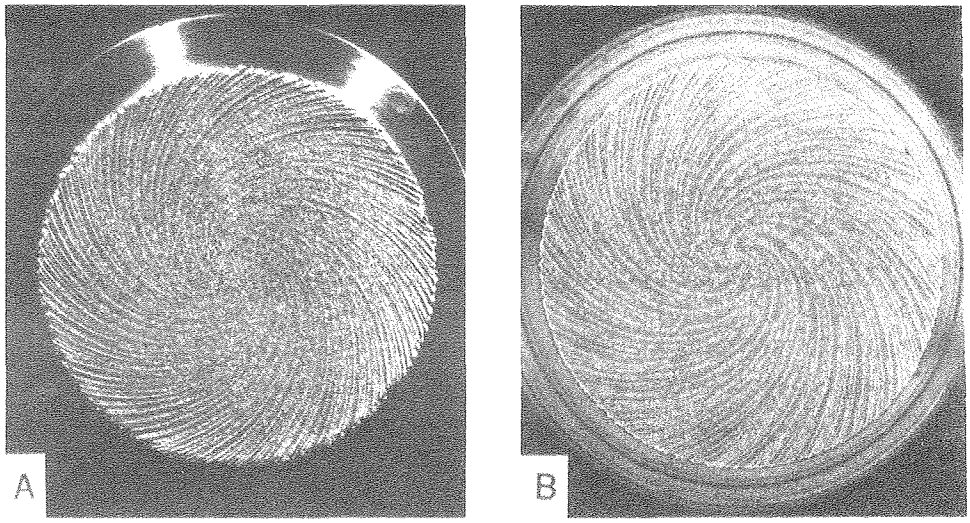

Figure 4.8 Photomacrographs showing the effect of lead content on the formation of spirals.

(A) 4.8 X 10^{-5} M Pb
(B) 4.8 X 10^{-6} M Pb

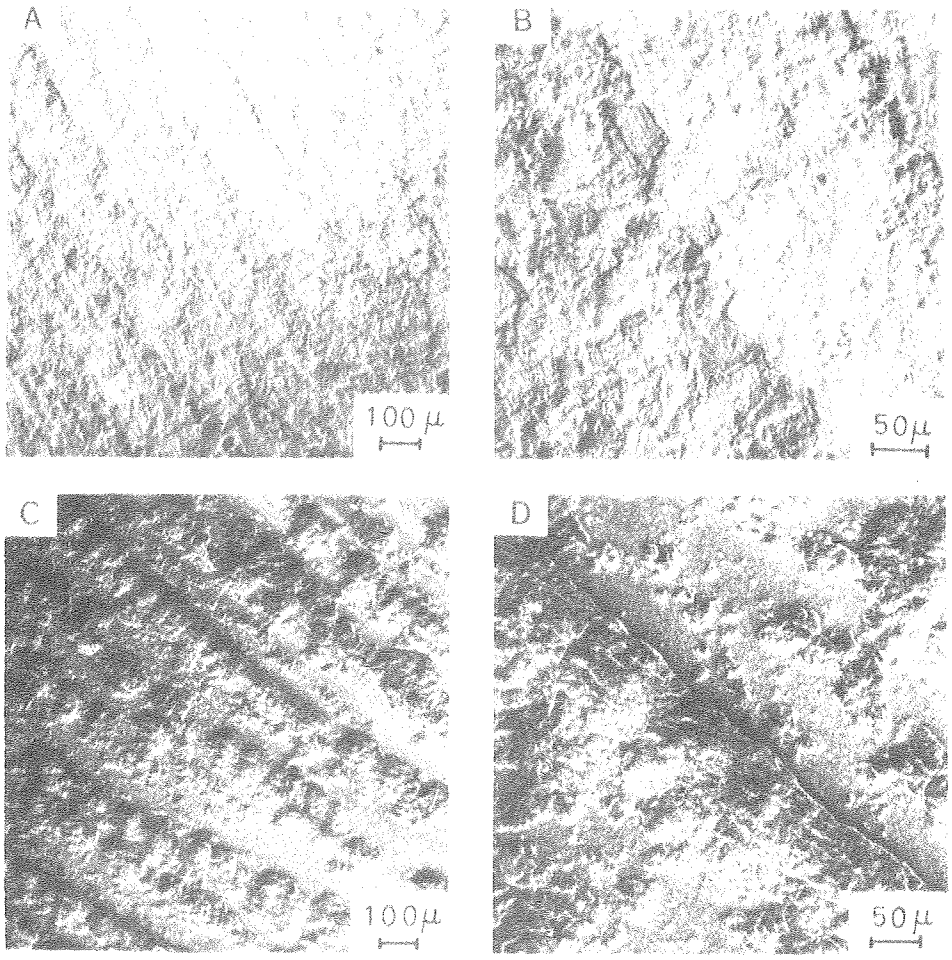

XBB 817-6790 A

Figure 4.9 SEM photographs showing the morphological changes with lead content in zinc chloride electrolyte.

(A),(B) 4.8 X 10^{-5} M Pb
(C),(D) 4.8 X 10^{-6} M Pb

10 mA/cm^2 X 45 min., 800 rpm.

TABLE 4.4 Effect of Pulsed Current on Spiral Formation

	Electrolyte	On-time / Off-time	Formation Time (min.)	Number of Spirals
1.	A.R. grade 1M $ZnCl_2$ solution	T 1ms / T'9ms	20 - 30	highly increased
		T 1s / T'9s	30 - 60	highly increased
2.	Zn-treated 1M $ZnCl_2$ with 4.8×10^{-6} M Pb ion	T 1ms / T'9ms	10 - 20	increased
		T 1s / T'9s	30 - 45	highly increased
3.	Zn-treated 1M $ZnCl_2$ with 4.8×10^{-5} M Pb ion	T 1ms / T'9ms	- 20	decreased
		T 1s / T'9s	- 5	slightly increased

Rotation speed 800 rpm
Average current density 10 mA/cm^2
Peak current density 100 mA/cm^2
Duty cycle $T/(T + T')$ 0.1
T : On-time , T' : Off-time

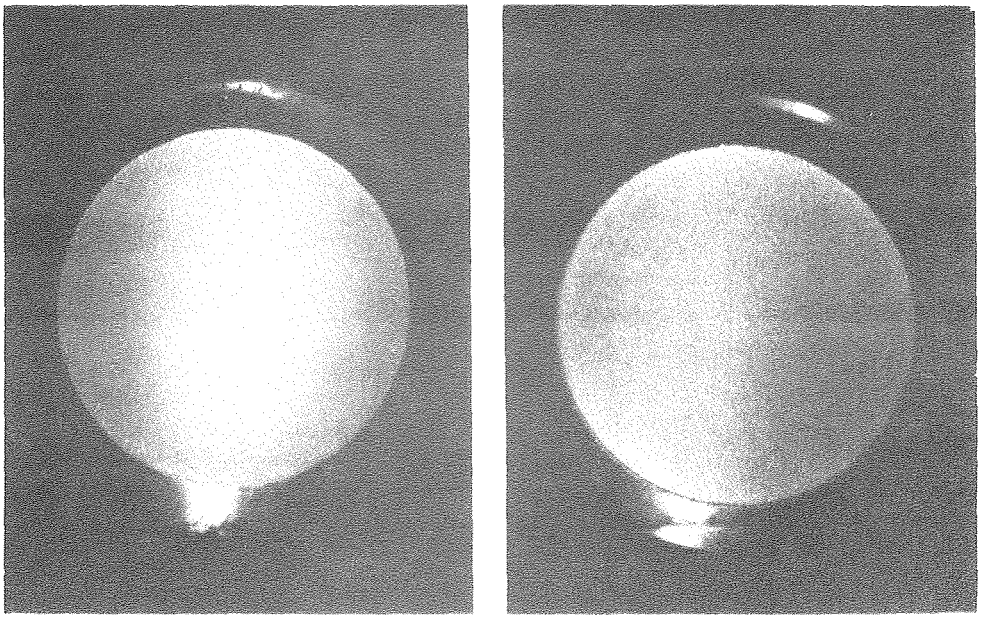

XBB 817-5959A

Figure 4.10 Photomacrographs showing the influence of pulse deposition in A.R. GRADE solution.

i_p = 100 mA/cm^2, 800 rpm.

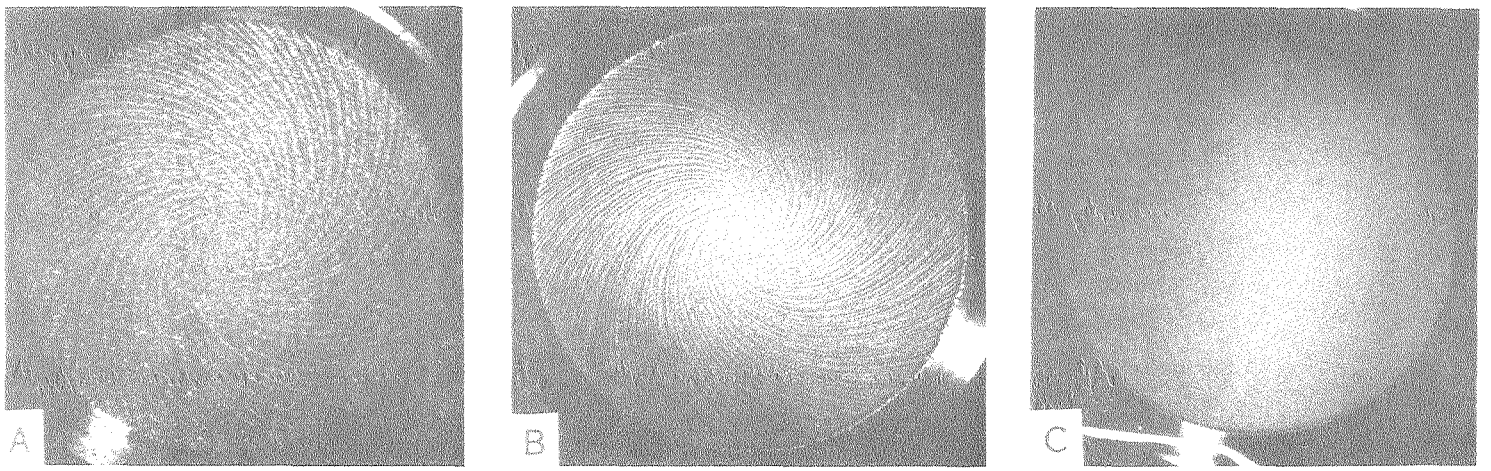

XBB 817-6479 A

Figure 4.11 Effect of pulse deposition in 1M $ZnCl_2$ with 4.8 X 10^{-6} M Pb.
800 rpm, i_p = 100 mA/cm^2, $i_{avg.}$ = 10 mA/cm^2.
(A) d.c. 10 mA/cm^2 (B) T 1ms, T' 9ms (C) T is, T' 9s.

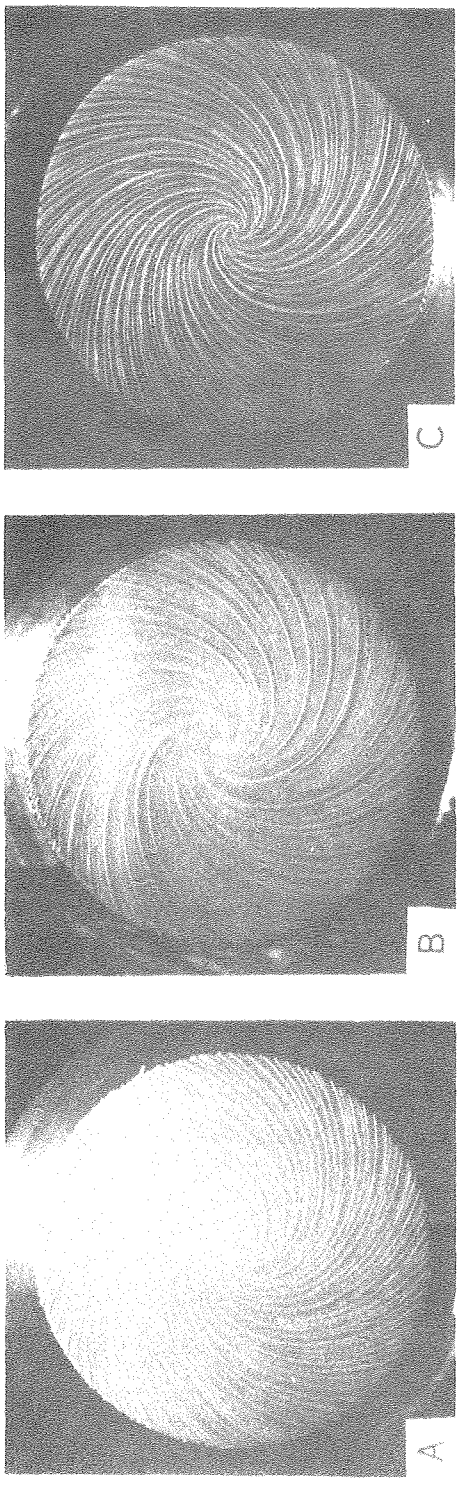

Figure 4.12 Effect of pulse deposition in 1M $ZnCl_2$ with 4.8 X 10^{-5} M Pb.

800 rpm, i_p = 100 mA/cm^2, $i_{avg.}$ = 10 mA/cm^2.

(A) d.c. 10 mA/cm^2 (B) T 1ms, T' 9ms (C) T 1s, T' 9s.

Morphological Observations of Initial Protrusions

(1) Influence of substrate

In general the number density of protrusions varied only slightly according to the orientation of the crystal grain of the polycrystalline substrate. Extreme example is shown in Figure 4.13. Here we believe that during silver-soldering the polycrystalline platinum disk to the stainless steel "sub"-disk it reached a relatively higher temperature than in the case of other platinum disks, and the resulting annealing led to over-grown grains with differential active sites. It is likely that different crystallographic facets of each grain provide different numbers of nucleation sites for zinc crystallization and impurity segregation. Zinc tended to deposit preferentially along the scratch lines created by mechanical polishing.

(2) Influence of current density

As illustrated in Figure 4.14, the number density of protrusions formed at the initial stage of deposition increased with an increase in current density, while the average size of these protrusions was reduced. The number of coulombs passed was in the range of 27 - 54 C per 1.65 cm^2.

(3) Influence of rotation speed

The number density of initial protrusions showed a slight decrease as rotation speed increased from 400 rpm to 1,200 rpm at 10 mA/cm^2. The tendency of protrusions to coalesce became more pronounced as the rotation speed was increased from 400 rpm to 1,200 rpm, at 30 mA/cm^2. This is clearly shown in Figure 4.15.

(4) Influence of lead content

The number density of initial protrusions decreased and their average size increased as the lead content of electrolytes increased as shown in Figure 4.16. The number density and the average size of these protrusions electrodeposited from A.R. grade solution were similar to those obtained from solution containing 4.8×10^{-6} M lead as can be seen in Figure 4.17.

(5) Influence of pulsed current

Pulse electrolysis increased the number density of protrusions and reduced the average size of these protrusions. This tendency became more pronounced as pulse frequency increased for solution containing 4.8×10^{-6} M lead; on the contrary, the opposite result was obtained from solution containing 4.8×10^{-5} M lead as shown in Figure 4.18 and 4.19.

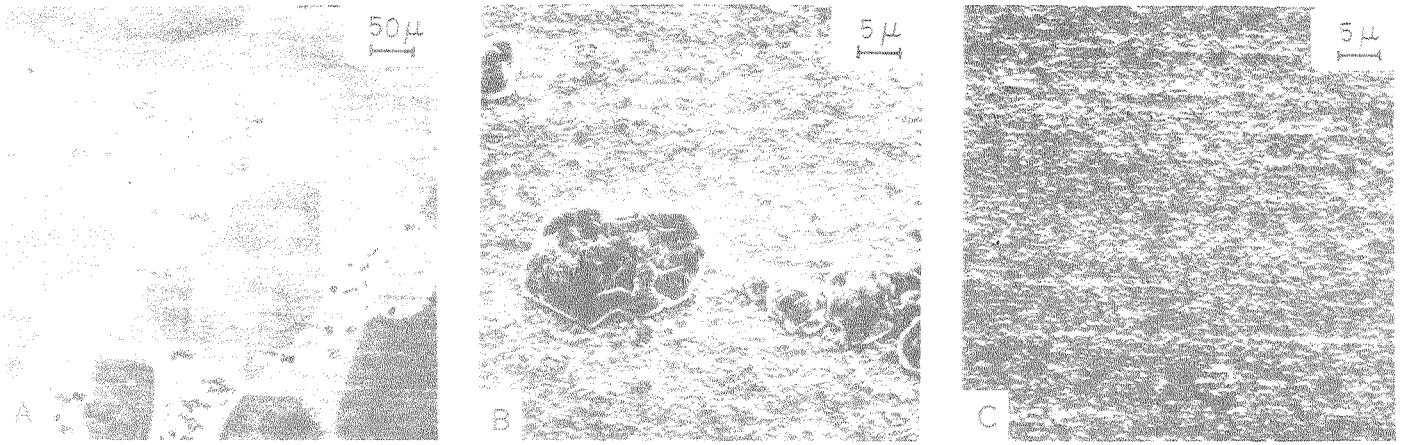

XBB 817-6761 A

Figure 4.13 SEM photographs showing the influence of crystallographic orientation of platinum substrates.

(A) Protrusion formation varies significantly with crystal grain.
(B) Area of the electrode where large protrusions appear.
(C) Area of the electrode without large protrusions.

Smaller disc electrode, 10 mA/cm^2 X 2.5 min., 3,200 rpm, 4.8 X 10^{-6} M Pb.

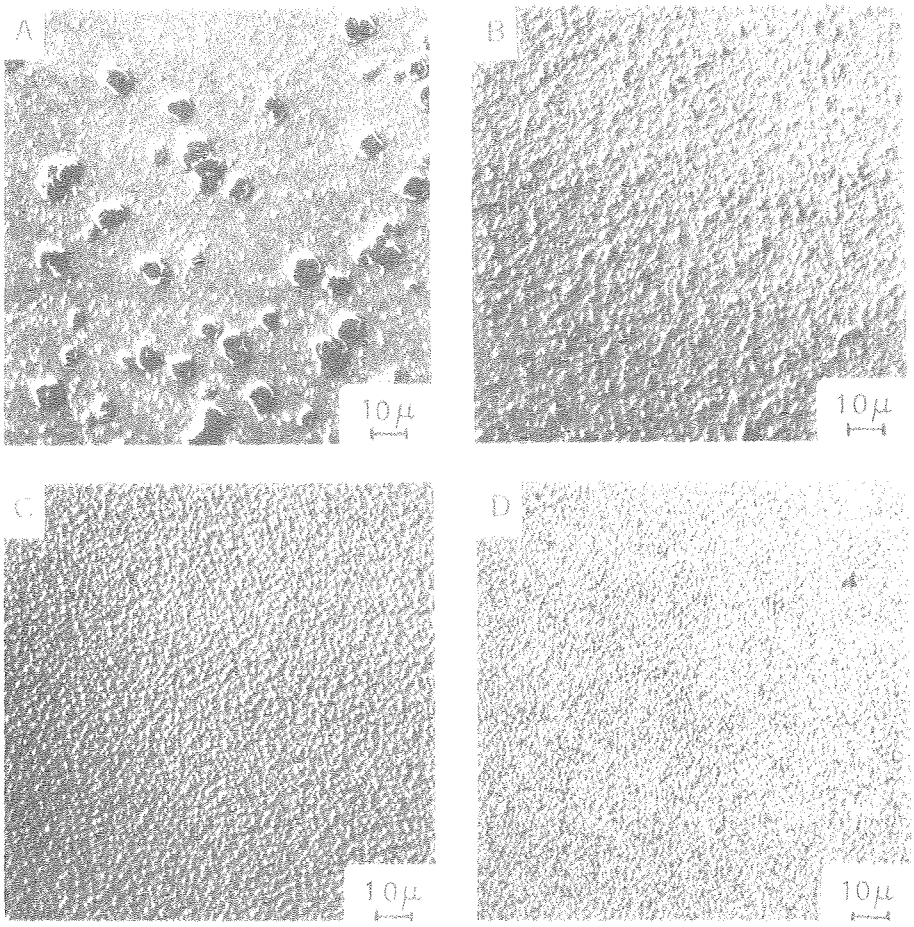

XBB 817-6791A

Figure 4.14 Effect of current density on the numbers and size of initial protrusions.

(A) 10 mA/cm^2 X 1.5 min.
(B) 30 mA/cm^2 X 0.5 min.
(C) 60 mA/cm^2 X 15 sec.
(D) 120 mA/cm^2 X 5 sec.

1M $ZnCl_2$ with 4.8 X 10^{-5} M Pb
800 rpm.

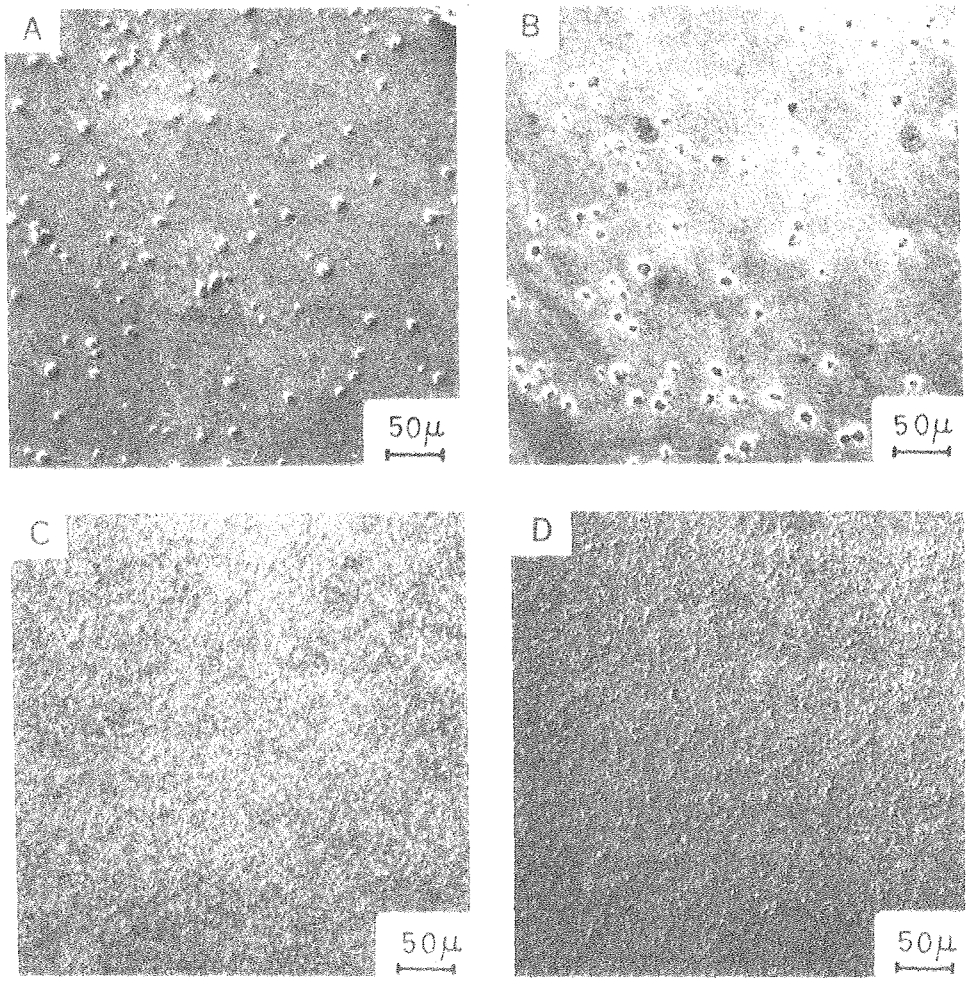

XBB 816-6792 A

Figure 4.15 Effect of rotation speed on the numbers and size of initial protrusions.

(A) 10 mA/cm^2 X 1.5 min., 400 rpm
(B) 10 mA/cm^2 X 1.5 min., 1,200 rpm
(C) 30 mA/cm^2 X 0.5 min., 400 rpm
(D) 30 mA/cm^2 X 0.15 min.,1,200 rpm

1M $ZnCl_2$ with 4.8 X 10^{-5} M Pb

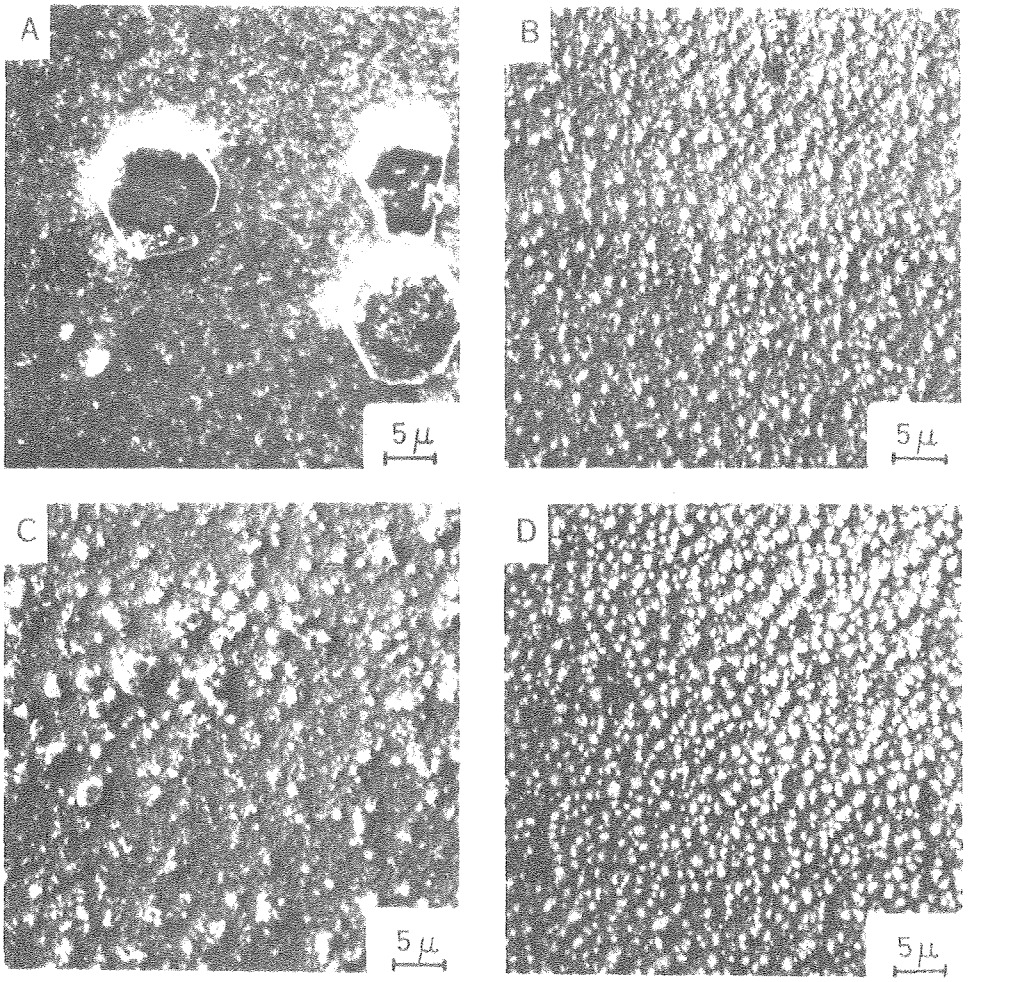

XBB 817-6781 A

Figure 4.16 Effect of lead content on the numbers and size of initial protrusions.

(A) 10 mA/cm^2 X 1.5 min., 4.8 X 10^{-5} M Pb
(B) 10 mA/cm^2 X 1.5 min., 4.8 X 10^{-6} M Pb
(C) 30 mA/cm^2 X 0.5 min., 4.8 X 10^{-5} M Pb
(D) 30 mA/cm^2 X 0.5 min., 4.8 X 10^{-6} M Pb

1M $ZnCl_2$, 1,200 rpm.

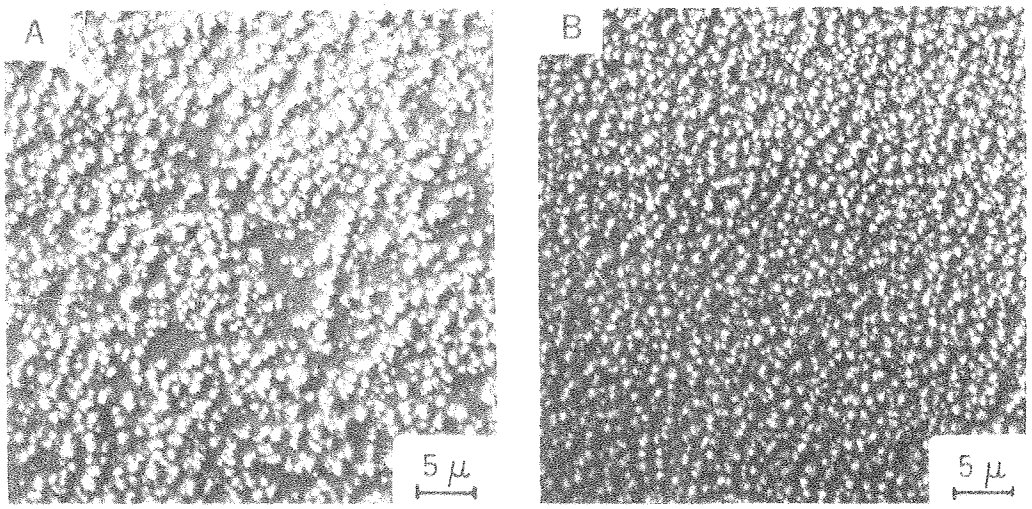

Figure 4.17 SEM photographs showing the initial protrusions obtained from A.R. grade 1M zinc chloride electrolyte.

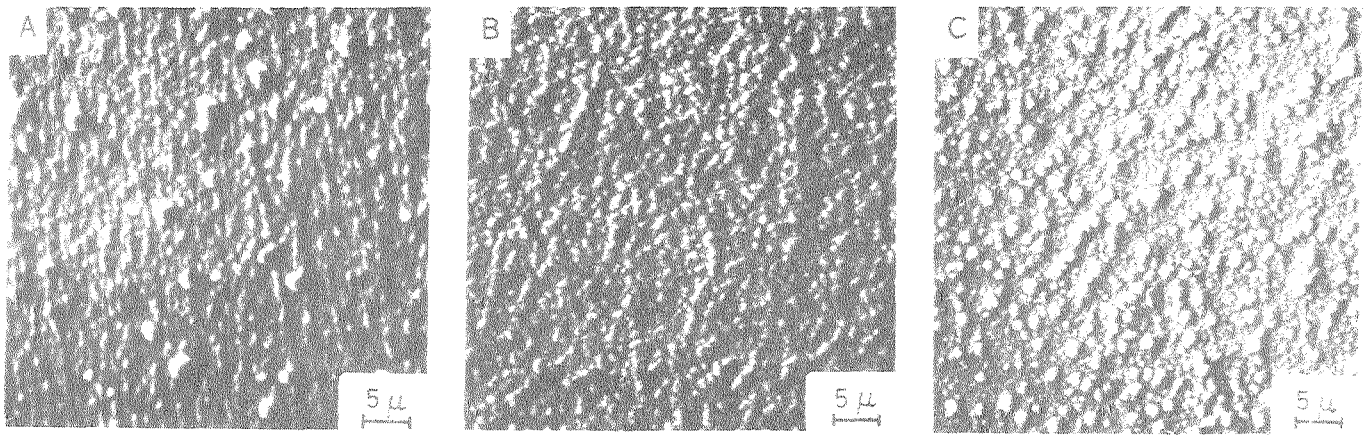

XBB 817-6759 A

Figure 4.18 Effect of pulse deposition on the number and size of initial protrusions obtained from 1M $ZnCl_2$ with 4.8 X 10^{-6} M Pb at 800 rpm.

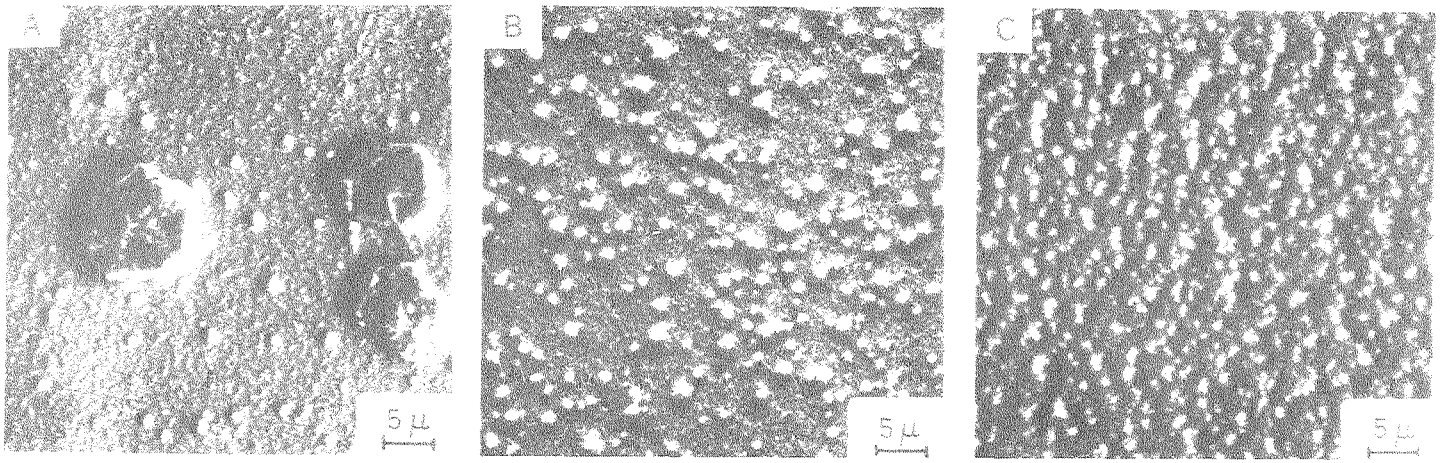

XBB 817-6758 A

Figure 4.19 Effect of puls deposition on the number and size of initial protrusions obtained from 1M $ZnCl_2$ with 4.8 X 10^{-5} M Pb at 800 rpm.

Protrusions Coalescence and Shaping of Spirals

Scanning electron micrographs of protrusions taken after different deposition times clearly show that numerous minute nuclei formed at the very beginning of deposition tended to coalesce with their closest neighbors into larger protrusion (i.e., Clusters of grown nuclei which were defined as "initial protrusions") as crystal growth proceeded, and these larger protrusions continued to grow preferentially coalescing with protrusions comparable in size or consuming smaller protrusions. It appears that connection of these protrusions along spiral trajectories does not occur until these protrusions reach a "critical" height. Eventually this bridging between protrusions gave rise to the formation of spiral ridges.

(1) Preferential growth and coalescence of protrusions

The degree to which coalescence of protrusions and their selective growth occurred, was dependent on current density and lead content of electrolytes; as is evident from Figure 4.20, 4.21, 4.22 and 4.23, this tendency was greatly marked by decreasing current density and/or increasing lead content in the electrolyte.

The number density of initial protrusions was much higher at low lead concentration than from high lead concentration; coalescence of protrusions, however, occurred as deposition proceeded, originating distributed roughness elements comparable in number to those generated from high lead content solution.

At 120 mA/cm^2, above the spiral forming region, coalescence of protrusions occurred only at the very beginning of deposition (i.e., 0 - 10 sec. deposition time), subsequent growth of protrusions occurred

evenly, instead of preferential growth of the larger ones (see Figures 4.24 and 4.25). The reason that surface roughening doesn't develop in this current density regime may be attributed to the high nucleation rate associated with high current densities.

In order to investigate the influence of the substrate on the coalescence of protrusions, zinc was deposited in 1M $ZnCl_2$ solution containing 4.8×10^{-5} M lead on a platinum surface, first at 120 mA/cm^2 for 30 sec. Electrolysis was cotinued at only 10 mA/cm^2 on this smooth surface. The spiral formation time was slightly prolonged. Figure 4.26 shows basically similar trends of coalescence of protrusions regardless of substrate.

(2) Connection of protrusions and formation of spirals

Figures 4.27 through 4.32 are scanning electron microscope views of the sequential development of the deposit morphology. The direction of flow is from bottom right towards top left in each photograph. Once surface roughness evolved to a certain degree, crystal growth of these protrusions was preferred upstream and more preferentially downstream behind each protrusion. It is likely that if the protrusions are sufficiently close to each other along the spiral trajectory, connection of protrusions occurs and initiates the formation of spiral ridges.

The number density of protrusions prior to the onset of connection of protrusions increased with current density.

Lateral growth of protrusions was favored as the lead content in the electrolyte was increased. Figure 4.32 well illustrates the layer growth characteristic of these protrusions.

(D) Surface analysis of spirals

The concentration of codeposited lead on a zinc deposited disk exhibits periodic spiral patterns as shown in Figure 4.33. All elements X-ray map showed uniformly distributed dots; this confirms that the periodic spiral patterns of the lead map were not caused by topographical shadowing effects.

As shown in Figure 4.34, lead map resulting from Auger spectroscopy clearly shows that lead was depleted near ridges and valleys, while it was rich on intermediate slopes.

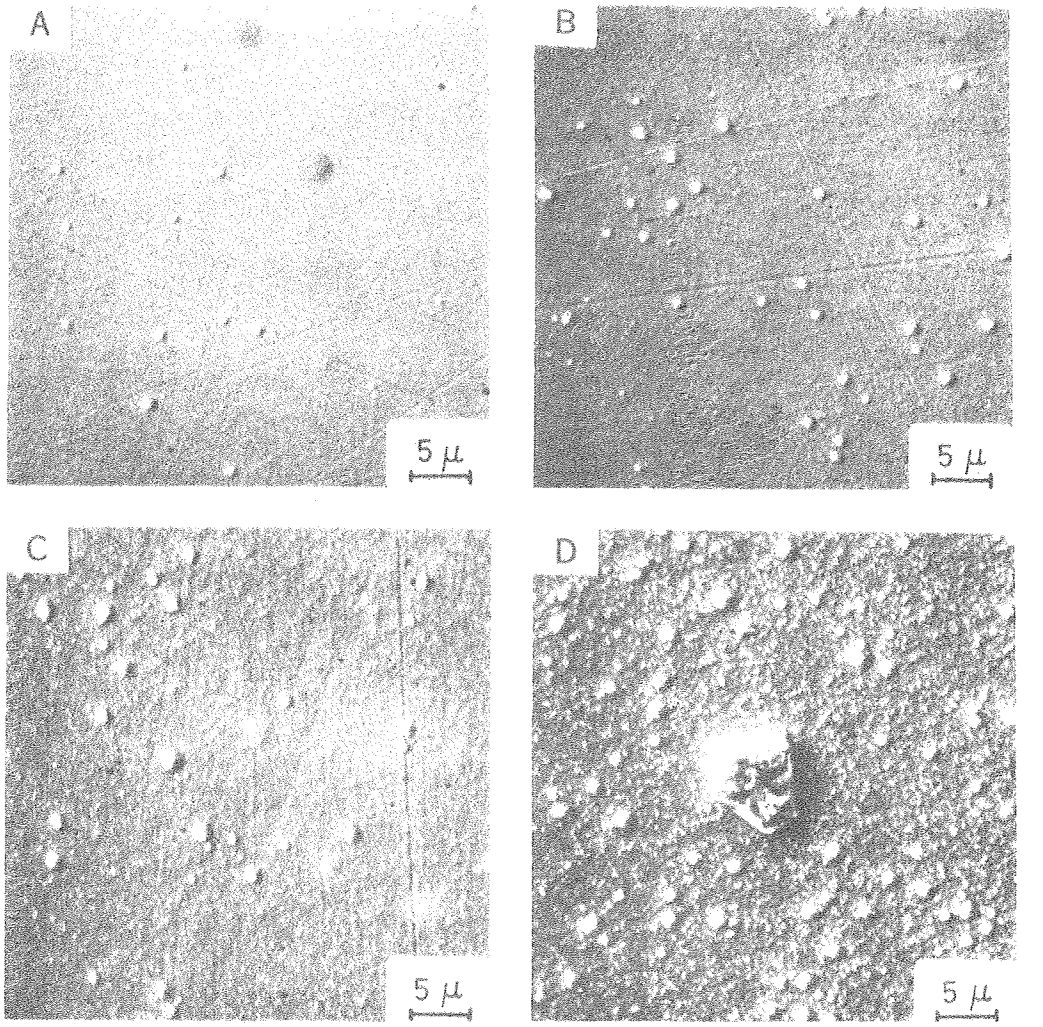

Figure 4.20 SEM photographs showing the sequence of growth of protrusions and their coalescence.

(A) 15 sec. (B) 30 sec. (C) 45 sec. (D) 60 sec.

1M $ZnCl_2$ with 4.8 X 10^{-5} M Pb, 10 mA/cm^2

800 rpm.

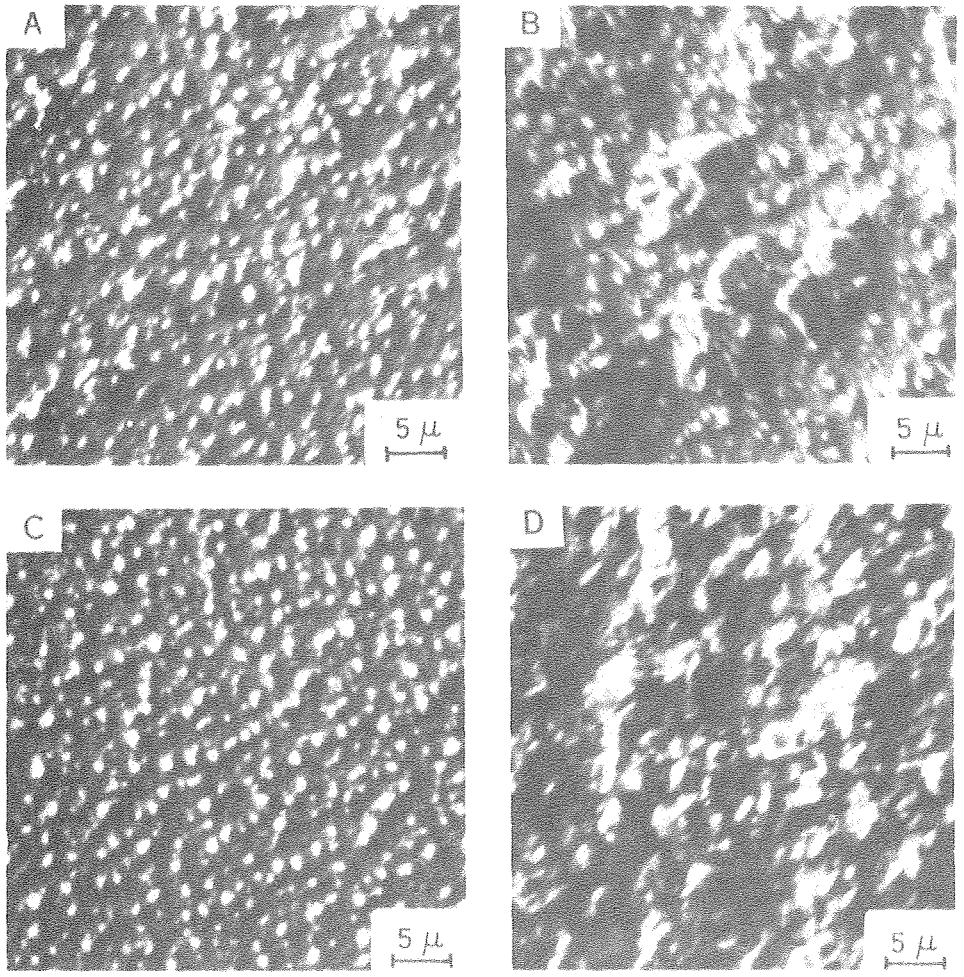

XBB 817-6782 A

Figure 4.21 SEM photographs showing the amplification of surface roughness through coalescence and preferred growth of protrusions.

(A) 30 mA/cm^2 X 0.5 min. (B) 30 mA/cm^2 X 1.5 min.
(C) 60 mA/cm^2 X 15 sec. (D) 60 mA/cm^2 X 90 sec.

1M $ZnCl_2$ with 4.8 X 10^{-5} M Pb, 800 rpm.

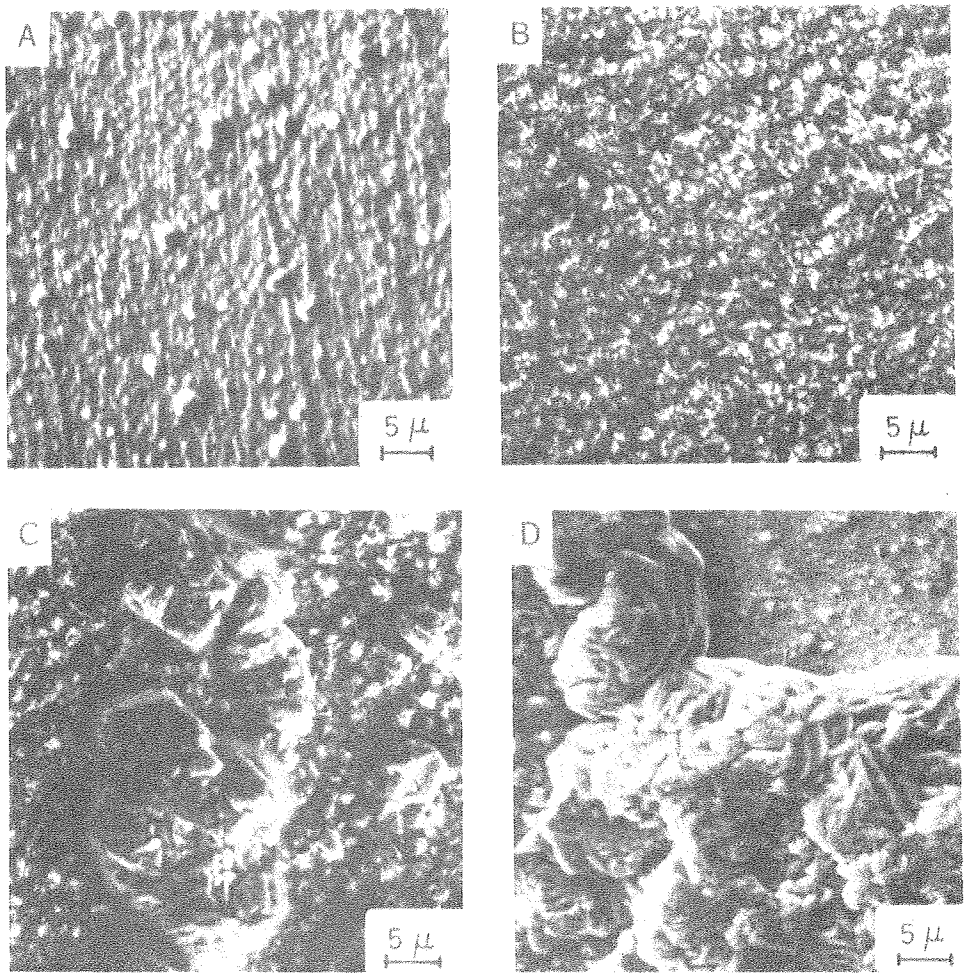

XBB 817-6779 A

Figure 4.22 Sequence of protrusion coalescence and preferred growth at 10 mA/cm^2 and 800 rpm in 1M $ZnCl_2$ containing 4.8 X 10^{-6} M Pb.

(A) 1.5 min. (B) 3 min. (C) 6 min. (D) 9 min.

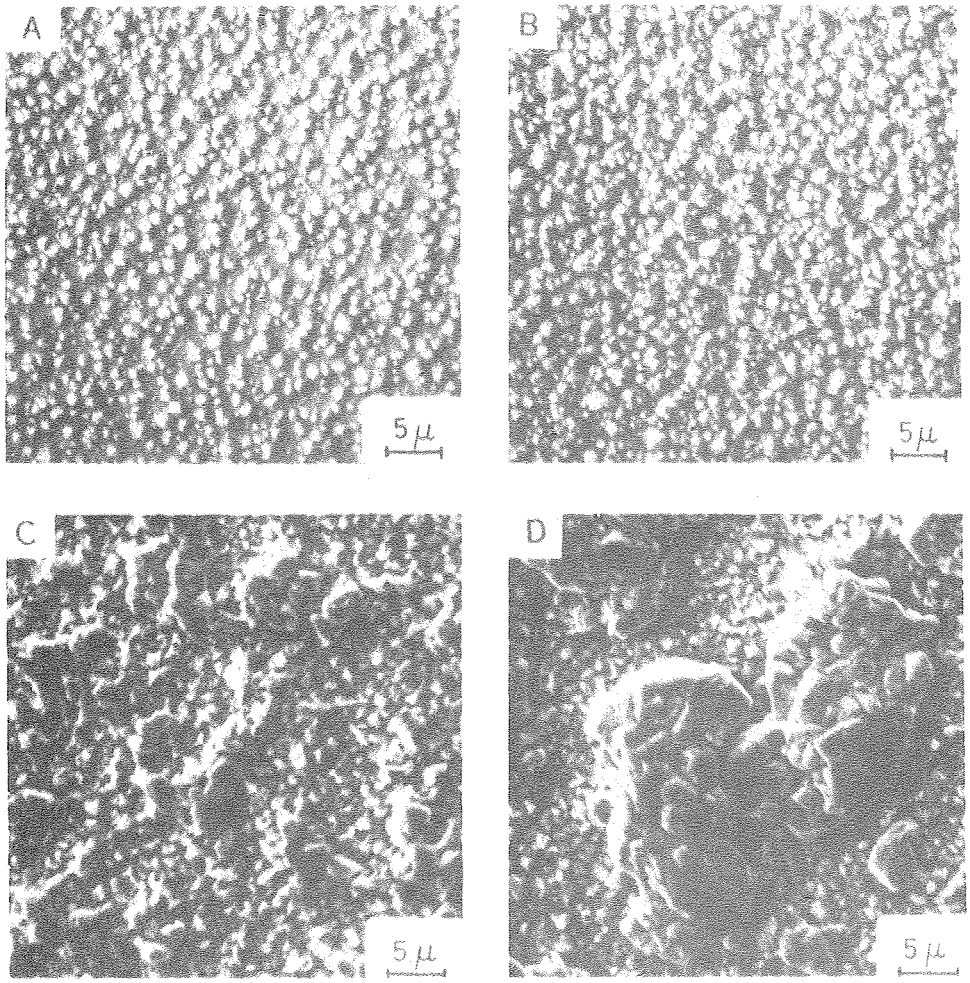

XBB 817-6780 A

Figure 4.23 Sequence showing protrusion coalescence and preferential growth, at 30 mA/cm^2 and 899 rpm in 1M $ZnCl_2$ with $4.8 \cdot X\ 10^{-6}$ M Pb.

(A) 0.5 min. (B) 1.5 min. (C) 3 min. (D) 6 min

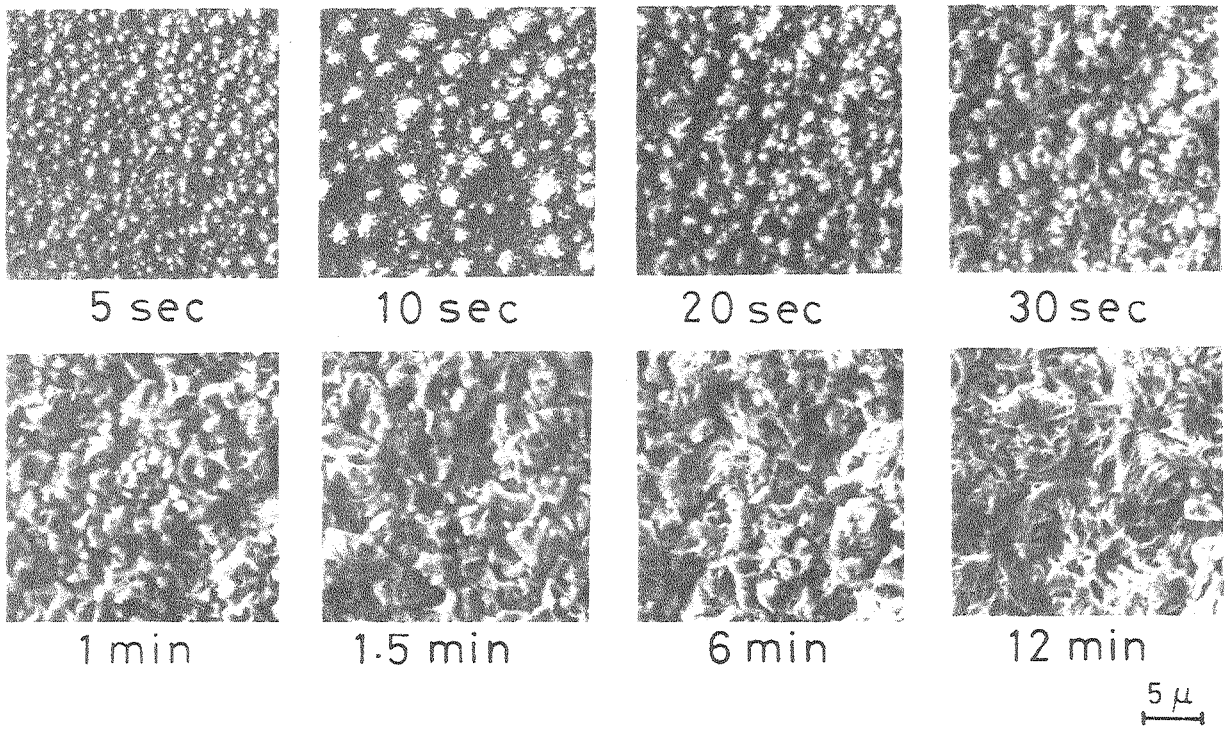

Figure 4.24 Scanning electron micrographs of the sequence of crystal growth at a current density above spiral forming region.

120 mA/cm^2, 800 rpm, 1M $ZnCl_2$ with 4.8 X 10^{-5} M Pb.

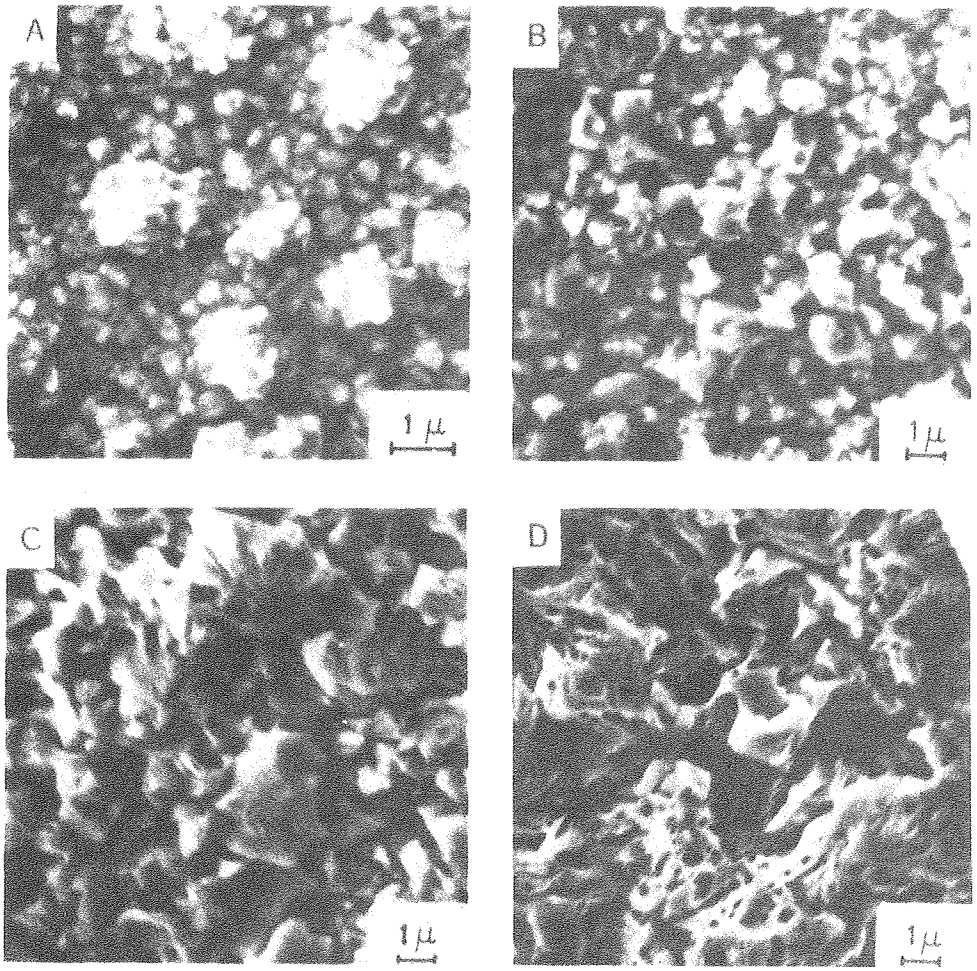

Figure 4.25 SEM photographs showing the sequence of crystal growth at a current density above the spiral forming region. Note that the magnification is approximately five times higher than in Figure 4.24.

(A) 10 sec. (B) 30 sec. (C) 1.5 min. (D) 12 min.

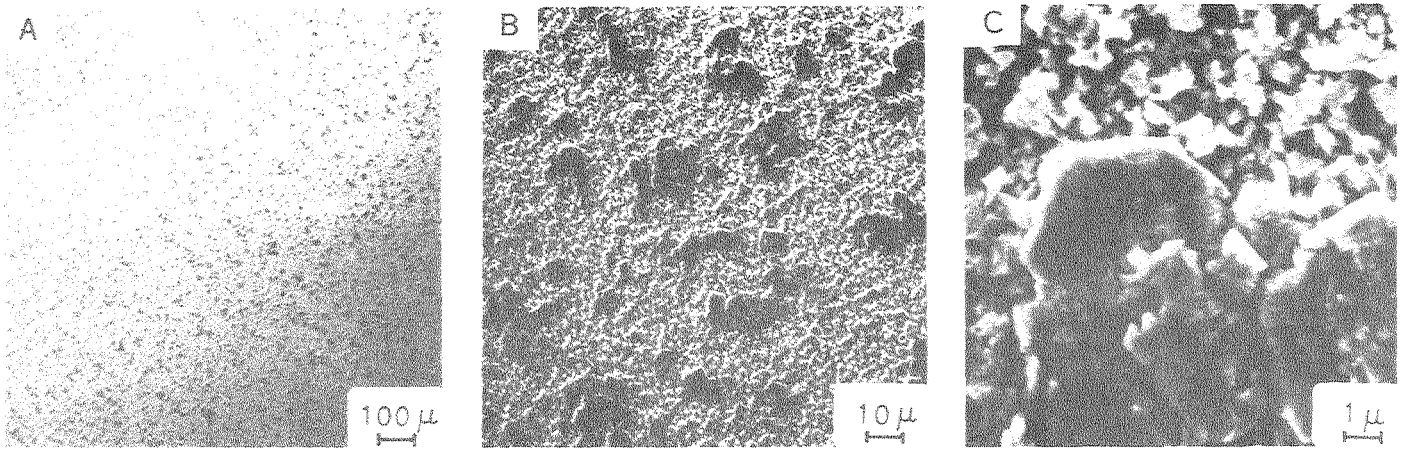

XBB 817-6762 A

Figure 4.26 Influence of substrate on coalescence of protrusions.

(A) SEM view showing onset of spiral formation.
(B),(C) SEM photographs of critical protrusions at higher magnification.

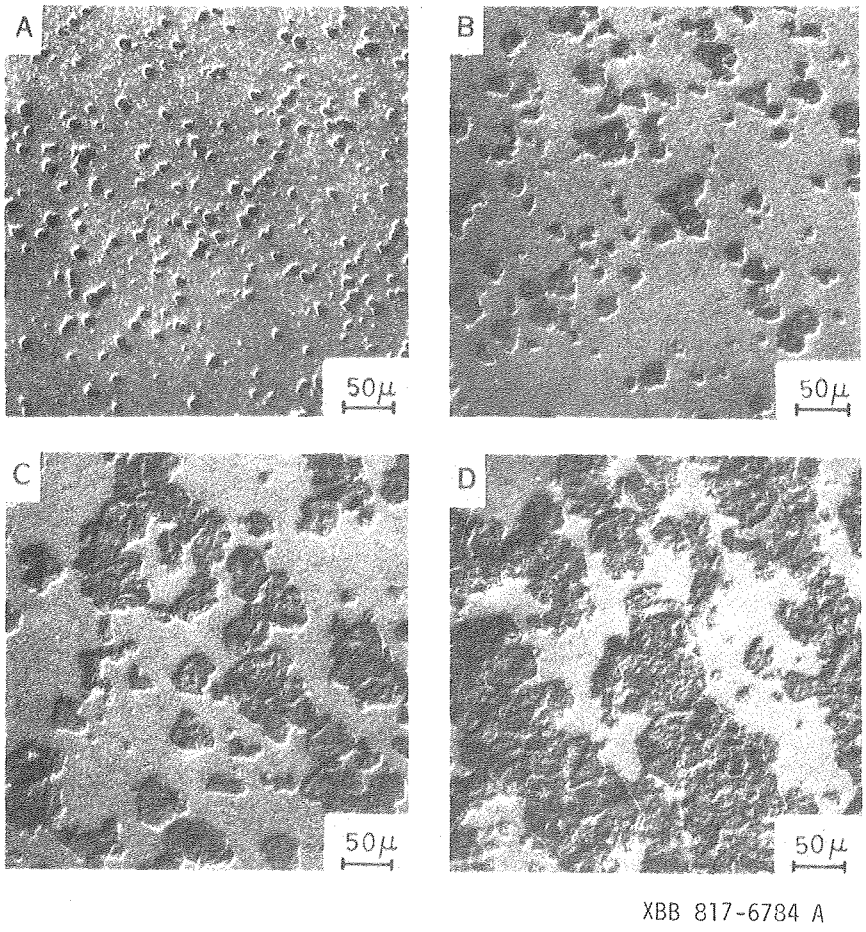

XBB 817-6784 A

Figure 4.27 Connection of protrusions and shaping of spirals, electrodeposited at 10 mA/cm^2 and 800 rpm in 1M $ZnCl_2$ with 4.8 X 10^{-5} M Pb.

(A) 1.5 min. (B) 3 min. (C) 6 min. (D) 9 min.

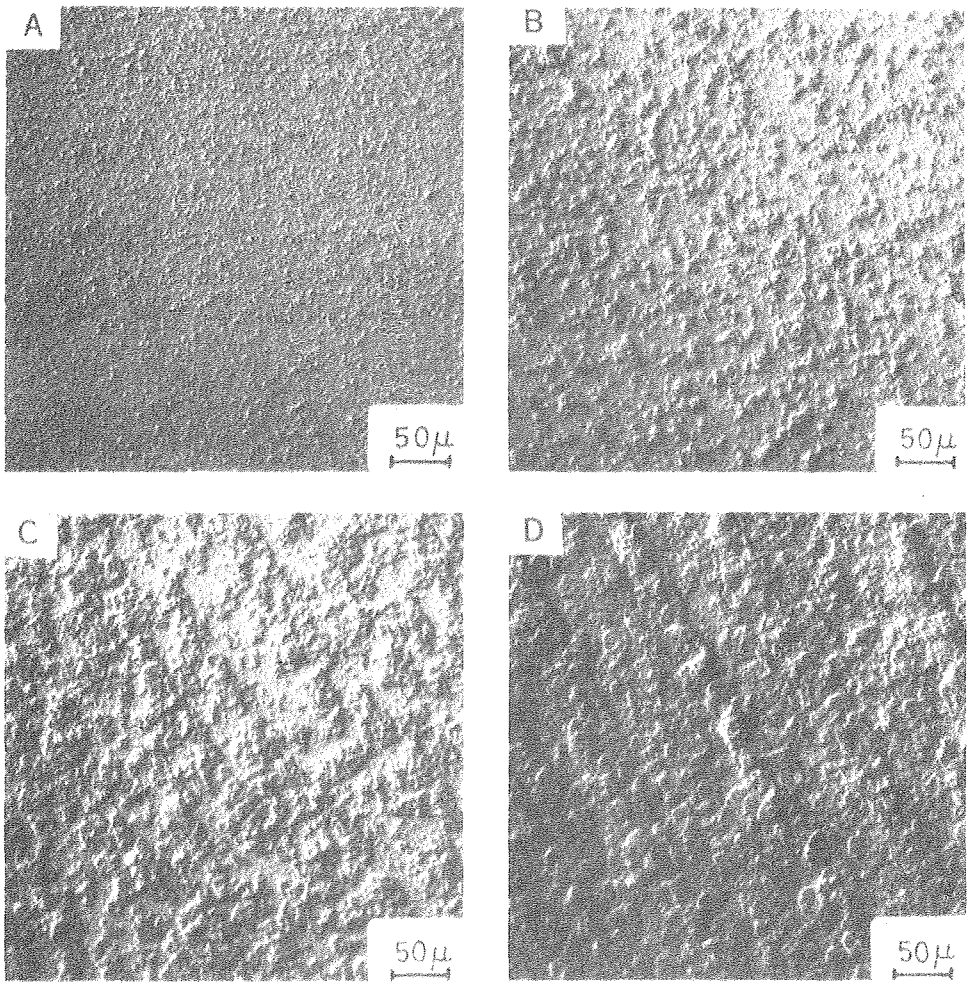

XBB 817-6786 A

Figure 4.28 Scanning electron micrographs showing the amplification of surface roughness and formation of spirals, deposited at 30 mA/cm^2 and 800 rpm in 1M $ZnCl_2$ with 4.8 X 10^{-5} M Pb.

(A) 0.5 min. (B) 1.5 min. (C) 3 min. (D) 6 min.

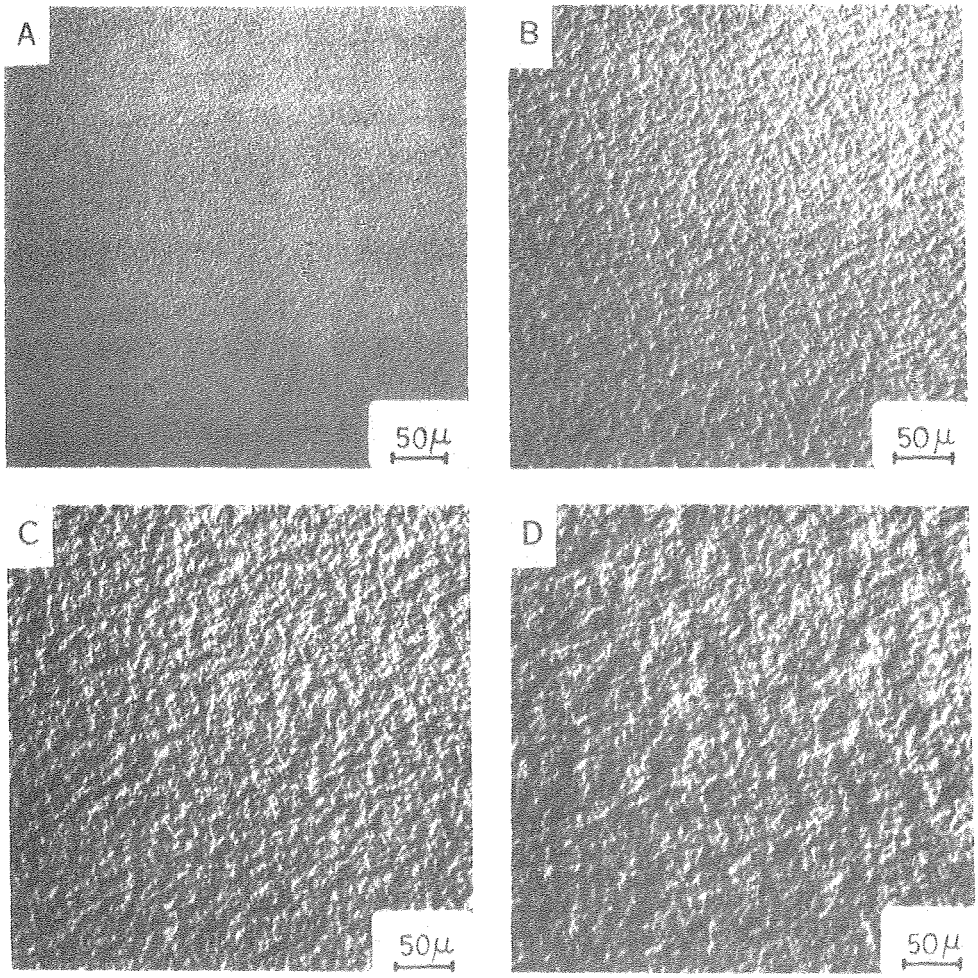

XBB 817-6775 A

Figure 4.29 SEM photographs showing the development of surface roughness and shaping of spirals, deposited at 60 mA/cm^2 and 800 rpm in 1M $ZnCl_2$ containing 4.8 X 10^{-5} M Pb.

(A) 15 sec. (B) 45 sec. (C) 1.5 min. (D) 3 min.

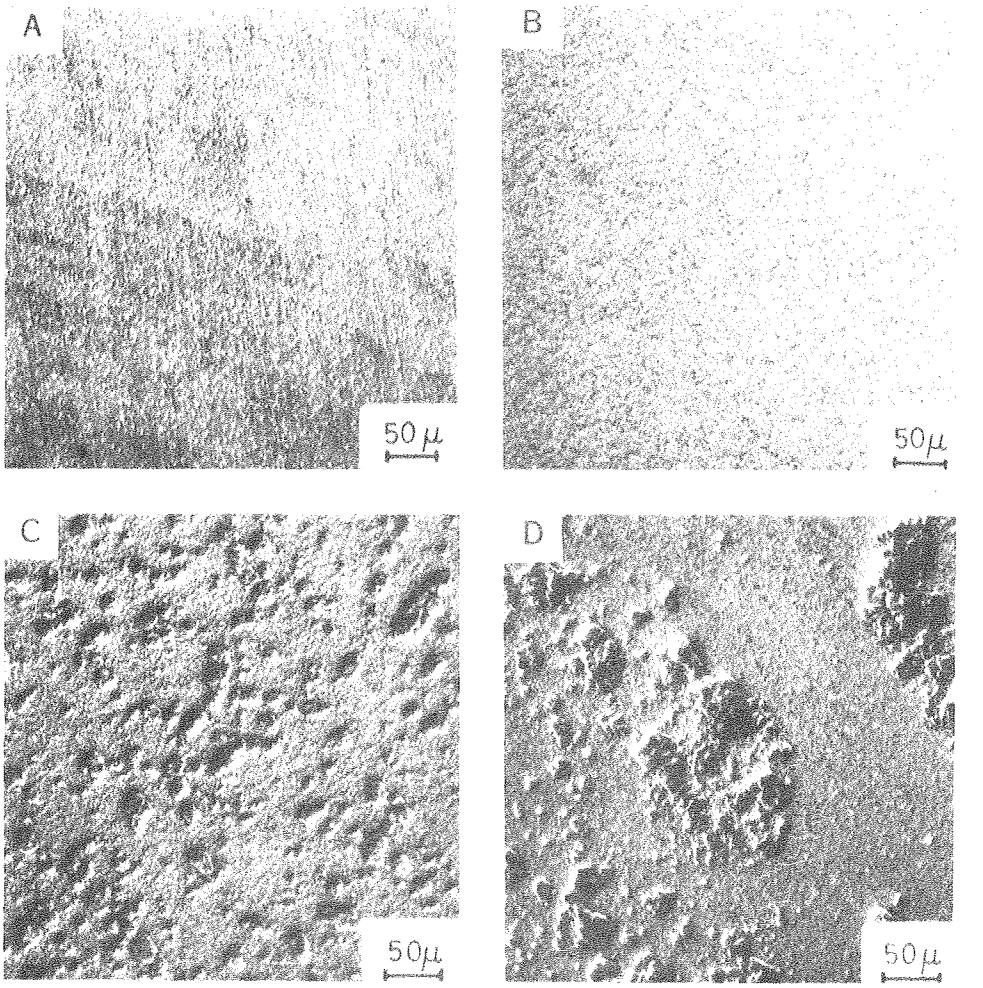

XBB 817-6776 A

Figure 4.30 SEM photographs showing the evolution of surface roughness and formation of spirals, deposited at 10 mA/cm^2 and 800 rpm in 1M $ZnCl_2$ containing 4.8 X 10^{-6} M Pb.

(A) 1.5 min. (B) 3 min. (C) 6 min. (D) 9 min.

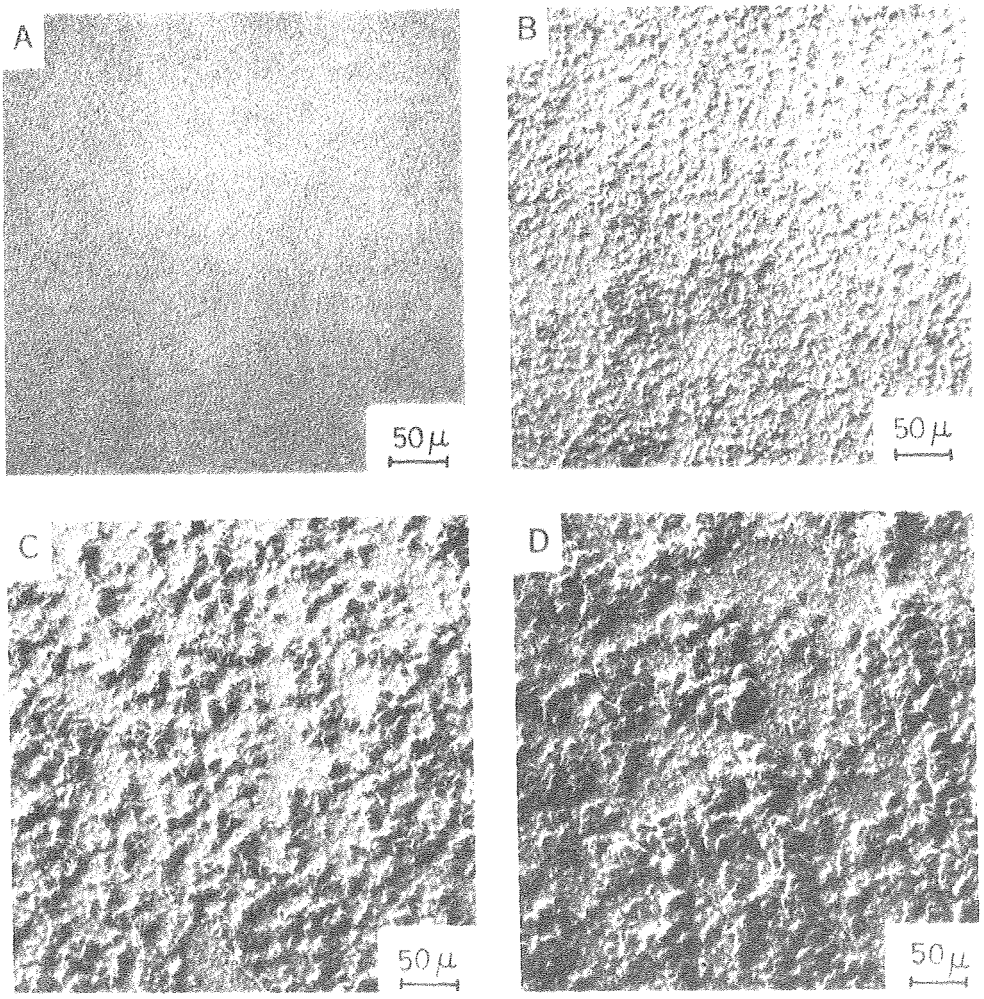

XBB 817-6777A

Figure 4.31 Scanning electron micrographs showing the evolution of surface roughness and formation of spirals, deposited at 30 mA/cm^2 and 800 rpm in 1M $ZnCl_2$ with 4.8 X 10^{-6} M Pb.

(A) 1.5 min. (B) 3 min. (C) 6 min. (D) 9 min.

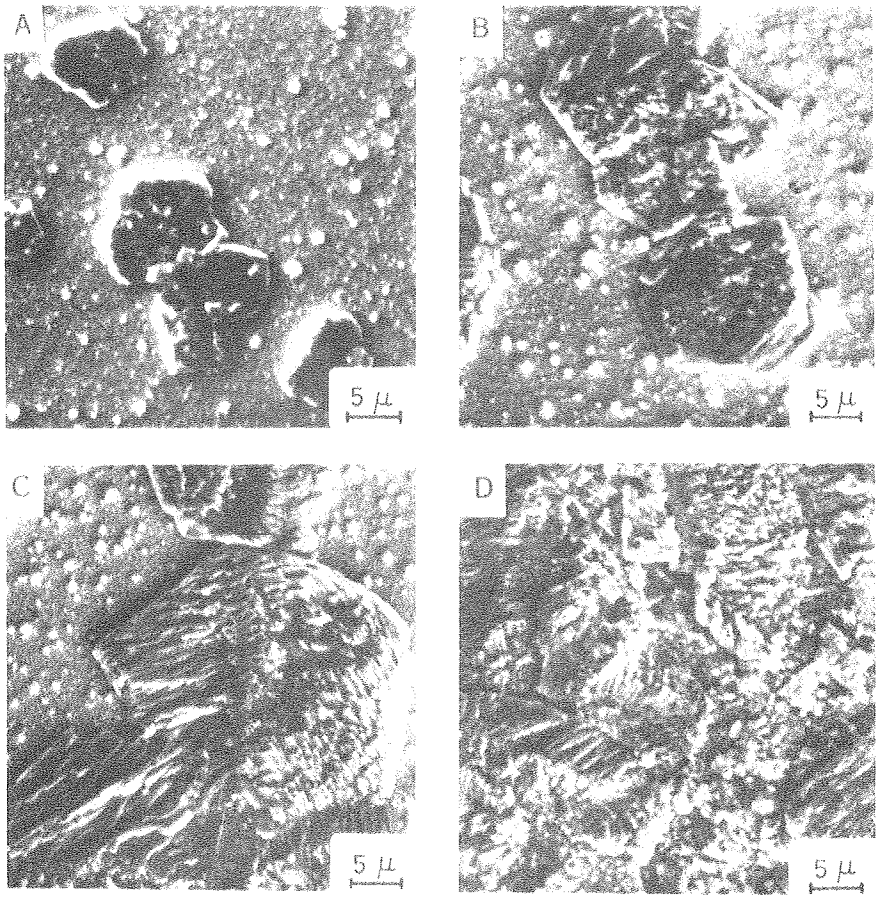

XBB 817-6785 A

Figure 4.32 SEM photographs showing the growth process from protrusion to spiral ridge, electrodeposited at 10 mA/cm^2 and 800 rpm in 1M $ZnCl_2$ with 4.8 X 10^{-5} M Pb.

(A) 1.5 min. (B) 3 min. (C) 6 min. (D) 9 min.

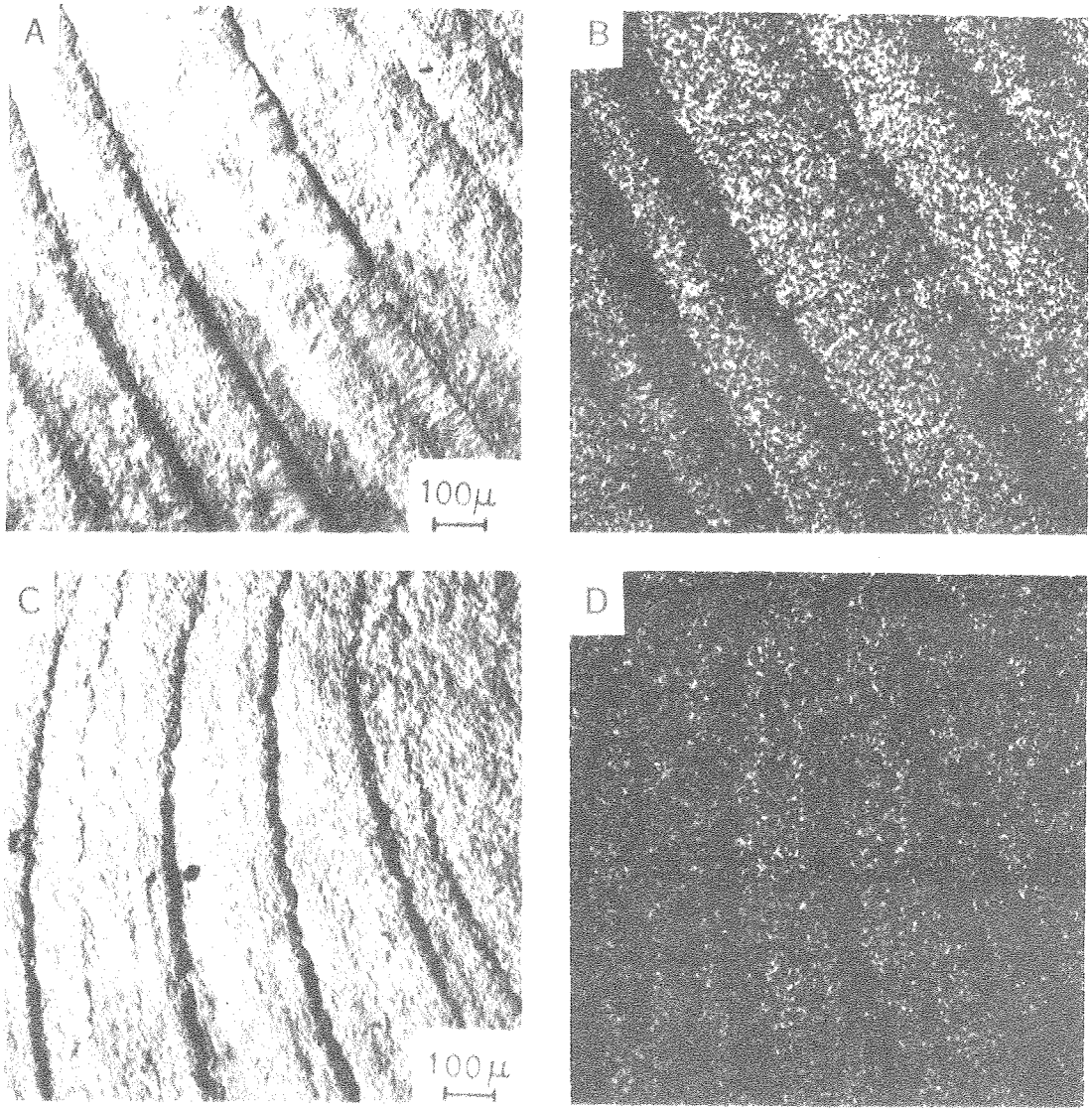

XBB 817-6772 A

Figure 4.33 Back scattered electron image of spirals and the corresponding lead x-ray map.

30 mA/cm^2 X 30 min. (A) BSE image (B) Pb map

10 mA/cm^2 X 60 min. (C) BSE image (D) Pb map

1M $ZnCl_2$ with 4.8 X 10^{-5} M Pb, 800 rpm.

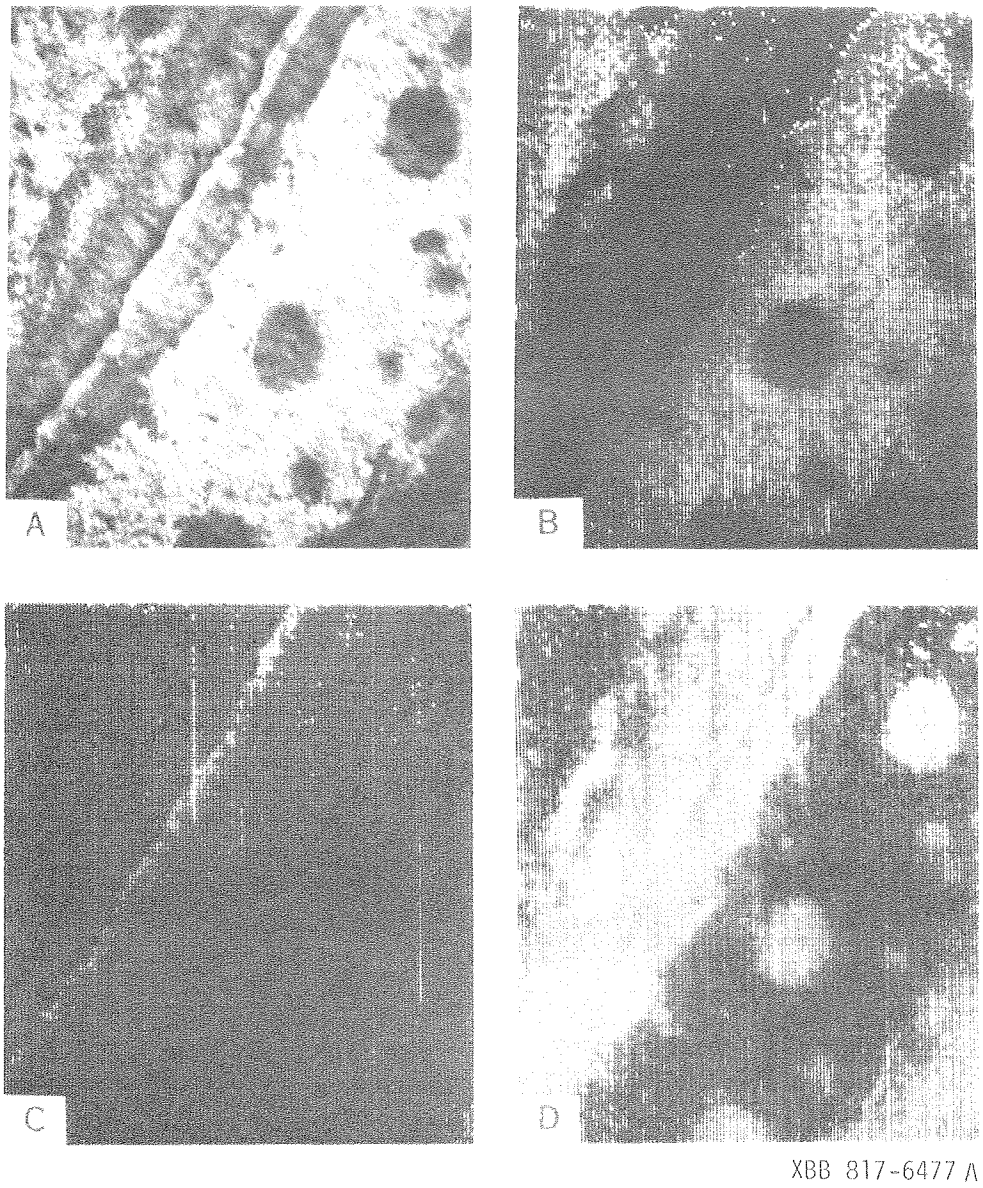

Figure 4.34 Elemental Auger mapping of spirals.

(A) Secondary electron image of spiral (X198)
(B) Pb map (C) Zn map (D) O map
beam voltage 5 kV, beam current 19 nA.
10 mA/cm^2 X 60 min., 800 rpm, 1M $ZnCl_2$ with
4.8 X 10^{-5} M Pb.

4-3. Ultra-pure Electrolytes

Most of the electrodeposition was carried out in a pH 5.2 solution to reduce the influence of hydrogen co-evolution.

Morphological Observations of Spirals

(1) Macroscopic characteristics of spirals

The number density of spirals was higher than those obtained from solution containing lead as illustrated in Figure 4.35. Very fine spirals were seen on the surface deposited at 90 mA/cm^2. The spiral formation time was prolonged to 10 - 20 min. at 10 - 30 mA/cm^2 at a rotation speed of 800 rpm. There was no noticeable difference in the shape (angle) of spirals.

(2) Micromorphology of zinc deposit

A very definite crystalline appearance was observed on zinc deposits obtained from ultra-pure electrolyte. As shown in Figure 4.36, in some cases hexagonal columns may be seen at the initial stage of electrodeposition. Figure 4.37 is intended to show the crystalline masses of ridges consisting of piles of polygonal layers.

(3) Non-homogeneity on the surface

The surface was coated by a thin zinc-platinum alloy layer for short time deposition from lead containing solution, whereas results of short time experiments with ultra-pure solution showed an extreme nonhomogeneity on the platinum surface. Initial crystallites were formed on discrete nucleation centers and the rest of the area exposed was a bare platinum surface (see Figure 4.36). It seems that microstructural defects on the platinum surface acted as preferred nucleation sites for zinc crystallization. Although no trace of hydrogen

bubbles could be visible on the surface of the rotating disk or in the solution during electrolysis, it is possible that hydrogen was produced as a side-reaction because of very low hydrogen overvoltage of platinum.

(4) Influence of pH

Zinc was electrodeposited at 120 mA/cm^2 from a solution containing 4.8×10^{-5} M Pb for 30 sec. to form a smooth layer of zinc and to reduce the hydrogen coevolution on the bare platinum surface. Subsequent experiments, using ultra-pure solution, were carried out at varying pH values. It made little difference whether the pH was high (5.2) or low (1.8), except that the crystalline appearance became more rounded in shape for low pH solution. Spiral formation time, the number density and shape angle of spirals did not vary with pH (see Figure 4.40 and 4.41).

Morphological Observations of Initial Protrusions

The number density of initial crystallites increased significantly as the current density increased as demonstrated in Figure 4.38.

Protrusion Coalescence and Shaping of Spirals

Coalescence of initial crystallites with closest neighbors occurred, and then connection of larger crystallites into spiral shape was observed after the crystallites grew to a certain size (see Figure 4.39). Spiral patterns could not at all be discerned in the first six min. deposition; they became distinct after nine minutes.

Surface Analysis of Deposits

Auger spectroscopic investigation showed that on the planar surface between distinct crystallites no zinc was deposited (see Figure 4.42). In contrast, both zinc and platinum were detected on such area when

deposition occurred from lead containing electrolytes. Apparently at the initial stage of the deposition process a zinc-platinum alloy was formed.

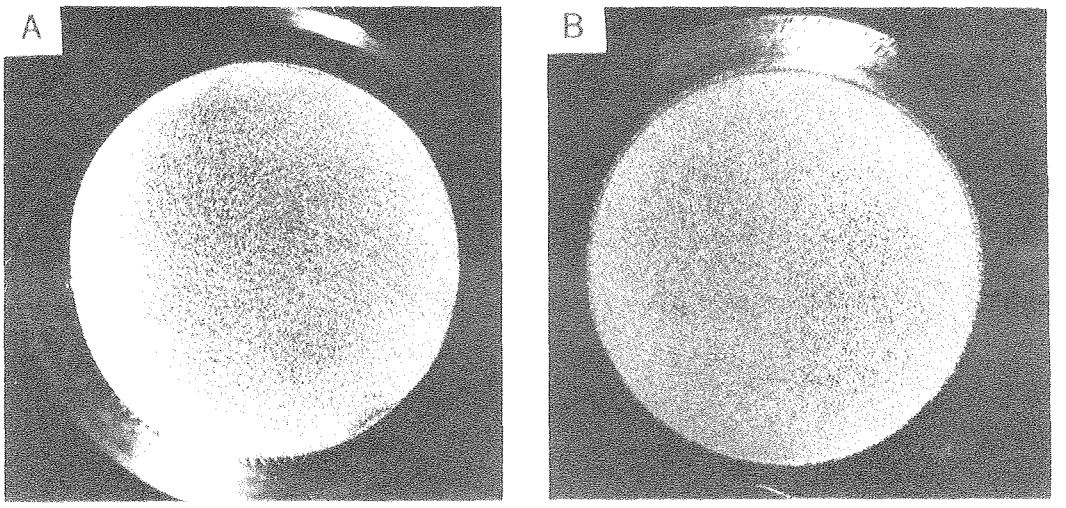

Figure 4.35 Spirals obtained from ultrapure solution 1M zinc chloride (pH 5.2), 6-nine zinc anode.

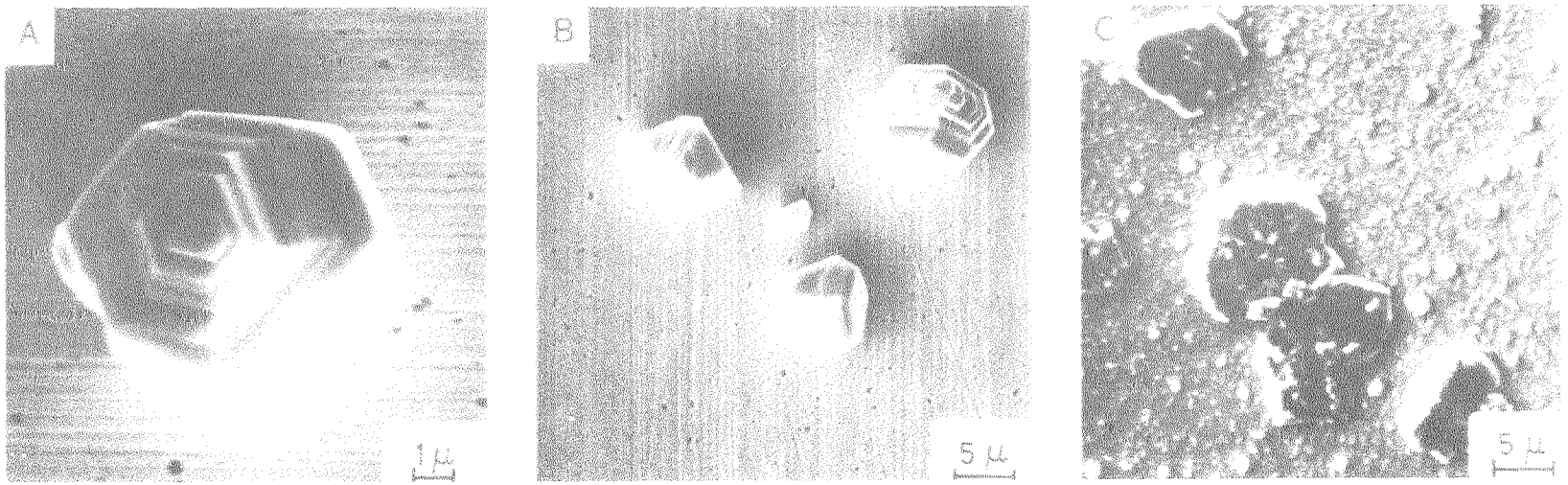

XBB 817-6763 A

77

Figure 4.36 The crystalline structure of initial protrusions.

(A) An ideally hexagonal crystallite.
(B) Crystallites formed on bare platinum surface.
(C) Protrusions formed from 1M $ZnCl_2$ with 4.8 X 10^{-5} M Pb.

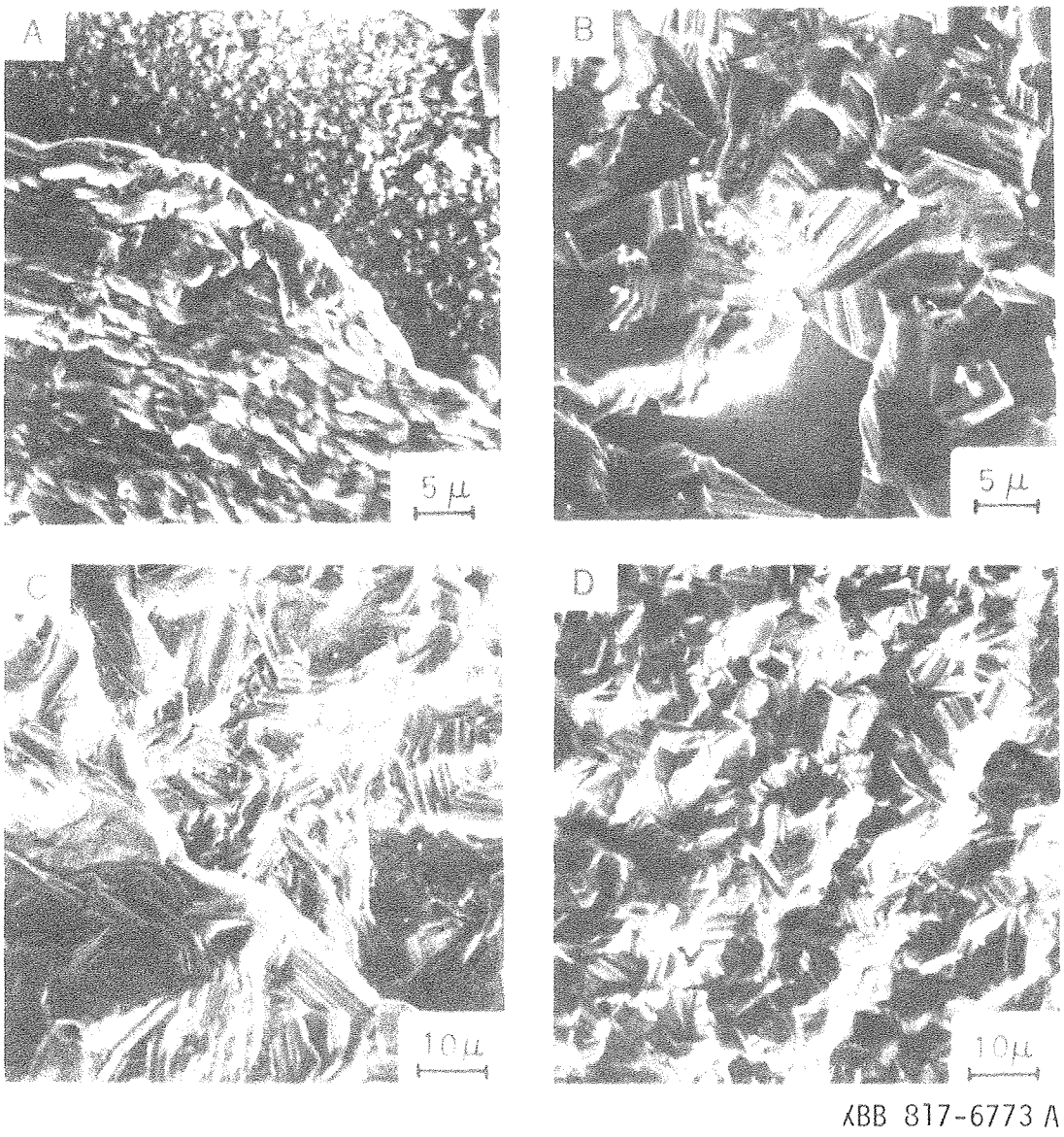

Figure 4.37 SEM photographs showing the crystalline structure of spirals from ultrapure solution.

(A) 10 mA/cm^2 X 45 min. 4.8 X 10^{-5} M Pb.
(B) 10 mA/cm^2 X 60 min. ultrapure
(C) 30 mA/cm^2 X 45 min. ultrapure
(D) 90 mA/cm^2 X 5 min. ultrapure

rotation speed 800 rpm.

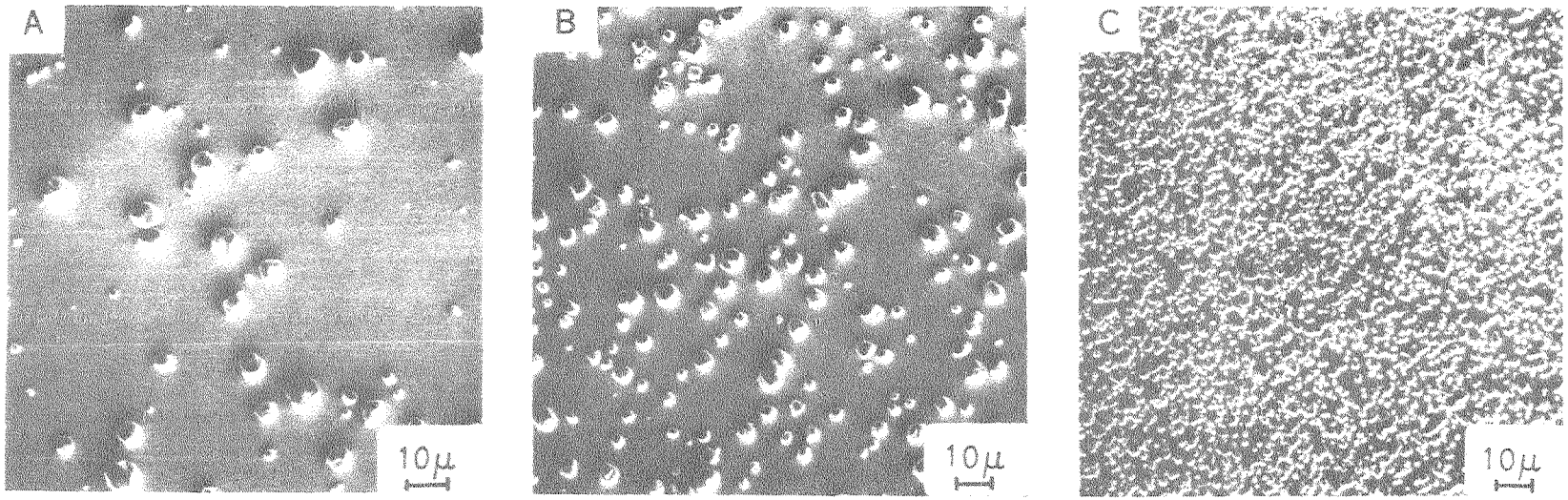

XBB 817-6764 A

Figure 4.38 Effect of current density on the number and size of initial crystallites.

(A) 10 mA/cm^2 X 90 sec. (B) 30 mA/cm^2 X 30 sec. (C) 90 mA/cm^2 X 10 sec. ultrapure 1M zinc chloride (pH 5.2), 800 rpm.

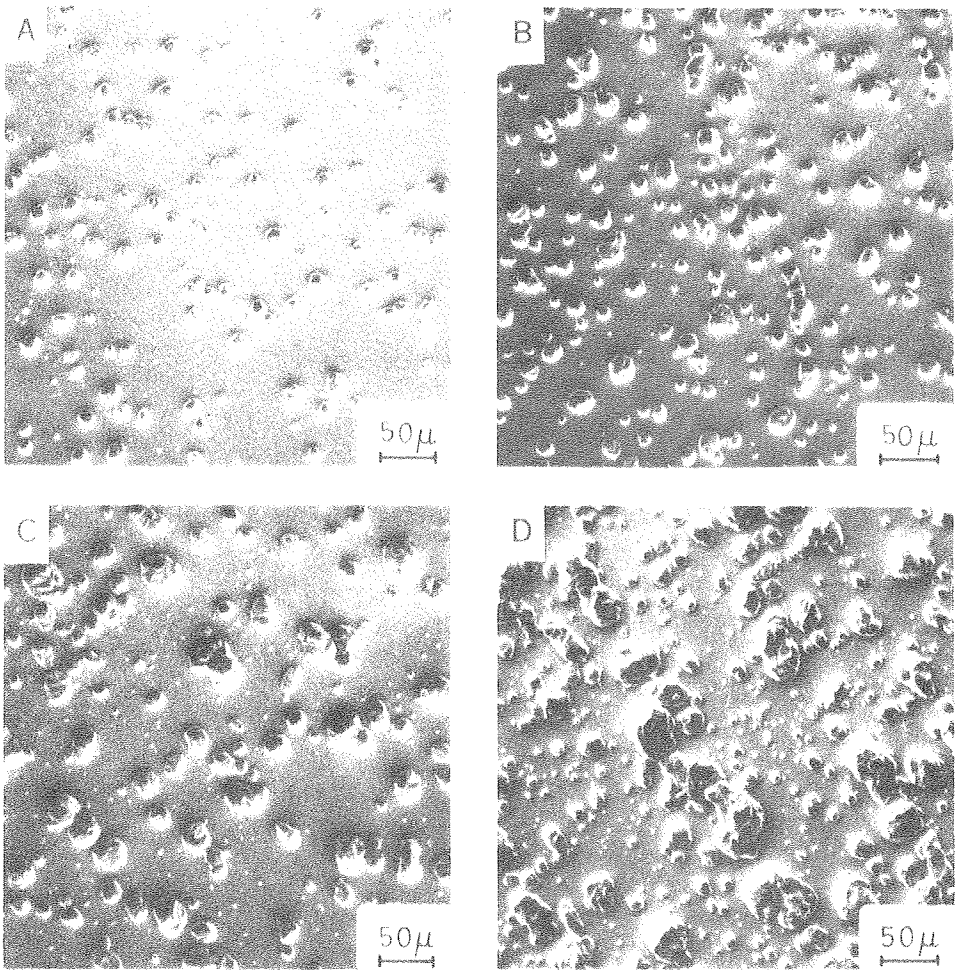

Figure 4.39 SEM photographs showing the sequential growth stage from initial crystallites to spiral ridges.

(A) 3 min. (B) 6 min. (C) 9 min. (D) 18 min. 10 mA/cm^2, 800 rpm, ultrapure 1M $ZnCl_2$

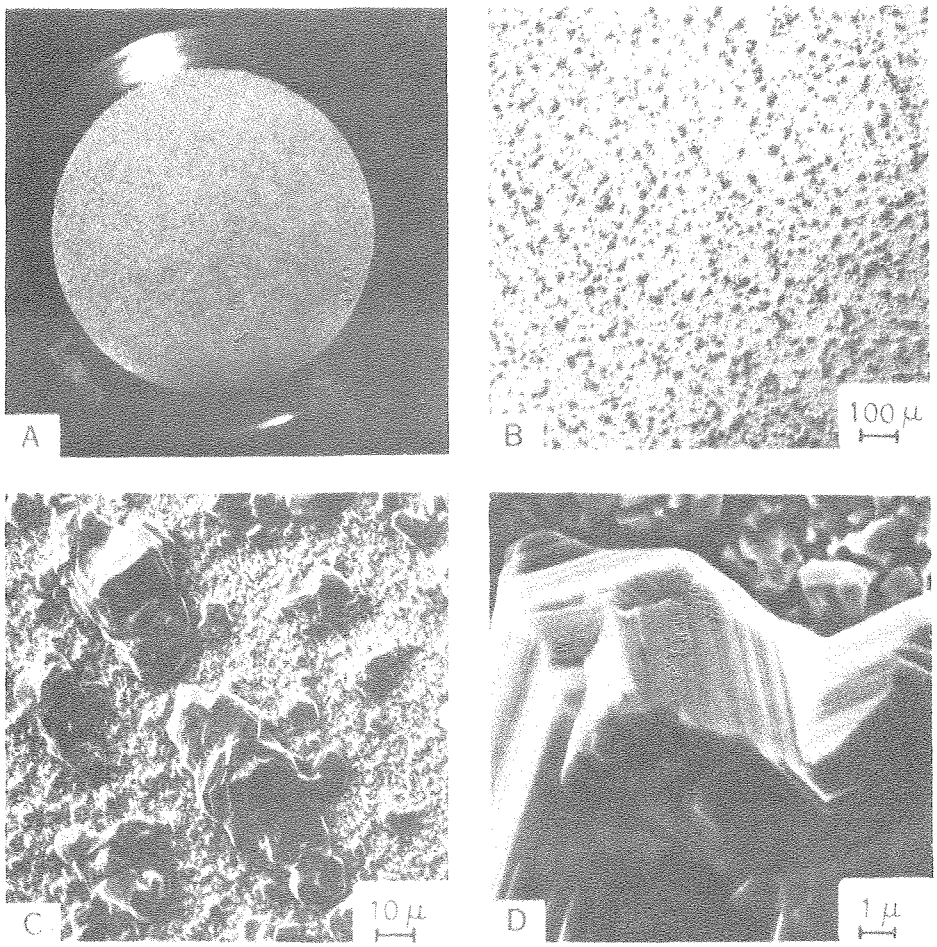

XBB 817-6770 A

Figure 4.40 Influence of substrate on spiral formation from ultrapure zinc chloride electrolyte.

(A) A photomacrograph of spirals.
(B) SEM photograph of spirals.
(C) Spiral ridges formed by connection of crystallites.
(D) Crystalline structure of spiral ridges.

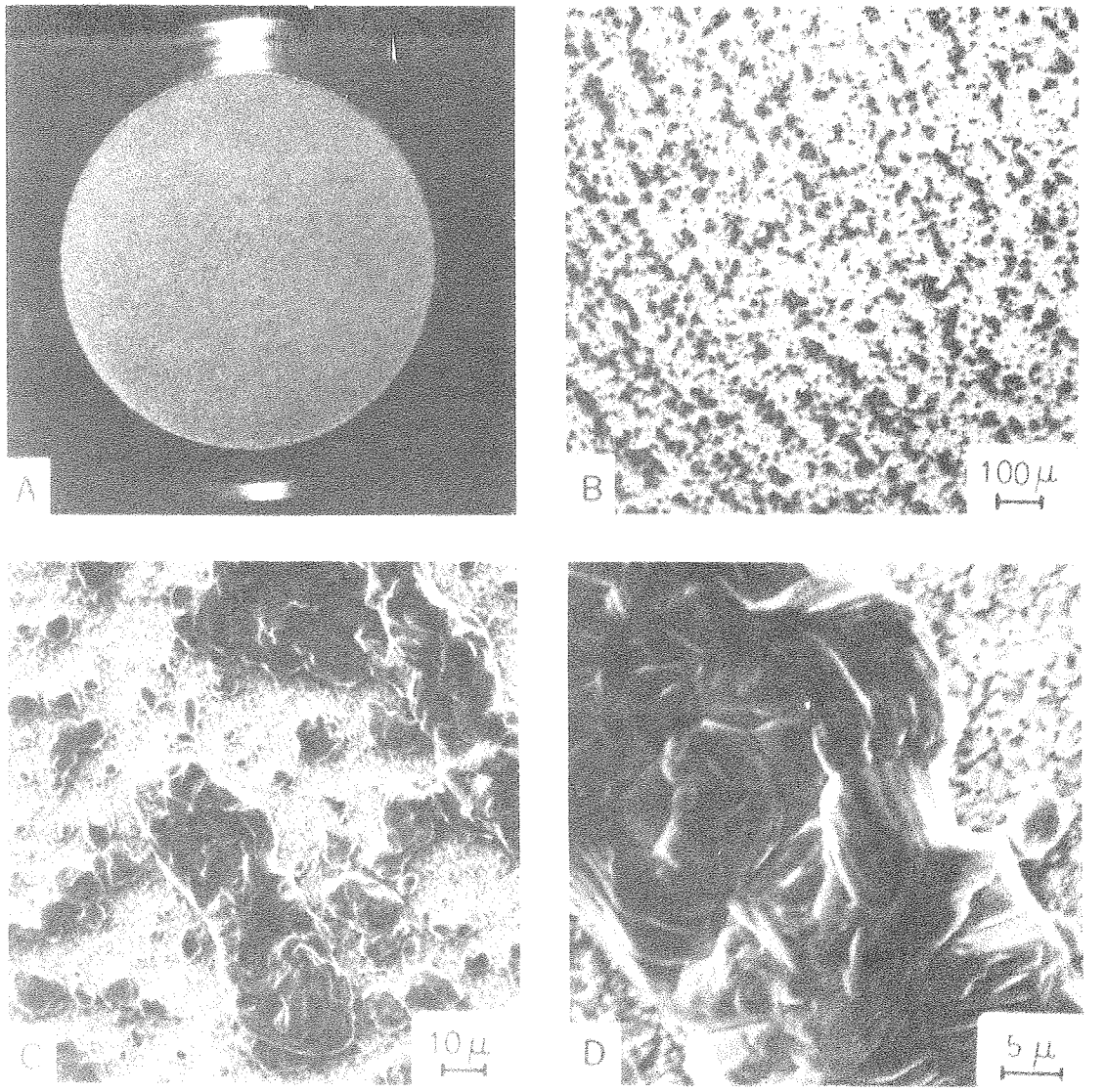

XBB 817-6771 A

Figure 4.41 Influence of pH on spiral formation from ultrapure zinc chloride electrolyte.

120 mA/cm^2 X 30 sec. in 1M $ZnCl_2$ with 4.8 X 10^{-5} M Pb followed by 10 mA/cm^2 X 30 min. in ultrapure solution (pH 1.8). Note rounded shape of spiral ridges (D).

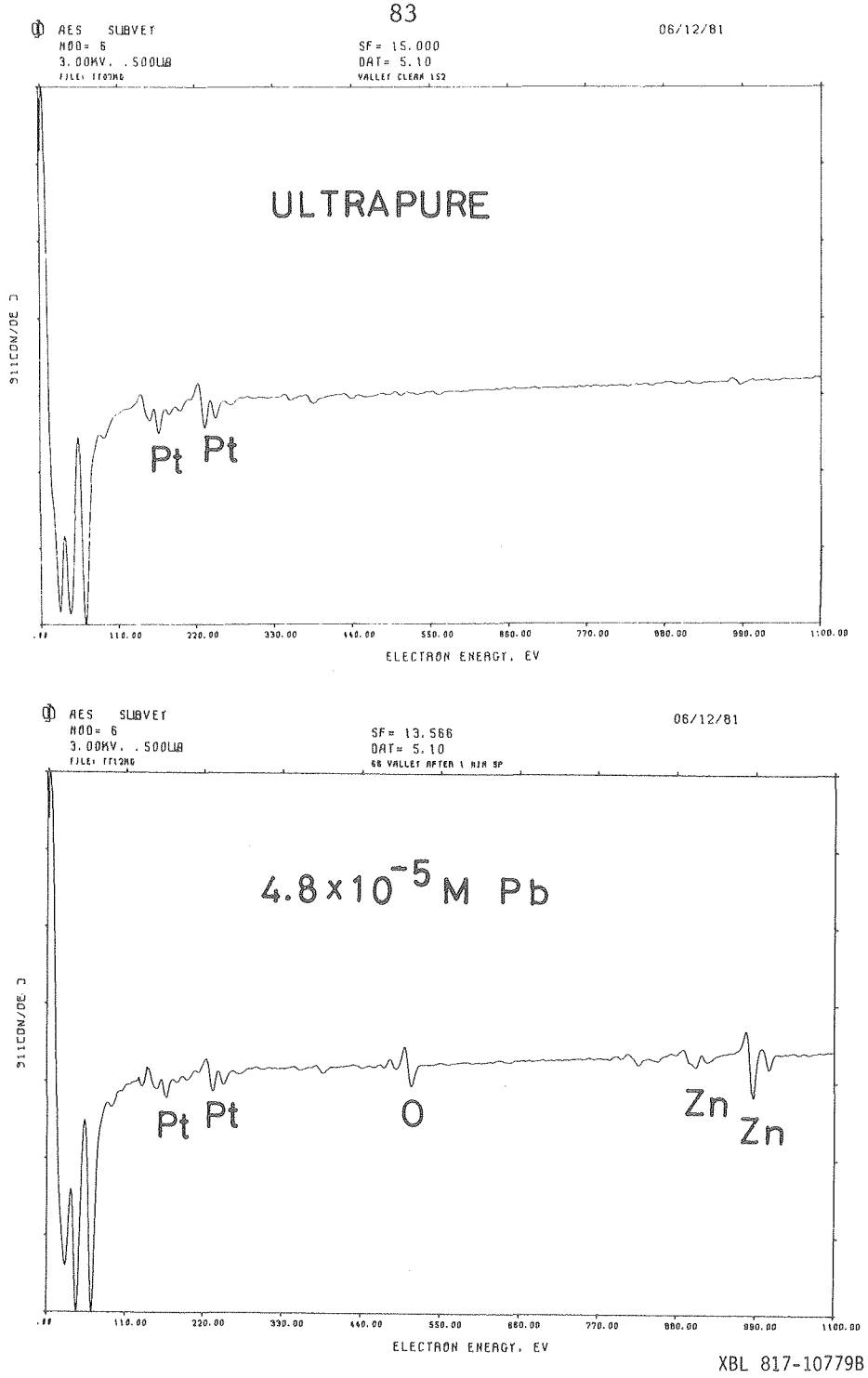

XBL 817-10779B

Figure 4.42 Auger spectra of flat and smooth area of the electrodes.

5. DISCUSSION

In an attempt to explain the hydrodynamic effect on macromorphology of zinc deposits well below the limiting current, Jaksić and Tobias (9) tentatively proposed a model based on a coupling mechanism between differential nucleation and growth due to slight variations of concentration and secondary flow phenomena within the fluid boundary layer initiated by developing roughness on the electrode surface with deposition. The present investigation was undertaken to gain further insight into the complex phenomena responsible for the formation of striations in zinc deposits, and to reinforce, modify or disprove the tentative models advanced by Jaksic et al. Jaksić and Komnenić's work raised a number of questions; these, along with primary results of the present investigation on impurity effects (see also Appendix C) led to raising the following questions:

(1) How is this surface roughening process (i.e., the initiation and growth of protrusions) related to the nucleation and growth of zinc electrocrystallization? In other words, what is the dominant factor controlling this roughening phenomenon?

   (a) The original substrate and its surface defects, whether they may be microscopic (e.g., kinks, dislocations, crystallographic facets, etc.) or macroscopic (e.g., grain-boundary, scratch marks, depressions, etc.).

   (b) The number density of nuclei initially formed on the substrate at the very beginning of electrodeposition.

   (c) Variations of mass flux of minor species affecting kinetics

of zinc electrocrystallization between peaks and valleys due to the difference in distance for diffusion.

(2) How do these growing protrusions, acting as distributed roughness elements, disturb the laminar flow and originate secondary flows?

   (a) Will this disturbance merely cause local eddies close to the protrusion and damp out shortly downstream?

   (b) Will this result in a fully developed Taylor-Goertler vortices and form spiral streaks as a consequence?

(3) Why does this local eddy mixing enhance preferred zinc deposition under kinetic control conditions? Can this be attributed to minor species in the electrolyte?

(4) What role does lead impurity play in the formation of spiral patterns of electrodeposited zinc on a rotating disk electrode well below the limiting current density?

Concerning question (1): "How is this surface roughening process related to the nucleation and growth of zinc electrocrystallization?"

The results of sequential observations of protrusions clearly show that the development of macroscopic roughness depends on the number density of protrusions that grow to a critical height which then presumably governs the number density of spirals generated on the disk. This number density of critical protrusions is affected by not only the initial nucleation density but also by the rate of coalescence and preferred growth of protrusions. The significance of the original substrate and its surface defects should be considered in a sense that these influence the number density of initial nuclei formed. In addition, major emphasis should be placed on the tendency for coalescence and on the selective growth of protrusions.

An attempt was made to compare the lead content of protrusions with that of the flat area in between protrusions at the early stage of deposition by means of Auger spectroscopy. This attempt was not successful because the Auger peak of lead is too close to that of platinum to be identified separately. No conclusion, therefore, can be drawn as to whether local differences in interfacial lead concentration might promote amplification of roughness or not.

A model explaining the mechanism of formation of spiral patterns should account for the following macroscopic characteristics of spiral striations.

(A) The number density of spirals increases with increasing current density, while it is independent of lead content in the electrolyte. It is also independent of rotation speeds for zinc chloride containing

trace amount of lead ions, but is an increasing function of rotational speed for A.R. grade zinc sulphate.

(B) The spiral formation time appears to be nearly independent of current density. It decreases with increasing rotational speed and also with increasing lead content in the electrolyte.

To explain the behavior as described above, the following explanations are advanced:

Number Density of Spirals

(a) Effect of current density

With increasing current density, initial nucleation density increases and the rate of coalescence and selective growth of protrusions slows down. Thus the number density of critical protrusions would increase as the current density increases.

(b) Effect of lead content of electrolytes

The initial nucleation density greatly increases with a decrease in lead content in the electrolyte, however, coalescence and preferential growth of these protrusions should eventually give rise to produce nearly the same number of critical protrusions.

(c) Effect of rotation speed

With increasing rotational speed, resulting in the reduction of the thickness of the diffusion boundary layer, the critical height is reduced. The mass flux of lead ions to the surface increases as well. In general, the smaller the critical height the larger the number density of aggregating protrusions, since surface roughening is a totally time-dependent phenomenon. On the other hand, the increased mass flux of lead ions lessens the nucleation density and strengthens the tendency

for coalescence of protrusions resulting in fewer numbers of critical protrusions. It seems that these two factors cancel out each other to generate almost identical number density of critical protrusions in the case of $ZnCl_2$. Although the effect of lead in zinc sulphate solution has not been adequately studied and should be subject to future investigation, it is conjectured that for zinc sulphate solution lead ions might influence the kinetics of zinc deposition to a lesser extent than in zinc chloride solutions. On this basis it could be expected that the number density of critical protrusions increases with rotation speed due to a diminution in critical protrusion height in the case of $ZnSO_4$.

Spiral Formation Time

(a) Effect of current density

With an increase in current density, the initial nucleation density increases and the average size of protrusions becomes smaller. Furthermore, the rate of coalescence of these protrusions is hindered as increasing current density. As a result, at higher current densities these growing protrusions reach the critical height more slowly than expected from the amount of charge passed.

(b) Effect of lead content of electrolytes

A significant increase in initial nucleation density and retarded rate of protrusion coalescence are observed with decreasing lead content in the electrolytes. It is likely that lead interferes with crystal growth, and that the large population of fine protrusions requires longer periods to grow to a critical size, through coalescence and preferred growth, than do less densely spaced initial protrusions.

(c) Effect of rotation speed.

The thickness of the boundary layer as it is reduced with increasing rotational speed is tabulated below. According to the Levich equation,

$$\delta_{hyd.} = 3.6\sqrt{\nu/\omega}$$

$$\delta_{diff.} = 1.61\,(D/\nu)^{1/3}\sqrt{\nu/\omega}$$

$D = 0.7 \times 10^{-5}$ (cm^2/s)

$\nu = 1.08 \times 10^{-2}$ (p)

$r = 0.725$ (cm)

ω (rad/s)	δ diff. (μm)	δ hyd. (μm)	Re
20.9 (200 rpm)	32	820	1,020
41.9 (400 rpm)	22	580	2,040
83.8 (800 rpm)	16	410	4,080
126 (1,200 rpm)	13	330	6,130

Even assuming the same growth rate of protrusions, the spiral formation time should be reduced due to a decrease in the critical protrusion height. Also the increased mass flux of lead to the surface may promote the coalescence of protrusions, leading to an increased growth rate of protrusions.

Concerning question (2): "How do these growing protrusions disturb the laminar flow and originate secondary flows?"

The shape of these spirals is most closely approximated by logarithmic spirals described by,

$r = a^{\theta}$ or equivalently $\theta - \theta_o = (1/\ln a) \ln r/r_o$

The most striking feature is that the shape (angle), or equivalently, the characteristic constant $(1/\ln a)$ is independent of rotation speed, current density and lead content in the electrolyte as well. If we assume that spirals are originated by protrusions which reached a critical height, disturbing the concentration field within the diffusion boundary layer, this critical protrusion height can be estimated in the same manner as suggested by Rogers and Taylor (3). If a protrusion of given height k originates a wake in the fluid at a distance k from the surface of a disc, the trajectory of this wake can be written as,

$$\theta - \theta_o = \frac{1 - G(\zeta)}{F(\zeta)} \ln r/r_\bullet$$

Here the dimensionless height

$$\zeta = k \sqrt{\omega/\nu}$$

Hill et al. (5) have explained this speed independence of spirals in terms of submicroscopic defects causing wakes along spiral stream lines in the presence of inhibiting film on the surface. That is to say, the characteristic constant $(1 - G)/F$ approaches the limit 1.21 as the dimensionless height ζ tends to 0. For extremely small protrusion (i.e., $k \sim 0$), $\zeta \sim 0$ regardless of rotation speed. Therefore $(1 - G)/F$ approximates 1.21 and becomes independent of rotation speed.

However, it is more likely that the contribution of roughness to the disturbance in the concentration field may be considered to depend on its height relative to the thickness of the diffusion boundary layer, along the lines of Dryden's work (18) on momentum instability in the hydrodynamic boundary layer caused by a roughness element. Thus the critical protrusion height, where local eddy-mixing initiates, may be written in the form as,

$$k = k^* \delta_{diff.} \qquad (0 \leq k^* \leq 1)$$

Here, k* denotes the critical relative roughness height. According to the Levich equation,

$$\delta_{diff.} = 1.61 \, (D/\nu)^{1/3} \sqrt{\nu/\omega}$$

$$\zeta_{crit.} = k^* \delta_{diff.} \sqrt{\omega/\nu}$$

By substitution,

$$\zeta_{crit.} = 1.61 \, k^* \, (D/\nu)^{1/3}$$

If k* is not a function of angular velocity , $\zeta_{crit.}$ becomes a constant. Hence (1 - G)/F does not depend on rotation speed.

As mentioned earlier by Rogers and Taylor (3), the roughness Reynolds number can be represented by,

$$Re_k = r \, \zeta \sqrt{\omega/\nu} \cdot \sqrt{F^2 + (1 - G)^2}$$

Associated pertinent calculated values are given below.

k	k*	ζ	Re_k	(1-G)/F
3.4 m	0.21	0.03	0.045	1.24
8 m	0.50	0.07	0.24	1.29
16 m	1.0	0.14	0.95	1.38

$r = 0.725$ (cm) , $\omega = 83.8$ (1/s) (i.e., 800 rpm)

$D = 0.7 \times 10^{-5}$ (cm^2/s), $\nu = 1.08 \times 10^{-2}$ (p)

Calculated values of Re_k are at least one order of magnitude smaller than the range of the critical roughness Reynolds number for an isolated roughness element (19), namely 7 - 20. It seems to suggest that a fully-established secondary flow does not occur at the onset of formation of spirals. Therefore a short range disturbance upstream and downstream the protrusion will more likely be initiated by these critical protrusions, facilitating connection of protrusions along spiral wakes.

The periodicity of lead distribution in the zinc deposits along spiral patterns indicates the possibility of existence of secondary flow. Presumably secondary flow might be initiated as connection of protrusions proceeds forming semi-continuous spiral ridges. Mass transfer to the valleys will be reduced because of a thicker diffusion boundary layer along the valley floor.

Concerning question (3): "Why does this local eddy-mixing enhance preferred growth of zinc under kinetic control conditions?"

Although it is impossible to exclude the possible influence of hydrogen co-evolution, preferred growth of zinc crystals towards higher concentration location occurs in the absence of minor species (i.e., ultra-pure solution) well below the mass transfer regime. It may be reasonably assumed that this preferred growth is due to a slight difference in crystallization over-potential caused by a slight difference in zinc concentration. More convincing support for this tentative mechanism will have to rely on future studies on nucleation and growth of zinc electrocrystallization.

Concerning question (4): "What role does lead impurity play in the formation of spiral patterns of electrodeposited zinc on a rotating disk electrode?"

Lead ions reduce the initial nucleation density and promotes the coalescence and preferential growth of protrusions. Therefore they tend to accelerate the amplification of surface irregularities. It is not at all clear on an atomic scale whether codeposited lead serves as a nucleation center enhancing nucleation rate or acts as an obstacle against the propagation of monoatomic layer, thereby retarding crystal growth. SEM photographs of protrusions show that growth of these protrusions proceeds by successive nucleation and growth of atomic layers, one over another. Experimental results appear to favour the reduction of growth sites due to incorporation of lead into active sites on the crystal.

6. SUMMARY AND CONCLUSIONS

On the basis of the foregoing discussion the cause for formation of spiral striations can be reasonably exlained by the following mechanism.

DEVELOPMENT OF SURFACE ROUGHNESS

Amplification of surface roughness proceeds sequentially in the following manner.

(1) Initial nucleation and growth of nuclei

(2) Coalescence of nuclei into larger protrusions

(3) Preferential growth of larger protrusions

(4) Successive coalescence, and consumption of smaller protrusions by larger ones.

DISTURBANCE OF THE CONCENTRATION FIELD

The concentration field is disturbed by these protrusions acting as distributed roughness elements. Eventually well established secondary flows occur.

(1) Short range disturbance

Local eddy mixing is originated by protrusions, the heights of which reach a certain portion of the thickness of the diffusion boundary layer.

Slight differences in zinc concentration results in slight differences in crystallization over-potential, causing enhanced crystal growth in well mixed locations. Thus connection of protrusions along spiral lines occurs.

(2) Long range disturbance

Secondary flow occurs as connection of protrusions proceeds.

Spiral ridges become more pronounced owing to greater mass transfer onto ridges than into recesses.

The role of minor species may be summarized as follows:

LEAD IONS

(1) Decrease the number of initial nucleation sites for zinc.

(2) Poison the platinum surface for hydrogen evolution. Hence, the whole surface can be covered by a thin layer of zinc-platinum alloy from the very beginning of deposition.

(3) Enhance successive coalescence and preferential growth of protrusions.

(4) Deform the crystalline structure to a rounded shape.

H^+ IONS

(1) Seem not to affect either the initial nucleation or successive coalescence of protrusions.

(2) Change the crystalline structure to a rounded shape with decreasing pH values.

APPENDIX A

Zinc Dust Purification

Cementation of the more noble metallic impurities by zinc dust has been utilized in electrolytic winning of zinc as one of the main purification steps. Such elements as copper and lead can be easily removed by cementation with zinc dust. Copper and arsenic are often added to the solution at an elevated temperature to activate zinc particles for further cementation of other impurities, which are more difficult to remove. It is widely accepted that cementation is a diffusion-controlled, first order rate process. The importance of the activity of the surface deposit (i.e., effective surface area, alloy formation or poisoning) should be emphasized (20). As a result, the cementation rate is a complicated function of temperature, agitation, concentration of metal ions and complexing ligands, zinc particle size, etc. (21). Shibuya and Nakamori have investigated several potential methods for the removal of lead impurity from acidic zinc electrolytes (22). Figure A-1 and A-2 are shown reproduced after Shibuya et al. with permission of Sumitomo Metal Ind., Ltd. The solution was 1.4M $ZnSO_4$ with supporting electrolyte: 0.5M Na_2SO_4. A.R. grade zinc dust was used. The lead concentration after cementation was below 0.1 mg/l (4.8×10^{-7}M) measured by atomic absorption spectroscopy associated with a special extraction procedure. Recently the residual concentration has been determined by Shibuya et al. to be about 0.05 mg/l (2.4×10^{-7}M) through the use of polarographic measurements.

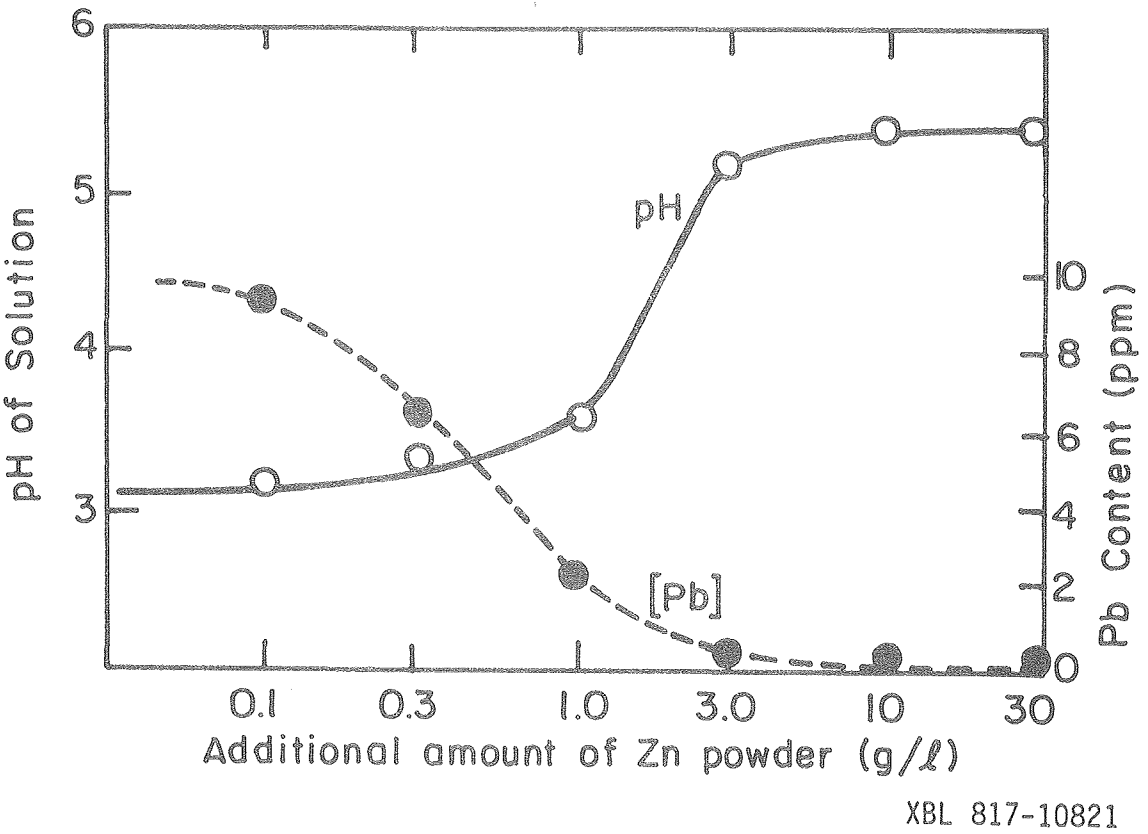

Figure A-1. Reduction Rate of Lead.
Temperature 60 °C
Reaction time 1 hr.

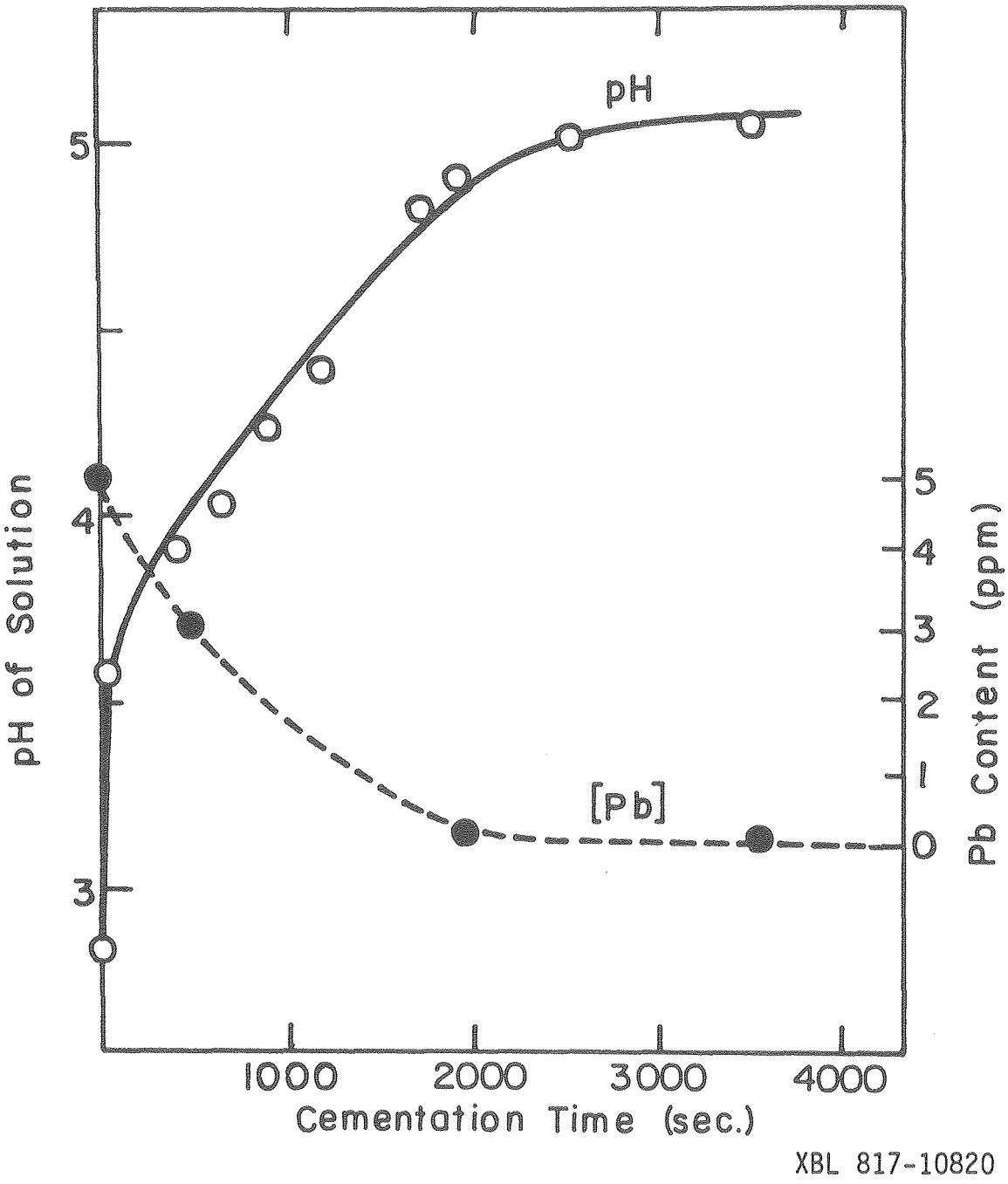

Figure A-2. Reduction Rate of Lead.
Temperature 60 °C
12.5 g/ℓ Zn powder added

APPENDIX B

Experiments with a Rotating Ring Electrode

Rotating ring electrodes were employed to examine the leading-edge effect of a rotating system. Experiments were conducted at a current density of 5mA/cm^2 and at rotation speeds of 200, 400, 800 and 1,600 rpm respectively in 1M zinc sulfate solution (A.R. grade, pH 2). The results may be summarized as follows:

(1) Spiral ridges appear originally from the outer edge of a ring electrode propagating inwards along spiral patterns. Then after about 3 min. deposition, spiral patterns appear at the inner edge propagating outwards. Spiral formation is much more pronounced at the outer edge. Finally many protrusions in the intermediate region were connected to each other to form complete spiral ridges.

(2) At 200 rpm, spiral formation at the inner edge did not occur. This might suggest that spirals may not form below certain low rpm.

(3) The number density of spirals increases with an increase of rate of rotation.

(4) Melding of spirals is more pronounced after prolonged deposition and with increasing the rotation speed.

(5) The formation time of spiral lines does not decline with an increase of the rotation speed (i.e., all shorter than 3 min.).

(6) Shapes of striations resemble those of logarithmic spirals. The characteristic constant (1/ln a) seems to be nearly independent of the rotation speed.

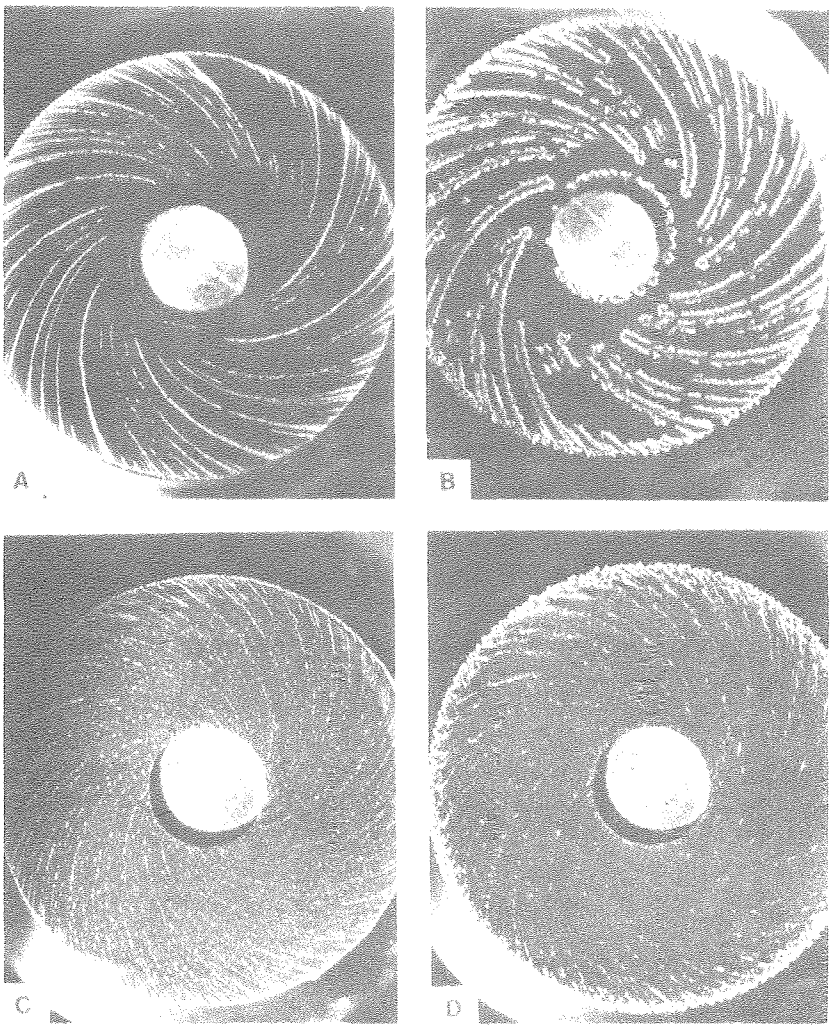

XBB 817-6475 A

Figure B. Effect of rotation speed on the number density of spirals and their melding characteristics. A.R. grade 1M zinc sulphate solution, 5 mA/cm^2. Ring electrode (r_{in} = 0.2 cm, r_{out} = 0.73 cm).

(A) 200 rpm, 30 min. (B) 200 rpm, 135 min.
(C) 1,600 rpm, 30 min. (D) 1,600 rpm, 120 min.

APPENDIX C

Effect of Other Impurities on the Formation of Spirals

In preliminary experiments on purification by means of zinc powder cementation, the formation time of spirals was remarkably retarded when the solution was replenished every 20 min. with purified solution (i.e., 80 - 90 min at 30mA/cm^2, 800 rpm) even when 99.99% zinc was used as anode. This was much longer than that obtained from purified solution with a platinum anode (i.e., 30 - 45 min at 30mA/cm^2, 800 rpm). It can be assumed that an infinitesimal amount of impurity, inhibiting the formation of spirals, was present in the purified solution and was consumed within 20 - 30 min. deposition. Moreover, once the purified solution was contaminated by an impurity dissolved from the zinc anode, the zinc-powder treatment was no longer effective. This seems to suggest that other impurities accelerating spiral formation exist besides lead, or that some impurities which prohibit the zinc-cementation reaction were introduced, or possibly some impurities which activate the zinc-cementation reaction, such as copper, were not present at concentration levels in contrast to A. R. grade zinc chloride solution.

At this stage investigations were aimed neither to provide a thorough screening of impurities affecting the formation of spirals nor to set forth the limiting value of each impurity. Instead it was intended to briefly seek elements which might enhance or inhibit the formation of spirals with a minimal number of experiments.

The presence of impurities such as lead, cadmium, tin, thallium, iron, nickel, cobalt, copper, arsenic, antimony, germanium, tellurium, selenium, manganese, magnesium, aluminum, sodium and potassium, is

common in electrolytic refined zinc. Bismuth, tungsten, gallium and indium are not likely to be contained. It is also known in electrolytic refining process of zinc that controlled amounts of cobalt reduce the amount of lead deposited with the zinc, whereas thallium tends to raise it (23).

Impurities may be classified into several groups, from different viewpoints, as follows:

(1) Hydrogen Overpotential

(a) High hydrogen overvoltage ----- Hg, Pb, Tl, In

(b) Low hydrogen overvoltage ------ Co, Ni, Cu, Sn

(2) Lowering current efficiency -------- Co, Ni, Cu, As, Sb, Ge, Te, Se, Mn

(3) Difficult removal by zinc cementation ----- Co, Fe, Ni

Finally, Cd, Sn, Co, Hg and Tl were chosen among them. Each metallic compound was dissolved in 1M zinc chloride solution pretreated by zinc-powder cementation method. Current density was 30mA/cm^2 mainly and for some impurities 10 mA/cm^2 in addition. Rotation speed was kept at 800 rpm.

Results are summarized in Table C and shown in Figure C.1 through C.4. Table C. leads to the following:

(1) The presence of Hg and Tl tends to inhibit the formation of spirals. Surprisingly no spirals were visible except for the area near the circumference even after 120 min. deposition in the presence of Tl at current density 30 mA/cm^2.

(2) Addition of trace amount of Cd, Sn, Co and Hg (4.8×10^{-5}M) result in an increase of number (density) or spirals, although their induction period for onset of spiral lines varies significantly.

(3) Hydrogen overpotential is not directly related to this phenomenon.

(4) It can reasonably be assumed that vigorous co-evolution of hydrogen occurs in the presence of Co. A portion of recess area among spiral ridges was not covered by zinc deposit as shown in Figure C.1.

(5) It is suggested that at the very beginning of deposition onto a platinum surface the impurity poisons active sites for discharge of hydrogen providing more uniform deposition of zinc in the presence of impurities, which have high hydrogen overpotential, as Pb, Hg and Tl.

(6) It might be worthwhile to search other reproducible electrodes such as glassy carbon, zinc-cyanide strike on platinum etc., since hydrogen overvoltage of platinum is extremely low. Particularly it may be desirable for experiments under "ultra-pure" condition to minimize the influence of hydrogen evolution in spite of the fact that it could be of a minor importance.

(7) The formation of spirals is sensitive to certain trace metal cations. They should be introduced as an addition agent in the electrolyte rather than allowing them to appear as an impurity.

The effect of two or more impurities in combination is a much more complicated problem leading to an everlasting project in terms of understanding the mechanism of spiral formation. But further investigations

on impurities may be beneficial in real application to improve the performance and reliability of zinc chloride batteries.

Table C. Effect of impurities on the formation of spirals.

Impurity	Current Density (mA/cm^2)	Formation Time (min.)	Number of Spirals	Comments
Cadmium	30	- 20	Much larger	
	10	- 30	Larger	Clouds of big bumps in center domain
Tin	30	- 30	Larger	Extremely rugged
Cobalt	30	10 - 20	Larger	Rugged deposit. Bare substrate partly exposed.
Mercury	30	45 - 60	Much larger	
Thallium	30	(45 - 60)	Visible only near the edge	Rough deposit
	10	- 15	Smaller	Huge bumps connected along spiral locus
Lead	30	5 - 10	Basis for Comparison	
	10	5 - 10		

The concentration of each impurity is 4.8×10^{-5} M respectively.
Rotation speed 800 rpm.

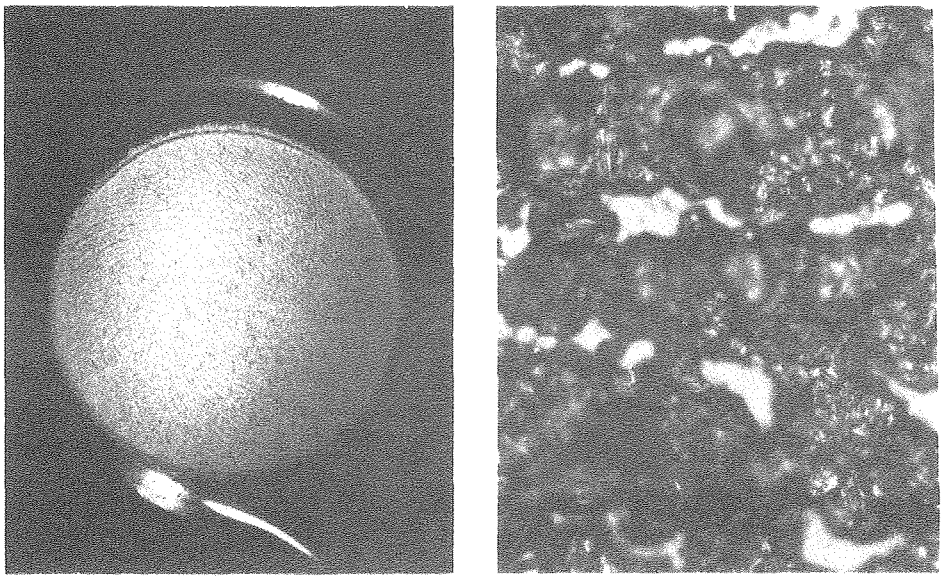

30 mA/cm^2 (X 192)

4.8×10^{-5} M Co

XBB 817-5955 A

Figure C.1 Effect of codeposition of cobalt.

1M zinc chloride with 4.8 X 10^{-5} M Co, 800 rpm.

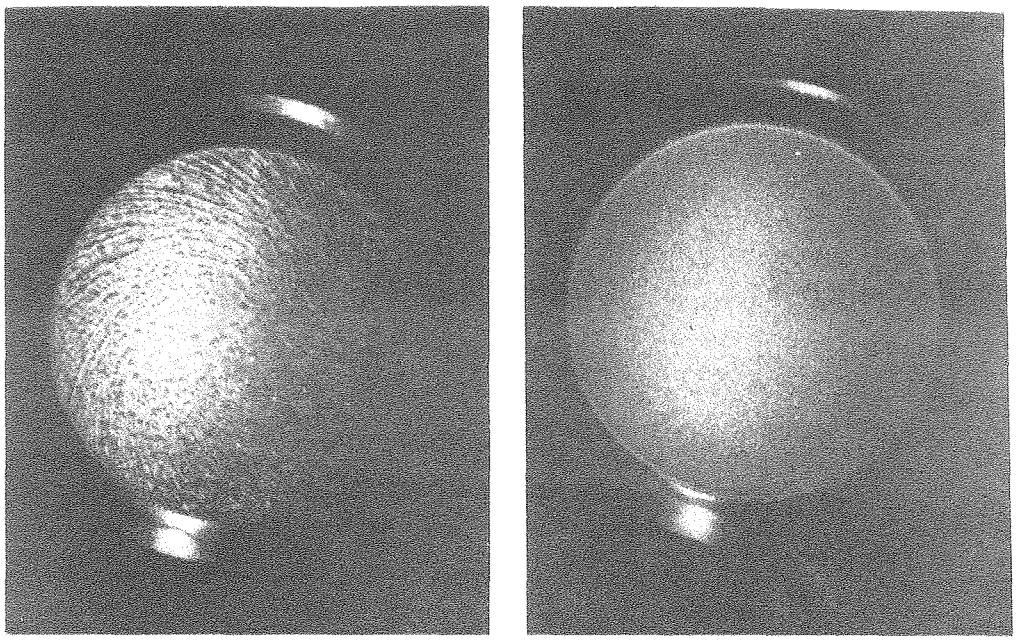

Figure C.2 Effect of codeposition of thallium.

1M zinc chloride with 4.8 X 10^{-5} M Tl
800 rpm.

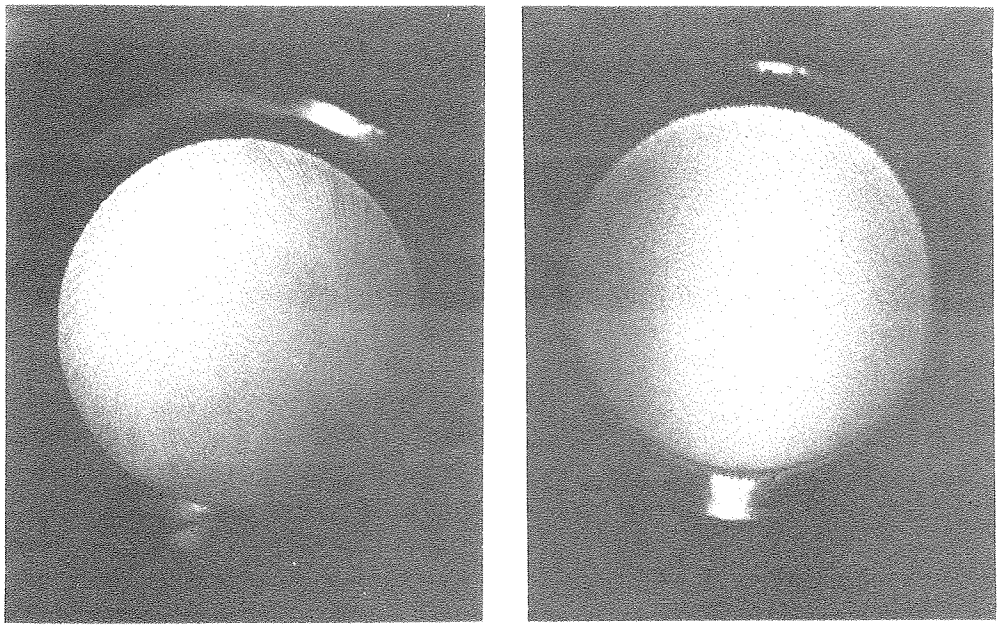

XBB 817-5957 A

Figure C.3 Effect of codeposition of cadmium.

1M zinc chloride with 4.8 X 10^{-5} M Cd
800 rpm.

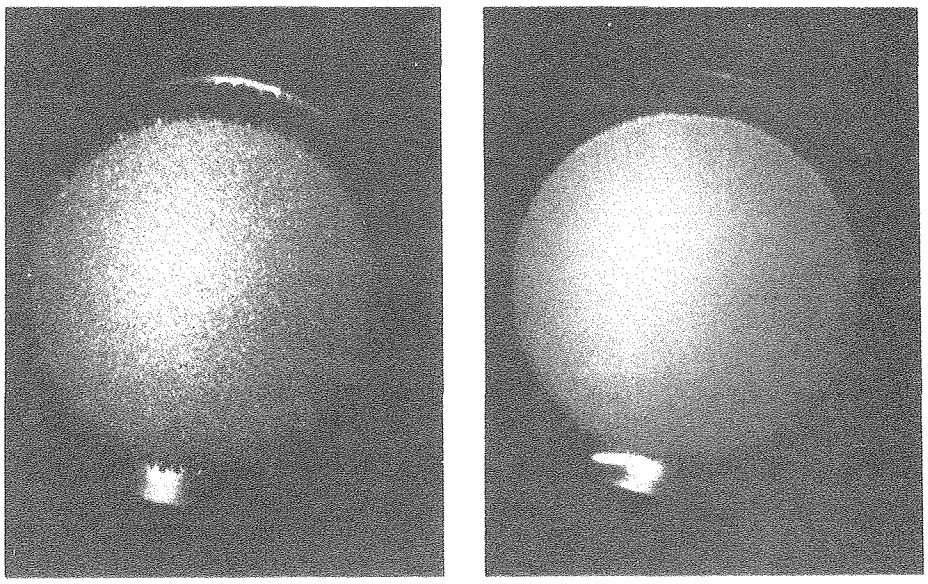

XBB 817-5958 A

Figure C.4 Effect of codeposition of tin or mercury

(a) 1M zinc chloride with 4.8 X 10^{-5} M Sn
(b) 1M zinc chloride with 4.8 X 10^{-5} M Hg

LIST OF SYMBOLS

i	current density
i_{avg}	time-average current density, pulse deposition
i_p	peak current density, pulse deposition
k	critical roughness height
k^*	critical relative roughness height
D	diffusion coefficient, cm^2/s
E	overpotential
L	characteristic dimension
T	on-time, pulse deposition
T'	off-time, pulse deposition

Greek Symbols

δ diff	thickness of the diffusion boundary layer
δ hyd	thickness of the hydrodynamic boundary layer
κ	electrolyte conductivity
ν	kinematic viscosity, cm^2/s
ω	rotation speed, rad/s
ζ	dimensionless axial distance from disc
ζ crit	critical dimensionless height

Dimensionless Groups

Re	Reynolds number, $r^2\omega/\nu$
Re_k	roughness Reynolds number, kv/ν
W	Wagner number, κ (dE/di)/L

Functions and Coordinates

$F(\zeta)$	function describing the centrifugal motion
$G(\zeta)$	function describing the rotational motion
(r,θ)	polar coordinates
(r_o,θ_o)	a certain point on a logarithmic spiral
$1/\ln a$	characteristic constant of a logarithmic spiral described by, $r = a^{\theta}$ or $\theta - \theta o = (1/\ln a) \ln r/r_o$

REFERENCES

(1) A. C. Riddiford, "The Rotating Disk System", Advances in Electrochemistry and Electrochemical Engineering, Vol. 4, (1966), p. 82 - 84.

(2) G. R. Johnson and D. R. Turner, J. Electrochem. Soc., 109 (1962), p. 918 - 922.

(3) G. T. Rogers and K. J. Taylor, Nature, 200 (1963), p. 1062 - 1064.

(4) M. R. Hill and G. T. Rogers, J. Electroanal. Chem., 86 (1978), p. 179 - 188.

(5) M. R. H. Hill, G. T. Rogers and K. J. Taylor, J. Electroanal. Chem., 96 (1979), p. 87 - 93.

(6) N. Gregory, J. T. Stuart and S. Walker, Phil. Trans. Roy. Soc., A298 (1955), p. 155 - 198.

(7) I. Cornet, W. N. Lewis and R. Kappesser, Trans. Instn. Chem. Engrs., 47 (1969), p. T222 - T226.

(8) Lawrence Berkeley Laboratory MMRD Annual Report 1976, LBL-6016, p. 427 - 428.

(9) Lawrence Berkeley Laboratory MMRD Annual Report 1977, LBL-7355, p. 509 - 510.

(10) Lawrence Berkeley Laboratory MMRD Annual Report 1978, LBL-8580, p. 489 - 490.

(11) Lawrence Berkeley Laboratory MMRD Annual Report 1980, LBL-12000, p. 475, 486.

(12) M. M. Jaksić and C. W. Tobias, "Hydrodynamic Flow Visualization by an Electrochemical Method", presented on Sept. 9, 1980 at Bochum, Germany.

(13) F. Mansfeld and S. Gilman, J. Electrochem, Soc., 117 (1970), p. 588 - 592.

(14) D. J. MacKinnon, J. M. Brannen and R. C. Kerby, J. Appl. Electrochem., 9 (1979), p. 55 - 70.

(15) J. Bressan and R. Wiart, J. Appl. Electrochem., 7 (1977), p. 505 - 510.

(16) J. Bressan and R. Wiart, J. Appl. Electrochem., 9 (1979), p. 43 - 53.

(17) J. Bressan and R. Wiart, J. Appl. Electrochem., 9 (1979), p. 615 - 621.

(18) H. L. Dryden, "Review of Published Data on the Effect of Roughness on Transition from Laminar to Turbulent Flow", J.A.S. 20 (1953), p. 477 - 482.

(19) H. Schlichting, "Boundary Layer Theory", Chap. 17, 7th ed., (1979), McGraw Hill.

(20) J. D. Miller, Miner. Sci. Engng., 5 (1973), p. 242 - 254.

(21) R. C. Kerby and T. R. Ingraham, Department of Energy, Mines and Resources (Canada), Report #R 243.

(22) A. Shibuya and T. Nakamori, Sumitomo Metal Ind., Ltd. Central Research Laboratory Report #4150 (1977).

(23) C. H. Mathewson, "Zinc: The Science and Technology of the Metal, Its Alloys and Compounds", Hafner Pub. Co., (1970).

(24) V. G. Levich, "Physicochemical Hydrodynamics", 2nd ed., (1962), Prentice-Hall, Inc.

TECHNICAL INFORMATION DEPARTMENT
LAWRENCE BERKELEY LABORATORY
UNIVERSITY OF CALIFORNIA
BERKELEY, CALIFORNIA 94720